

\$5

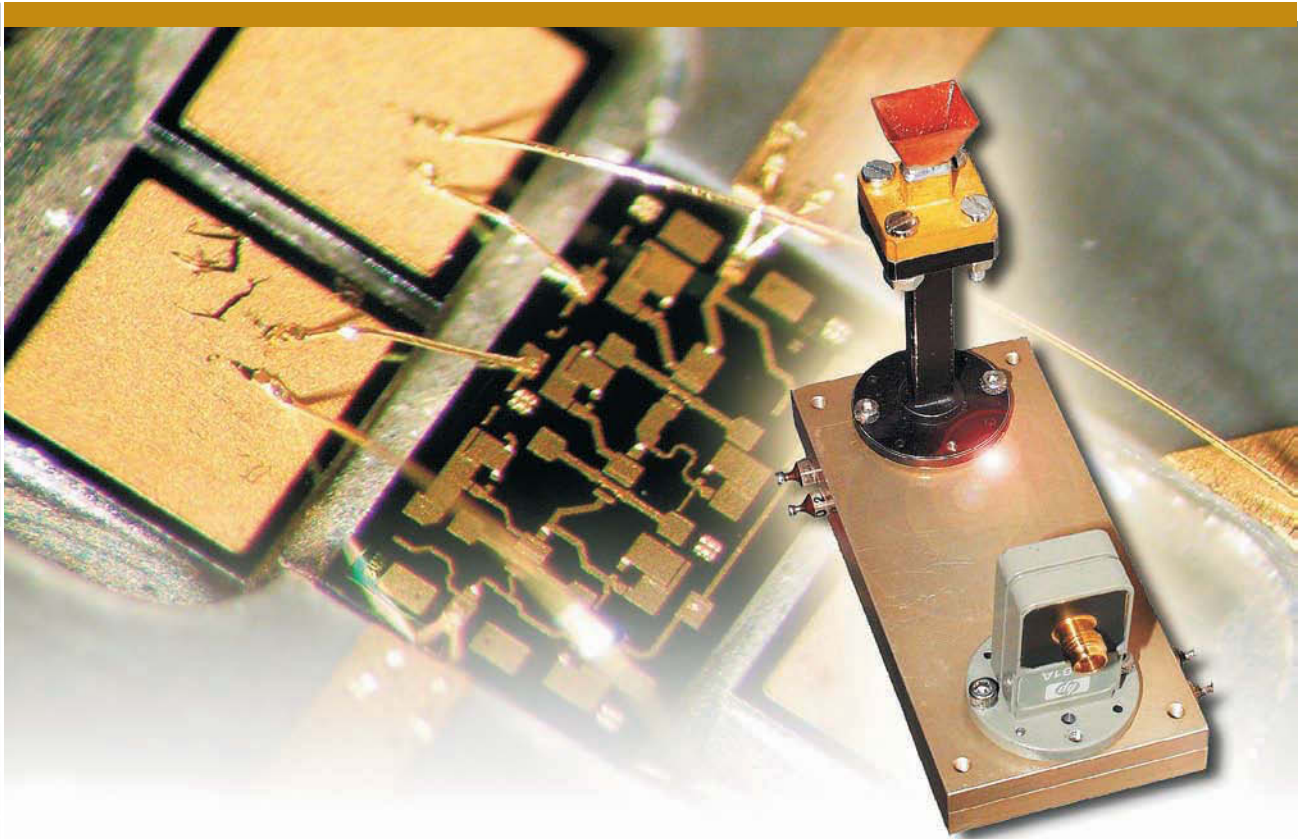


QEX

INCLUDING:
COMMUNICATIONS
QUARTERLY

Forum for Communications Experimenters

July/August 2005
Issue No. 231



From Italy, **IWØFGR** and **IØLVA**
present an LNA for 47 GHz.

ARRL The national association for
AMATEUR RADIO

225 Main Street
Newington, CT USA 06111-1494

Continuing Education



**Sign Up for
Summer
Classes!**

Register Online! www.arrl.org/cce

There's no better time to improve your skills. Online Classes are Available Now through the ARRL Certification and Continuing Education Program. Complete 100% of your training via the Internet:

- **Self-paced (asynchronous) format**—you attend class when and where you want.
- **High quality web experience** enhanced with graphics, audio, video, hyper-linking and interactive modules.
- **Online Mentoring.** Individually assigned instructors help advance each student toward successfully completing the course material.
- **Pre-register Now!** Classes open regularly.

Available Courses

Antenna Design and Construction...EC-009

Students become familiar with antenna design theory and experience hands-on construction techniques. The course includes several optional antenna construction projects for HF, VHF, and UHF.

Member: \$65 / Non-member: \$95

Antenna Modeling...EC-004

This course is an excellent way to learn the ins and outs and the nitty-gritty details of modeling antennas. In the last decade the science of modeling antennas using computer software has advanced by huge leaps and bounds. While some absolutely unique, brand-new antenna designs have resulted from computer studies, the real progress has been in our understanding of how even common, ordinary antennas work.

Member: \$85 / Non-member: \$115

HF Digital Communications...EC-005

Understanding HF digital Amateur Radio communications and developing awareness and stronger skills for many HF digital modes. **Member: \$65 / Non-member: \$95**

Level 1 Amateur Radio Emergency Communications...EC-001

Introduction to Amateur Radio Emergency Communications. A basic course to raise awareness and provide additional knowledge and tools for any emergency communications volunteer.

Member: \$45 / Non-member: \$75

Level 2 Amateur Radio Emergency Communications...EC-002

Intermediate Amateur Radio Emergency Communications. A more in-depth study into amateur radio emergency communications to enhance the skills and knowledge received from previous experience. Requires prior completion of EC-001.

Member: \$45 / Non-member: \$75

Level 3 Amateur Radio Emergency Communications...EC-003

Advanced Amateur Radio Emergency Communications. Bridging the gap between basic participation and leadership. Requires prior completion of EC-001 and EC-002.

Member: \$45 / Non-member: \$75

Radio Frequency Propagation...EC-011

Explore the science of RF propagation, including the properties of electromagnetic waves, the atmosphere and the ionosphere, the sun and sunspots, ground waves and sky waves, and various propagation modes—including aurora and meteor scatter.

Member: \$65 / Non-member: \$95

Radio Frequency Interference...EC-006

Learn to identify sources and victims of interference. Tips and suggestions for solutions and for handling those ticklish problems that crop up with difficult neighbors and other aggrieved parties. Tools to help foster ingenuity, intuition, and determination for solving interference problems.

Member: \$65 / Non-member: \$95

VHF/UHF—Life Beyond the Repeater...EC-008

An introduction to Internet linking, amateur satellites, direction finding, APRS, weak signals, VHF contesting, microwaves, amateur television, and high speed multimedia radio. Great for both the newly licensed and more experienced hams.

Member: \$65 / Non-member: \$95

Technician License Course...EC-010

The course prepares students to earn their first Amateur Radio license. There are no prerequisites. Individually assigned online mentors assist students as they advance toward successfully completing the course. Registration includes the ARRL book, *Now You're Talking!* and online graduate support.

Member: \$99 / Non-member: \$139

Analog Electronics...EC-012

Students learn about the use of instrumentation, Kirchoff's Laws, Diodes, Rectifier circuits, Bipolar and Field Effect Transistors, various amplifier configurations, filters, timers, Op-Amps, and voltage regulators. Most lessons include a design problem and optional construction project. (College-level course.)

Member: \$65 / Non-member: \$95

Digital Electronics...EC-013

Student learn about Basic Boolean, Basic Gates, Flip-Flops, Counters and Shift Registers, Latches, Buffers and Drivers, Encoders and Decoders, Parallel Interfaces, Serial Interfaces, Input Devices, Displays, Logic Families, Microprocessor Basics, Connecting to Analog Electronics, Understanding Data Sheets and Design Resources. Most lessons include a design problem and optional construction project. (College-level course.)

Member: \$65 / Non-member: \$95

Online courses are produced by American Radio Relay League, Inc. and are available through ARRL's partnership with the Connecticut Distance Learning Consortium (CTDLC), a nonprofit organization that specializes in developing on-line courses for Connecticut colleges and universities. Continuing Education Units (CEUs) are available for all ARRL Certification and Continuing Education courses. The ARRL Certification and Continuing Education Program is funded in part by course fees from interested hams who support public service and quality continuing education.

For further information, e-mail your questions to cce@arrl.org, or write to ARRL C-CE, 225 Main Street, Newington, CT 06111.

ARRL The national association for
AMATEUR RADIO
www.arrl.org/cce

QEX

INCLUDING: COMMUNICATIONS
QUARTERLY

QEX (ISSN: 0886-8093) is published bimonthly in January, March, May, July, September, and November by the American Radio Relay League, 225 Main Street, Newington CT 06111-1494. Periodicals postage paid at Hartford, CT and at additional mailing offices.

POSTMASTER: Send address changes to: QEX, 225 Main St, Newington, CT 06111-1494 Issue No 231

Harold Kramer, WJ1B
Publisher

Doug Smith, KF6DX
Editor

Robert Schetgen, KU7G
Managing Editor

Lori Weinberg, KB1EIB
Assistant Editor

L. B. Cebik, W4RNL
Zack Lau, W1VT
Ray Mack, WD5IFS
Contributing Editors

Production Department

Steve Ford, WB8IMY
Publications Manager

Michelle Bloom, WB1ENT
Production Supervisor

Sue Fagan
Graphic Design Supervisor

Mike Daniels,
David Pingree, N1NAS
Technical Illustrators

Joe Shea
Production Assistant

Advertising Information Contact:

Janet L. Rocco, *Account Manager*
860-594-0203 direct
860-594-0200 ARRL
860-594-0303 fax

Circulation Department

Kathy Capodicasa, *Circulation Manager*
Cathy Stepina, *QEX Circulation*

Offices

225 Main St, Newington, CT 06111-1494 USA
Telephone: 860-594-0200
Fax: 860-594-0259 (24 hour direct line)
e-mail: qex@arri.org

Subscription rate for 6 issues:

In the US: ARRL Member \$24,
nonmember \$36;

US by First Class Mail:
ARRL member \$37, nonmember \$49;

Elsewhere by Surface Mail (4-8 week delivery):
ARRL member \$31, nonmember \$43;

Canada by Airmail: ARRL member \$40,
nonmember \$52;

Elsewhere by Airmail: ARRL member \$59,
nonmember \$71.

Members are asked to include their membership control number or a label from their QST when applying.

In order to ensure prompt delivery, we ask that you periodically check the address information on your mailing label. If you find any inaccuracies, please contact the Circulation Department immediately. Thank you for your assistance.

Copyright ©2005 by the American Radio Relay League Inc. For permission to quote or reprint material from QEX or any ARRL publication, send a written request including the issue date (or book title), article, page numbers and a description of where you intend to use the reprinted material. Send the request to the office of the Publications Manager (permission@arri.org)



About the Cover

The completed LNA levitates above a close-up of a MMIC and its wiring. Read about the project on page 45.



Features

3 Receiver Measurements, How To Evaluate Receivers

By Dr Ulrich L. Rohde, N1UL

12 The Quest for the Elusive TBWB4EQ (The Triband Wideband 4-Element Quad)

By L. B. Cebik, W4RNL

28 Ground System Configurations for Vertical Antennas

By Al Christman, K3LC

38 A Blind Automatic Frequency Control Algorithm

By Gary A. Geissinger, WA0SPM

45 A 47-GHz LNA

By Silvano Ricci, I0LVA, and Daniele Moretti, IW0FGR

52 A Do-It-Yourself Noise Figure Meter

By Fred Brown, W6HPH

54 A Space-Saving Antenna for 40 Meters

By Ron Skelton, W6WO

57 Octave for Signal Analysis

By Maynard A. Wright, W6PAP

Columns

62 Letters

63 Next issue in QEX

Jul/Aug 2005 QEX Advertising Index

American Radio Relay League: Cov II,
63, Cov III, Cov IV
Atomic Time: 53
Down East Microwave, Inc.: 64
Expanded Spectrum Systems: 27
J-TEC, LLC: 64
National RF: 64

Nemal Electronics International, Inc.: 53
Noble Publishing Corp.: 64
RF Parts: 11
Teri Software: 56
Tucson Amateur Packet Radio Corp.: 44
Walter H. Volkmann: 63

THE AMERICAN RADIO RELAY LEAGUE



The American Radio Relay League, Inc. is a noncommercial association of radio amateurs, organized for the promotion of interests in Amateur Radio communication and experimentation, for the establishment of networks to provide communications in the event of disasters or other emergencies, for the advancement of radio art and of the public welfare, for the representation of the radio amateur in legislative matters, and for the maintenance of fraternalism and a high standard of conduct.

ARRL is an incorporated association without capital stock chartered under the laws of the state of Connecticut, and is an exempt organization under Section 501(c)(3) of the Internal Revenue Code of 1986. Its affairs are governed by a Board of Directors, whose voting members are elected every two years by the general membership. The officers are elected or appointed by the Directors. The League is noncommercial, and no one who could gain financially from the shaping of its affairs is eligible for membership on its Board.

"Of, by, and for the radio amateur," ARRL numbers within its ranks the vast majority of active amateurs in the nation and has a proud history of achievement as the standard-bearer in amateur affairs.

A bona fide interest in Amateur Radio is the only essential qualification of membership; an Amateur Radio license is not a prerequisite, although full voting membership is granted only to licensed amateurs in the US.

Membership inquiries and general correspondence should be addressed to the administrative headquarters at 225 Main Street, Newington, CT 06111 USA.

Telephone: 860-594-0200

FAX: 860-594-0259 (24-hour direct line)

Officers

President: JIM D. HAYNIE, W5JBP

3226 Newcastle Dr, Dallas, TX 75220-1640

Chief Executive Officer: DAVID SUMNER, K1ZZ

The purpose of QEX is to:

- 1) provide a medium for the exchange of ideas and information among Amateur Radio experimenters,
- 2) document advanced technical work in the Amateur Radio field, and
- 3) support efforts to advance the state of the Amateur Radio art.

All correspondence concerning QEX should be addressed to the American Radio Relay League, 225 Main Street, Newington, CT 06111 USA. Envelopes containing manuscripts and letters for publication in QEX should be marked Editor, QEX.

Both theoretical and practical technical articles are welcomed. Manuscripts should be submitted on IBM or Mac format 3.5-inch diskette in word-processor format, if possible. We can redraw any figures as long as their content is clear. Photos should be glossy, color or black-and-white prints of at least the size they are to appear in QEX. Further information for authors can be found on the Web at www.arrl.org/qex/ or by e-mail to qex@arrl.org.

Any opinions expressed in QEX are those of the authors, not necessarily those of the Editor or the League. While we strive to ensure all material is technically correct, authors are expected to defend their own assertions. Products mentioned are included for your information only; no endorsement is implied. Readers are cautioned to verify the availability of products before sending money to vendors.

Empirical Outlook

Immaculate Reception

We tend to dote on receiver articles here at QEX. That's probably because receivers are some of the more complex and perhaps the most difficult machines that one can design. We've certainly seen some good designs lately, too. But the recent rise of direct-conversion and similar DSP-based designs has given rise to fresh discussions about test methods. It's becoming increasingly difficult to make comparisons among new and old receivers, as in the ARRL product-comparison chart. If our test methods change—as they have done several times in the past—then that difficulty may increase.

But change they must because we have to be sure that we're measuring what we think we are. Increased dynamic ranges and bandwidth capabilities of receivers may force changes in test instrumentation as well. Here are a few of the issues as we see them.

One of the first mandatory measurements for any receiver is to ascertain its noise-floor power. For proper comparisons with other receivers, that must be specified in a standard bandwidth. Then it's possible to compute a noise figure, which we feel is the best figure of merit when it comes to noise performance. But simply selecting, say, a 500-Hz filter on an SSB rig doesn't guarantee that the actual bandwidth is the same as another receiver's 500-Hz filter. Yes, you can measure the bandwidth to get your result, but what about the shape of the passband and stopbands? One way to compensate for those factors would be to compute the equivalent rectangular bandwidth for the filter (infinite shape factor). There are other ways to measure noise figure, but then you must reverse the process to compute the noise-floor power. That's because it's used in dynamic-range calculations. So, we must have that number.

A possible pitfall of using an audio voltmeter during noise-floor testing arose a few years ago. It turns out the engineer was using a meter that did not read true-RMS, but more like average-reading calibrated to RMS. That meant that the peak-to-average ratio of what he measured affected the result. During his procedure and with no sig-

nal into the receiver, he calibrated his meter to 0 dB; then he injected a signal producing a 1-kHz tone and increased its level until the meter reading rose 3 dB. It turns out his results were off by almost 2 dB because the peak-to-average ratio of the noise was about 2 dB different than that of the sine wave.

To measure the upper end of any type of dynamic range, a good way to go seems to be to examine the receiver output on a spectrum analyzer. Then it's easy to determine when the interference produces the effect sought. But it's possible to design a receiver with an AGC knee at the noise floor. If that AGC could not be turned off or the knee not raised, the receiver's peak output level would remain constant. Then during a so-called blocking dynamic range measurement, an increase in on-channel noise would force the on-channel signal's level downward, giving a possibly false indication. You wouldn't be measuring blocking at all but some phase-noise effect. That could be a problem for testing of FM rigs.

Then there is this accuracy and precision business, which I've discussed before. Those are just a few of the things currently being considered. Your comments are welcome!

In This Issue

Ulrich Rohde, N1UL, brings us discussions and examples of receiver tests using European standards. Contributing Editor L. B. Cebik, W4RNL, discusses three-band four-element quads with an eye toward bandwidth, among other things. Al Christman, K3LC, has some notes on ground-system configurations for vertical antennas. Gary Geissinger, WA0SPM, shows how SSB voice signals might be tuned automatically. Our Italian friends Silvano Ricci, I0LVA, and Daniele Moretti, IW0FGR, relate their recent experiences on the 6-mm band with a 47-GHz LNA. Fred Brown, W6HPH, has a neat homebrew noise-figure meter design. Ron Skelton, W6WO, delivers a space-saving antenna for 40 m. Maynard Wright, W6PAP, has more on *Octave*. This time, the subject is signal analysis.—73, Doug Smith, KF6DX, kf6dx@arrl.org.

□□

Receiver Measurements, How To Evaluate Receivers

Want to test your receiver? Here's the right way.

By Dr. Ulrich L. Rohde, N1UL, ex KA2WEU

When evaluating a receiver, it is useful to have a set of guidelines by which to evaluate the receiver. In this paper, I am focusing on some specific modulation and tests because there are agreed upon measuring standards. They can be used for AM if the carrier is modulated 60%, as an example, instead of FM deviation. By not modulating the carrier, they are applicable for SSB, too. Some of modulation tests are applicable for all three modulation types (AM/FM and SSB).

For evaluation of the quality of a

receiver, different procedures of measurements with different standard values have been developed. All these receiver measurements, however, have in common that the RF-input signal is varied and the corresponding AF-output signal measured. The AF signal is a function of the RF signal.

Two groups of measurements apply

- Single-generator measurements, with one RF signal at the receiver input
- Two-generator measurements, with two RF signals at the receiver input

In the following, some test procedures specified by FTZ (German government standards) or recommended by CEPT (Conference of European Telecommunication Administrations) will be used as examples. The US standards follow these rules or vice versa.

Table 1 shows the guaranteed/measured characteristics of a high performance short wave receiver, Rohde & Schwartz model EK895. The measurements are done with the preamplifier off. If the preamplifier is switched on, the large signal parameters deteriorate. Please note that this receiver does not have FM capabilities.

Note: In most cases, the “receiver sensitivity” is specified as the criterion for receiver measurements. This fundamental parameter is defined either by the S/N of the modulated to the unmodulated RF signal (FTZ) or by the so-called SINAD method (CEPT); see Figs 5 and 6. Fig 1 shows the basic setup. RT refers to the transceiver. The signal generator or both signal generators (they need to be combined with a hybrid coupler) must be connected to the antenna terminal

of the receiver. The AF meter must be connected to the audio output of the receiver of the devices under test or better to the line output.

SINGLE-TONE MEASUREMENTS

1. Measurement of Receiver Noise

In order to measure the receiver noise, the AF-output voltage of the receiver is measured with an unmodulated RF signal applied. The RF level must be high enough for the RF limiter to operate (about 10 μ V EMF): see Fig 2.

Make sure to switch off the frequency modulation or the amplitude modulation.

Measurement of the AF voltage:

Increase the RF level with the attenuator starting from about 1 μ V EMF (-113 dBm) to approximately 10 mV EMF until the AF level no longer decreases (RF limiting). Read the residual level of receiver noise on the meter. This measurement defines the maximum S/N ratio or quieting.

EMF (electromotive force) refers to the open voltage without terminating the original generator. When terminating the generator into 50 Ω , the resulting voltage will be EMF/2.

Fig 1 shows a simplified test setup which consists of an RF generator, which can be modulated and an AF analyzer. The generator needs to cover the necessary frequency range and must be capable of very linear AM and FM modulation. The generator also needs to have low phase noise and high frequency stability. Generators in radio communication test-equipment units typically do not have sufficiently low phase noise, but they can handle all modulation requirements and have the audio analyzer built in. Some tests require two different low-noise generators.

Starting from about 0.1 μ V, Fig 2 shows the AF signal as a function of the RF input signal. Different input voltages result in different S/N ratios. The value of 40 dB shown here is typical, but the ultimate S/N ratio can be as high as 90 dB on high fidelity FM receivers. This requires a very low phase-noise oscillator.

2. Measurement of the S/N (FTZ)

For FM or AM the S/N is the ratio of the wanted signal level to the noise level that is:

$$S/N = \frac{V_{AF(1kHz:2.8kHz \text{ deviation})}}{V_{AF(no \text{ modulation})}}$$

Measurement of the wanted signal level:

V_{AF} (1 kHz: 2.8 kHz deviation)

The AF frequency will be set to 1 kHz. Adjust the frequency deviation to 2.8 kHz, or for AM, to 60% modulation. Adjust the RF level with the attenuator (about 10 mV, maximum, EMF); read the resulting S/N and the signal on the meter.

If the S/N is to be determined from the ratio of the set deviation (peak

value) to the residual deviation (RMS value), either the indicated resulting deviation must be converted to the RMS value (measured value/ $\sqrt{2}$) or the S/N obtained must be reduced by 3 dB.

In the AM case, the generator needs to be 60% modulated and then the value of the input signal for 10 dB S/N as the modulation is switched off must be determined. AM measurements are typically done with 3-6 kHz bandwidths.

Table 1

Sensitivity (for S/N= 10 dB, $f_0 = 0.1$ to 30 MHz)

A1A (CW)	0.4 μ V EMF (-121 dBm), bandwidth = 300 Hz
J3E (SSB), J7B	1.0 μ V EMF (-113 dBm), bandwidth = 2.7 kHz
H3E (AME), 1 kHz, m = 60% with preamplifier, f = 0.2 to 30 MHz	2.7 μ V EMF (-104 dBm), bandwidth = 6 kHz
A1A (CW) Bandwidth = 300 Hz	0.2 μ V EMF (-127 dBm),
J3E (SSB), J7B BW=2.7 kHz	0.4 μ V EMF (-121 dBm),
H3E (AME), 1 kHz, m = 60%	1.0 μ V EMF (-113 dBm), BW = 6 kHz

Immunity to interference, non-linearities

Intermodulation (1.5 to 30 MHz;

Δf	>30 kHz; interfering signal 0 dBm)
IP_2	>60 dBm (typical 70 dBm)
IP_3	>30 dBm (typ 35 dBm)

Cross-modulation (0.1 to 30 MHz,

Interfering signal 5 V EMF (+21 dBm)
 Δf >30 kHz; m = 0.3; f = 1 kHz;
 signal level 10 mV EMF (-33 dBm)), <10% modulation transfer

Blocking (0.1 to 30 MHz;

Interfering signal 6.3 V EMF
 (+23 dBm); Δf >30 kHz;
 signal level 1 mV EMF (-53 dBm);
 m = 0.3; f = 1 kHz), > 1 signal dB attenuation

Desensitization

(interfering signal 300 mV EMF
 Δf >30 kHz; signal level
 30 μ V EMF; bandwidth 3.1 kHz) >20 dB SINAD

Inherent spurious signals

(f > 100 kHz)	<-113 dBm (nominal -124 dBm)
Image frequency rejection	>90 dB
IF rejection	>90 dB

Weighted S/N ratio

For 1 mV EMF, >46 dB SINAD

Measurement of AF noise level:

V_{AF} (no modulation).

Switch off the frequency modulation. Read the noise level on the AF meter: V_{AF} (unmodulated). The RMS value of the noise needs to be measured.

In Fig 2, the levels of the wanted AF signal and AF noise are shown as a function of the EMF of the signal generator.

For SSB measurements, the receiver had to be set into SSB or CW mode. In SSB the receiver should be tuned to that frequency that produces a 1 kHz beat note. The same applies for CW. The bandwidth for SSB is typically 2.2 kHz to 3.1 kHz, depending upon the application. For CW the bandwidth is either set to 500 Hz or 250 Hz depending upon the available filters. For FM, the bandwidth depends on the modulation index. In the case of $m=1$ the applied bandwidth is typically 10 kHz in a 25 kHz spacing. This allows the recognition of the higher pitched female voices.

While the standard test is done with 1 kHz, it is recommended to check the frequency response of the receiver by varying the modulation frequency or the beat note from typically 300 Hz to 3 kHz, or higher, bandwidth permitting.

3. Measurement of SINAD Ratio (CEPT)

Under item 2 above, the quality of the AF signal of a receiver is evaluated using the ratio of the signal to noise. In practice, however, the quality of a receiver depends on the AF distortion factor as well. Therefore, in receiver measurements according to CEPT recommendations, the distortion is evaluated in addition to noise:

$$SINAD = \frac{S + N + D}{N + D}$$

Where,

S = signal.

N = noise.

D = distortion.

That is, the ratio of signal + noise + distortion to noise + distortion. Contrary to the S/N measurement (FTZ), the signal generator is no longer operated alternately in the modulated and unmodulated modes but is always modulated.

The ratio of $(S + N + D)$ to $(N + D)$ can now be evaluated automatically.

Set the normal test modulation according to CEPT,

$$f_{AF} = 1 \text{ kHz}; f_{\text{deviation}} = 60\% \text{ of } f_{\text{maximum deviation}}$$

That is:

$$f_{\text{maximum deviation}}, \text{ for example,} = 4 \text{ kHz.}$$

Adjust the deviation to 2.4 kHz.

Measurement of AF voltage:

Evaluation in the SINAD mode:
Read SINAD value on the meter in percent. The most important SINAD values are:

6 dB = 50%, 12 dB = 25%, 20 dB = 10%.

If there is no 1 kHz signal applied or the signal level is too high, the dynamic range of the SINAD ratio evaluation circuitry may be exceeded. (A similar condition applies for distortion-factor measurement.)

4. Measurement of Receiver Sensitivity in S/N Mode (FTZ)

In accordance with item 2, the RF level of the signal generator is reduced until the S/N equals 20 dB; normal modulation is $f_{AF} = 1 \text{ kHz}$; 2.8 kHz deviation. For SSB, this is typically done for 10 dB S/N.

Measurement of the AF signal level:
 V_{AF} (1 kHz (no modulation), 2.8 kHz deviation)

Switch off the frequency modulation of the Signal Generator: reduce RF level until the noise level is 20 dB below the AF signal level. When the frequency modulation is switched on again, the AF voltage should increase

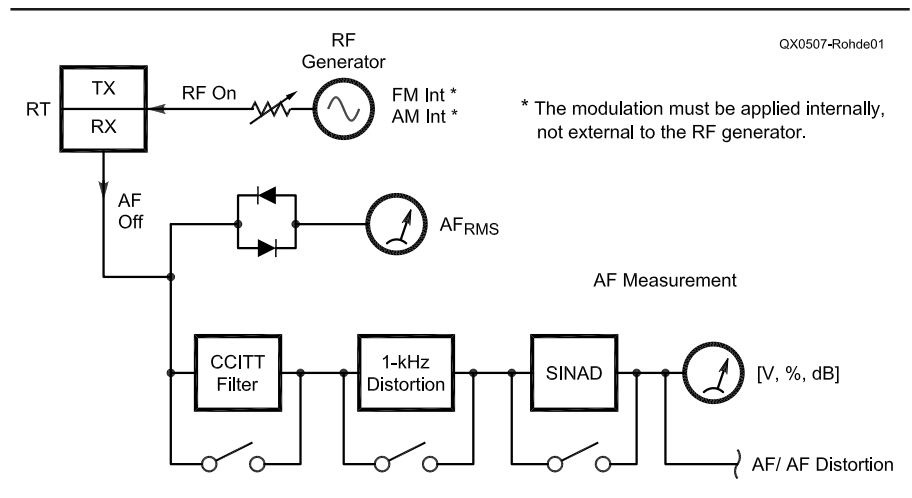


Fig 1—Block diagram of the setup to measure receiver sensitivity and S/N.

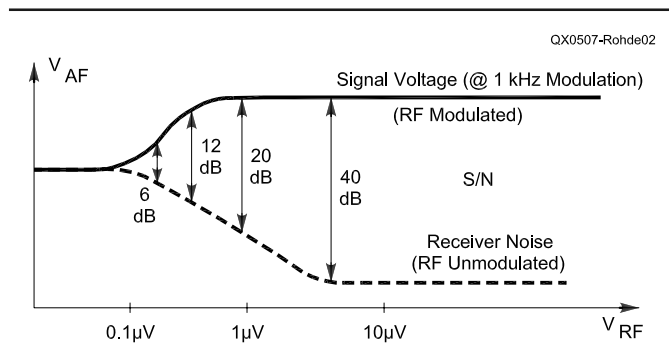


Fig 2—S/N for a typical receiver as a function of input level.

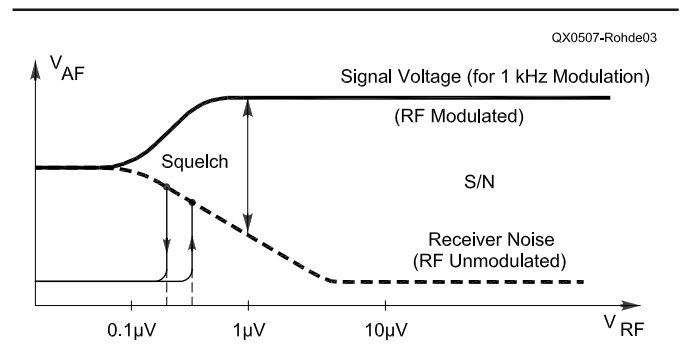


Fig 3—Squelch behavior as a function of S/N showing hysteresis.

by 20 dB. If this is not the case, the RF level must be varied again until S/N is 20 dB.

Read the receiver sensitivity directly in V_{EMF} or dBm . The actual numbers will be in the μV range. See Fig 2 for details.

The same technique applies for AM (60% modulation) and for SSD/CW (no modulation).

5. Measurement of Receiver Sensitivity in SINAD Mode (CEPT)

Adjust the normal test modulation (CEPT), that is $f_{AF} = 1$ kHz and, for example, 2.4 kHz deviation.

Adjust the RF level of the signal generator with the attenuator until the SINAD value equals 20 dB. Read the receiver sensitivity (20 dB) on the scale in V_{EMF} or dBm directly.

Note: In many cases, the sensitivity values measured in the S/N or the SINAD mode differ only slightly. The SINAD measurement, however, is by far simpler, more reliable and comfortable.

6. Squelch Measurement (see Fig 3)

If the RF signal level goes down below a certain threshold, the AF

channel is switched off automatically. Thus the residual noise is no longer heard.

Measurement:

Switch on the AF voltmeter:

a. Determination of the lower squelch response:

Reduce RF level (from about 10 μV) until the S/N deteriorates and the squelch closes.

The AF voltage goes to 0 V:

b. Determination of the upper squelch response:

Starting from about -145 dBm, increase RF level of the Signal Generator until the AF is switched on automatically: Read the value

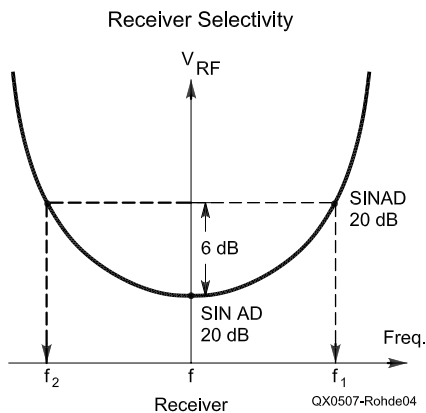


Fig 4—Typical input selectivity of a receiver. It assumes a single tuned filter.

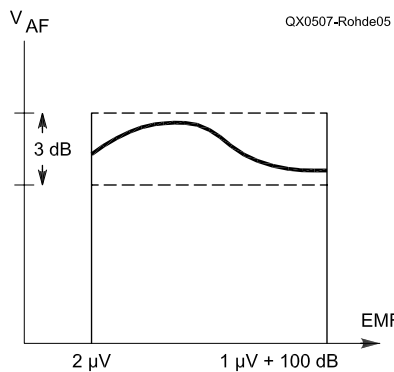


Fig 5—Receiver limiting as a function of input signal. The audio should not change more than 3 dB.

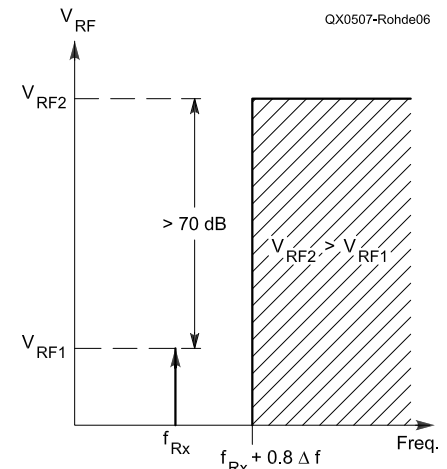


Fig 6—Attenuation of spurious signals should be at least 70 dB. V_{RF2} is the wanted signal and V_{RF1} is the spurious signal. The difference should be at least 70 dB. The spurious signal is caused by receiver non-linearity.

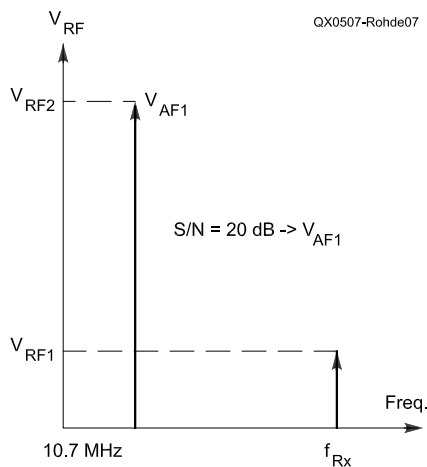


Fig 7—Measure of IF rejection. The difference between the wanted signal V_{RF2} and V_{RF1} for a good receiver should be 90 dB.

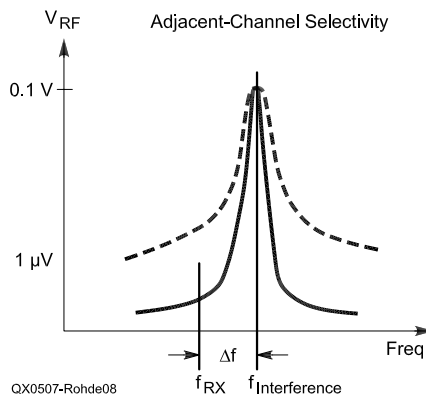


Fig 8—Adjacent-channel selectivity measurement. The interfering signal is only a few channels away. The difference in signal level between the two should be about 100 dB.

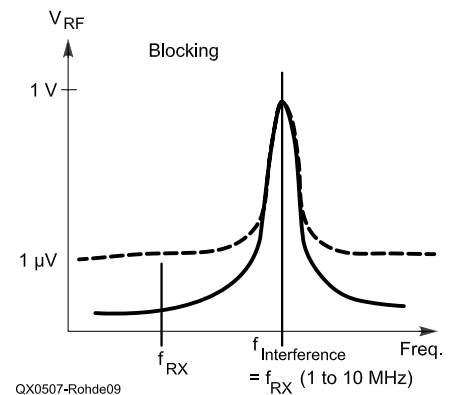


Fig 9—The blocking measurement refers to wider spacing, like an offset of 1-10 MHz. This points out the ultimate phase noise of the oscillator, like 145 dBc/Hz.

of the RF input signal.

The *squelch hysteresis* is obtained from the ratio of the two squelch response points.

A similar condition applies for measurement of the squelch hysteresis in the SINAD mode.

It may be useful to monitor this on a speaker.

7. Measurement of Receiver RF Bandwidth

The receiver RF bandwidth is evaluated with the aid of the AF criterion “receiver sensitivity” measured by the S/N or SINAD method. Tune the signal generator exactly to receiver frequency. Switch on normal test modulation (AM or FM). Find the 20-dB sensitivity (SINAD or S/N) and read corresponding EMF; increase EMF by 6 dB.

Increase the frequency of the signal generator until the value for sensitivity equals 20 dB (SINAD or S/N) again.

Read the new frequency: f_1 .

Repeat the same procedure for frequency f_2 (below the receiver frequency): The difference between f_1 and f_2 is the 6-dB bandwidth of the receiver. The receiver frequency should be in the middle of the 6-dB bandwidth. If this is not the case, the receiver input stage should be re-tuned. This is valid only for receivers with selective input stages.

8. Measurement of Limiting Characteristics of Receiver (CEPT)

This measurement is used to check the RF-limiting characteristics of the FM receiver. Adjust the normal test modulation ($f_{AF} = 1$ kHz with, for example, 2.4 kHz deviation). For AM, set the signal generator to 60% modulation; for SSB no modulation required. There will not be limiting, but the AGC should maintain a constant AF output voltage.

Tune the signal generator to the receiving frequency.

Adjust the RF level to 2 μ V EMF, measure the AF output level of the receiver and read the corresponding value in decibels, the RF level by 100 dB (referred to 1 μ V EMF). The AF level should not change by more than 3 dB. This is shown in Fig 5.

9. Measurement of Spurious Responses (FTZ)

For FM, unmodulated RF carriers, which are at more than $0.8 \times$ the channel spacing from the minimal frequency, should be attenuated by at least 70 dB referred to an unmodu-

lated RF carrier in the wanted channel. This is shown in Fig 6.

Measurement:

Adjust the test modulation and set Signal Generator to the receiving frequency.

Adjust the RF level of VFR1 to a value that the S/N ratio, for instance, is 20 dB

Switch off the modulation; read the AF level V_{AF1} .

Increase EMF to $V_{RF2} = V_{RF1} + 70$ dB; increase or reduce the frequency of the Signal Generator and read simultaneously the AF level V_{AF2} on the meter.

Requirement: $V_{AF2} > V_{AF1}$ for frequencies higher or lower than $0.8 \times$ the channel spacing.

Note: With other test methods, the modulation remains switched on.

10. Measurement of IF Rejection

Find the RF level at the receiver input, which gives a S/N of 20 dB. Switch off internal modulation. Measure AF output level. Tune the signal generator to the IF of the receiver (for example 10.7 MHz) and increase the RF level until the same AF output level is obtained. The difference between these two RF levels is the value for the IF rejection in dB. This is shown in Fig 7.

B. THE MOST IMPORTANT TWO-TONE MEASUREMENTS

Two-tone measurements are used to test the response of the receiver to interfering signals. For two-tone measurements according to CEPT, a very high spectral purity of the RF signal is required, especially for the interfering signal. For FM, these measurements are based on AF evaluation. For intermodulation tests, the AGC voltage should be used.

Measurement of Blocking and Adjacent-channel Selectivity

The S/N, referred to 1-Hz test bandwidth, has to be >140 dB at 20 kHz

from the carrier to permit measurement of an adjacent channel selectivity of >80 dB.

A S/N of more than 150 dB (at 1-Hz test bandwidth) is required at 1 MHz from the carrier for blocking measurements (>90 dB).

This means $L = -150$ dBc/Hz 1 MHz off the carrier. See Fig 8.

In the case of two-tone measurements, both signal sources have to be extremely stable.

Note: For all measurements complete matching is required, that is, the receiver and both RF sources should be terminated with 50 Ω . This is achieved by a T-section. See Fig 10.

When determining the EMF at the input of the receiver, the attenuation of the T-section must be taken into account! One can also use a low IMD hybrid coupler.

B1. Blocking Measurement (CEPT)

The blocking measurement is used to test the behavior of a receiver in the presence of strong interfering signals far off the receiver frequency (from 10 kHz to 1 MHz).

Tune the Signal Generator to the receiving frequency; adjust RF level to 2 μ V EMF using the normal test modulation. Adjust now the unmodulated interfering signal to 10 kHz-1 MHz above or below the receiver frequency.

Increase the interfering RF level until the sensitivity in the SINAD mode—with a CCITT filter—is reduced to 14 dB (or the AF level goes down by 3 dB).

$$\text{Result: } \frac{V_{RF \text{ unwanted}}}{1 \mu V}$$

should be >90 dB. This is shown in Fig 11.

B2. Measurement of Dynamic Adjacent Channel Selectivity (CEPT, FM-Test)

Similarly to the blocking measurement, now the behavior of the receiver

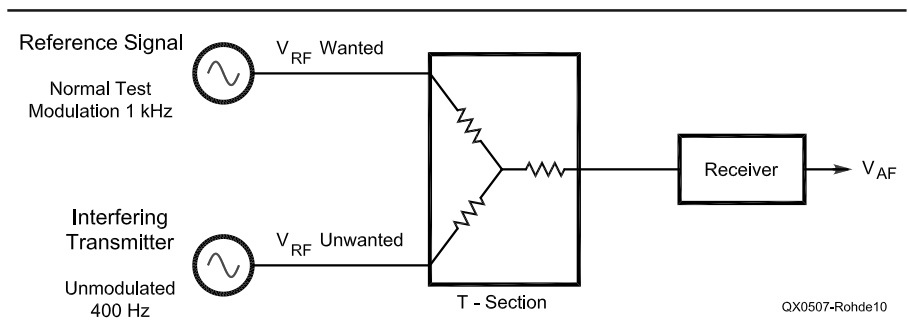


Fig 10—Set up for all two-tone measurements.

is tested in the presence of a strong interfering signal in the adjacent channel.

Find the receiver input voltage V_{RF1} for the 20-dB sensitivity (SINAD) using a CCITT filter.

Tune interfering signal to upper or lower adjacent channel, adjust interfering modulation ($f_{AF} = 400$ Hz, for example, 2.4 kHz deviation) and increase RF level V_{RF2} until the SINAD value of 20 dB is reduced to 14 dB.

Note: The ratio of the RF levels, $V_{RF2} : V_{RF1}$ should be >70 dB for a good receiver.

B3. Measurement of Interchannel Modulation (CEPT, FM Test)

This measurement is similar to the measurement of cross-modulation and useful for AM receivers. It permits checking whether two interfering signals present in the adjacent channels mix in the receiver input stage to simulate a "wanted" signal.

Find the receiver input level V_{RF1} for the 20-dB sensitivity (SINAD);

Then the reference signal (with normal test modulation) is tuned to the second channel above the receiver frequency, the interfering transmitter (unmodulated) to the first channel above the receiver channel.

The levels V_{RF2} of both signals should be equal at the receiver input: increase V_{RF2} until the SINAD value of 20 dB is measured again at the AF output of the receiver.

Note: The ratio of both voltages V_{RF2} :

V_{RF1} should be >70 dB for a good receiver. This measurement is repeated up to four and eight times the channel spacing, also for the channels below. This is shown in Fig 13.

Note: For this interchannel modulation measurement, it must be guaranteed that the spurious products which might be generated in the output stages of the two signal generators do not occur in the measurement. This is ensured by suitable attenuators of about 30 to 40 dB which are inserted between the transmitter output stage and the T-section. This, however, requires an output voltage, which is high enough, like +10 dBm.

B4. Measure of Spurious Response Rejection

The spurious response rejection indicates how much the reception of a desired signal is influenced by an interfering signal with a level 70 dB higher than the wanted signal (measurement in accordance with CEPT).

Tune the signal Generator to the receiving frequency; adjust the normal test modulation and RF-output voltage V_{RF1} for 20-dB SINAD sensitivity. Apply the interfering signal with modulation (400 Hz; 60% of maximum deviation). The level of the interfering signal V_{RF2} should be 70 dB above the wanted signal level. The frequency of the interfering signal is continuously varied; at the same time, the SINAD value, which should not be lower than 14dB, is measured. If the SINAD value

goes down below 14 dB, a spurious response of the receiver is indicated. This is shown in Fig 13.

B5. Two-tone Intermodulation

For AM and CW/SSB receivers, an important quantity is the two-tone dynamic range. While the dynamic range of a system is:

$$DR = \frac{2[IP_3 - MDS]}{3}$$

this formula can be solved for the measurement of the intercept point.

$$IP_n = \frac{n \cdot P_{ref} - P_{IMD}}{(n-1)}$$

$$IP_3 = \frac{3 \cdot P_{ref} - P_{IMD}}{2}$$

For example: When the Input = 2×-10 dBm, IMD products are -90 dBm.

$$IP_3 = \frac{3 \cdot (-10) - (-90)}{2} = \frac{-30 + 90}{2} = 30 \text{ dBm}$$

For example, Fig 15 shows the measured response of a doubly balanced mixer.

Fig 15 shows the measured two-tone response of a doubly balanced mixer. The input signals are 0 dBm, the insertion loss is 8 dB and the IMD products are -74 dBm.

From Fig 15 we can see that the

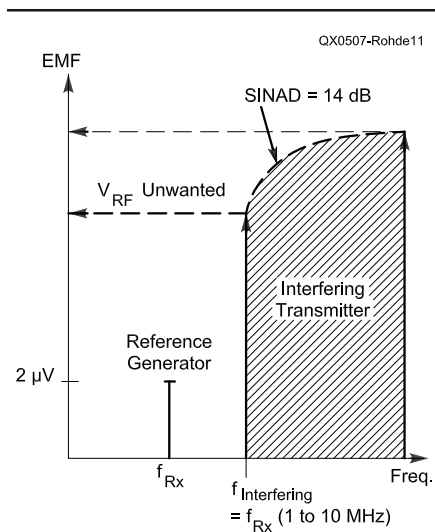


Fig 11—Two-tone blocking measurement with an interfering transmitter (signal generator) and a reference generator.

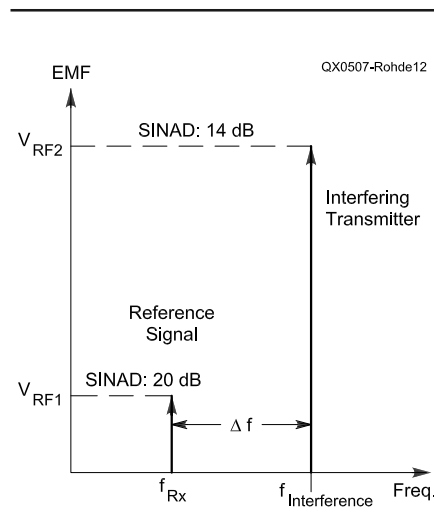


Fig 12—Two-tone measurements for dynamic adjacent-signal selectivity. The difference between V_{RF2} and V_{RF1} should be more than 90 dB.

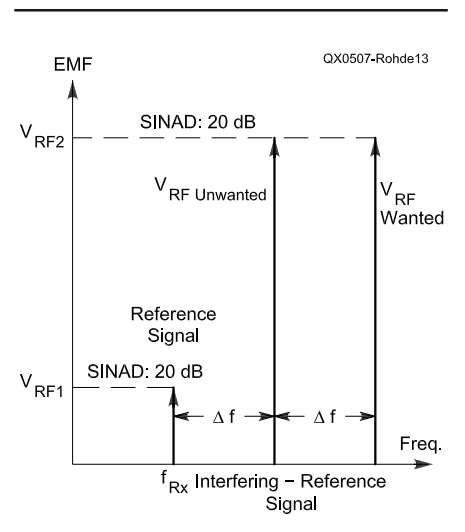


Fig 13—Measurement of spurious response rejection. There are two signals: a wanted signal and an interfering signal. Both at the level V_{RF2} resulting in an intermodulation product V_{RF1} .

input intercept point ($IP_{3(IN)}$) can be calculated as follows:

$$IP_{3(IN)} = \frac{3 \times [0 - (-74)]}{2} = 37 \text{ dBm}$$

Similarly, the output intercept point is calculated to be:

$$IP_{3(Out)} = \frac{3 \times (-8) - (-74)}{2} = 25 \text{ dBm}$$

If the assumed mixer is now active instead of passive (+8 dB loss) with 8 dB gain, and the IMD products are at -60 dBm, we now calculate:

$$IP_{3(In)} = \frac{3 \times 0 - (-60)}{2} = 30 \text{ dBm}$$

and

$$\frac{3 \times 8 - (-60)}{2} = \frac{24 + 60}{2} = 42 \text{ dBm}$$

Now the $IP_{3(Out)} > IP_{3(In)}$

As can be seen, this measurement is done with two generators. They can be set at two close frequencies such as 14.250 MHz and 14.300 MHz. The IMD products are then 14.200 MHz and 14.350 MHz. For the level of -10 dBm from the signal generator, they must be at -90 dBm down for $IP_3 = 30$ dBm. A set of generators is required that can deliver +20 dBm or more output and the level after the hybrid coupler must be set at -10 dBm for each tone. Since the generator can deliver +20 dBm and only 13 dBm is required (3 dB losses as-

sumed in the hybrid coupler) the built-in attenuator sits at 27 dB attenuation. Since both signal generators now have 27 dB attenuation, the attenuator between the two is 54 dB. If the generator can not supply that much of the power, use 1 watt class A amplifiers. Make absolutely sure that there is *no* crosstalk between the generators and no distortion produced by the 3 dB hybrid coupler.

Since this is a two-tone measurement based on RF levels, the device under test requires an AGC meter or an AGC/DC output. This is valid for all amplitude modulation based receivers which includes AM, SSB and CW. The absolute level of the IMD products are then -100 dBm (-10 -90 = -100). This can be calibrated with a single tone measurement measuring the reference signal of -100 dBm.

Many measurements are done at the MDS (Minimum Detectible Signal) level and use a 3 dB noise change above MDS. Unfortunately, this gives no insight in the nonlinear characteristic of the receiver. For multi-stage systems such as a receiver, the 3 dB/dB rule for IMD products is *not* valid. It is better to describe the levels of the input and the IMD products rather than call this an intercept point. To complicate matters, the distortion products vary as a function of the offset between the two carriers for narrow band applications such as CW

and SSB. The offset should be about three to four times the bandwidth. As an example at 2.4 kHz bandwidth, a frequency separation of 7 to 10 kHz is recommended. For FM applications, the Δ should be 2 channels apart. The FM measurement for different channels was shown above. Unfortunately, most medium performance receivers have a roofing filter of 15 kHz or wider bandwidth. Therefore, this test evaluates the second mixer. The standard test which is frequently found used 30 to 50 kHz spacing between the generators and gives no real insight into the receiver two-tone performance. In reality, these measurements should be performed from 2 kHz offset (CW) to 50 kHz (FM). This results in a set of curves for intermodulation distortion products (IMD).

The second order IMD products which are the sum and difference of two signals must also be measured. They should have values definitely above 70 dB, better 90 to 100 dBm as second-order intercept point should be reached.

Example: Set one signal generator at 6 MHz and one at 8.2 MHz. The resulting spurious signal will occur at 14.2 MHz. The measurement process is the same as evaluating the third-order products which follow the formula

$$2 \times F_1 + -F_2$$

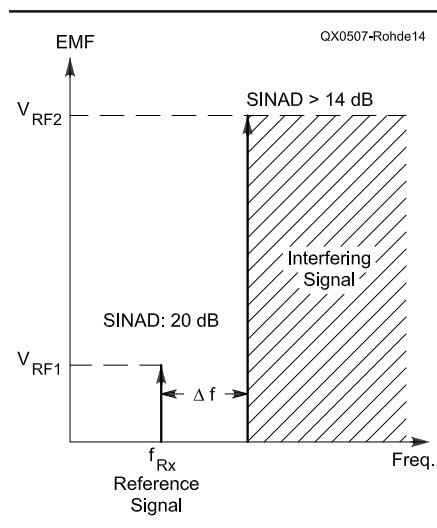


Fig 14—Measurement of spurious response rejection. This again is a two-tone test, where one signal generator is V_{RF1} and the transferring signal is V_{RF2} . The interfering frequency this time is varied and the SINAD value shall not change more than 6 dB (from 20 dB to 14 dB).

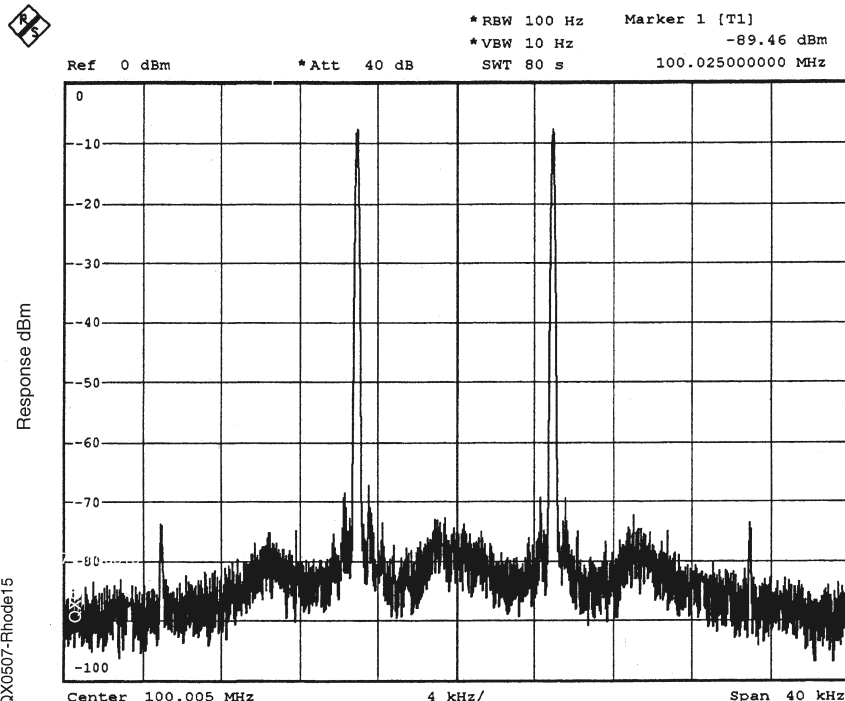


Fig 15—Measured two-tone response of a doubly balanced mixer.

C. Noise Figure

Rather than show the sensitivity of a system such as a receiver in terms of signal to noise ratio, the Noise Factor or the Noise Figure = $10 \times \log(F)$ can be used. This number which is the ratio between two powers is absolute and does not depend on the bandwidth of the system or receiver. The definition of the noise factor is

$$F = \frac{\text{available } S/N \text{ at input}}{\text{available } S/N \text{ at output}}$$

The noise at the output of a linear system then is kTB_n .

With $k = 1.38 \times 10^{-23} \text{ J/K}$

T = Operating temperature in Kelvins, 290 at room temperature.

B = Effective noise bandwidth in Hz.

This equation can be redone to be

$$V_n = \sqrt{4kTRB_n}$$

With V_n = RMS open noise voltage, and R = resistance of the conductor used. In terms of the S/N the complete formula is:

$$V_n = \sqrt{4kTRB_n F}$$

For $S/N = 1$, $F = 1$

Once the S/N is known, we can solve the equation for F .

Example: We measured the S/N ratio of an SSB receiver to be 10 dB (3.16 for $0.3 \mu\text{V}$ ($0.6 \mu\text{V}$ EMF)). Then the noise floor is about $0.1 \mu\text{V}$ for 0 dB S/N.

This means

$$0.1 \mu\text{V} =$$

$$\sqrt{2kT50 \times 2.4 \text{ kHz} \times F \text{ (terminated)}}$$

$$(0.1 \mu\text{V})^2 = 2kT50 \times 2.4 \text{ E}3 \times F$$

$$F = \frac{(0.1 \mu\text{V})^2}{\frac{2 \times 290 \times 50 \times 2.4 \text{ E}3 \times 1.38 \text{ E} - 23}{9.6 \text{ E} - 16}} =$$

$$\text{For } 3 \text{ dB } S/N = \frac{14.1}{9.6} = 14.7;$$

$$NF = 11.67 \text{ dB}$$

A noise figure meter would show this for a 3-dB increase in power which is required for the noise figure measurement. Remember, noise figure is expressed in dB and derived from the noise factor.

Total Dynamic Range

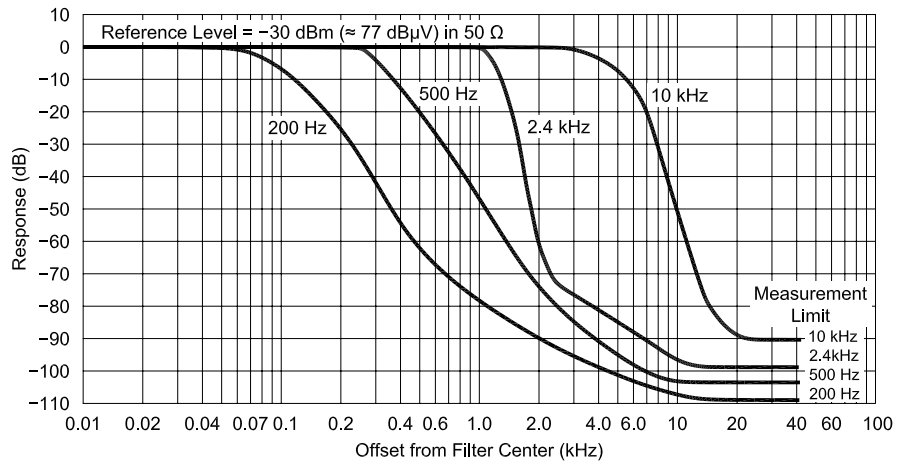
There are some issues about the

dynamic range which are difficult to measure, but need to be mentioned here. When talking about the skirt of a filter, we are referring to the 3 dB bandwidth, the 6 dB bandwidth, the 60 dB bandwidth and the ultimate rejection. The ultimate rejection depends on the cross talk off the filter when inserted on the board, for digital filters it depends on the filter implementation. Because of the noise of the oscillator, the "dynamic" bandwidth differs from the static bandwidth. To explain this better, here are two examples:

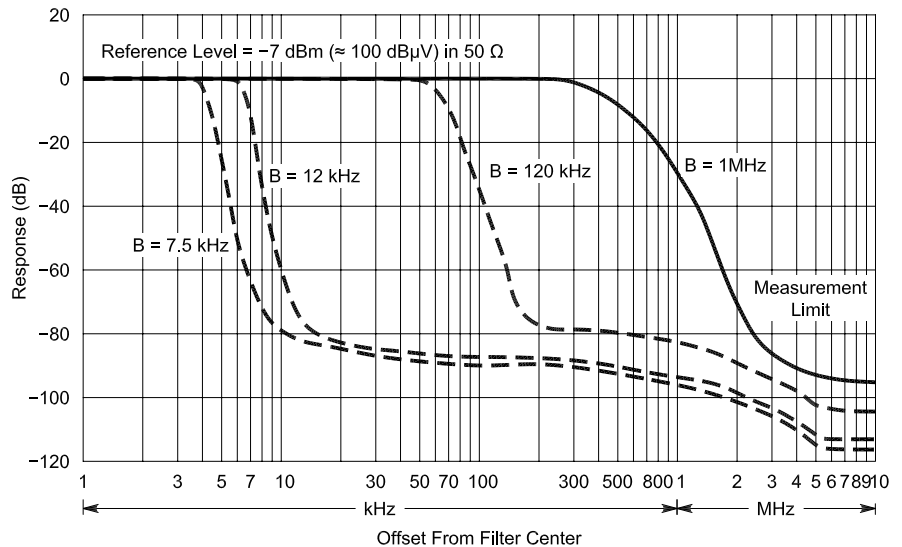
Fig 16 A and B show the measured dynamic selectivity as a function of the IF bandwidth for two commercial receivers. The R & S receiver ESH-2 has

a very low phase noise oscillator with about a -145 dBc/Hz phase noise at 10 kHz offset from the carrier. The crystal filters shown have different shape factors and Fig 16 A and B show the bleeding due to the noise.

There is a relationship between the phase noise (dBc/Hz) and the nonharmonic spurious (dBc). This is a frequently overlooked fact. I always wonder why people today only look into the mixer performance and forget the phase noise contribution. It seems to be a goal to have a 90 dB dynamic range for a receiver. According to Fig 17, one needs to have a phase noise of at least -142 dBc/Hz and a freedom of non-harmonic spurious of at least -107 dBc . These items



(A)



(B)

Fig 16—Dynamic selectivity versus IF bandwidth: At A, the Rohde & Schwarz ESH-2 test receiver (9 kHz to 30 MHz). At B, the Rohde and Schwarz ESV test receiver (10 MHz to 1 GHz). Reciprocal mixing widens the ESH-2's 2.4 kHz response below -70 dB (-00 dBm) at (A), and the ESV's 7.5, 12 and 120 kHz responses below approximately -80 dB (-87 dBm) at (B).

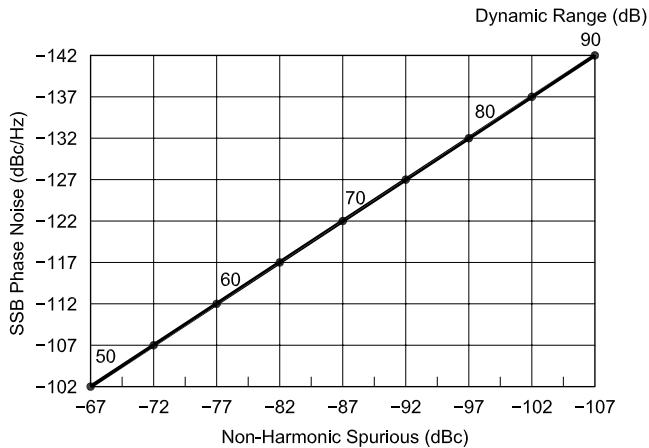


Fig 17—This graph shows the available dynamic range, which is determined either by the masking of the unwanted signal by phase noise or by discrete spuri. As far as the culprit synthesizer is concerned, it can be either the local oscillator or the effect of a strong adjacent-channel signal that takes over the function of the local oscillator.

6 dB Reserve for errors less than 1 dB
 Carrier-to-spurious ratio for 14 dB SINAD = 11 dB
 Carrier-to-noise for 14 dB SINAD = 46 dB

QX0507-Rohde17

are covered by measurements in the various topics above but have not been shown together in this form.

More information about these various topics are found in the references.

References:

1. "Modern Receiver Design Including Digital Signal Processing," *Communications Quarterly*, Winter 1997.
2. "Theory of Intermodulation and Reciprocal Mixing: Practice, Definitions and Measurements in Devices and Systems, Part 1," *QEX*, Nov/Dec 2002; Part 2, *QEX*, Jan/Feb 2003.
3. U. L. Rohde and J. Whitaker, *Communications Receivers: DSP, Software Radios, and Design* Third Edition, ISBN 0-07-136121-9 McGraw-Hill, 2001.
4. U. L. Rohde, N1UL, and D. P. Newkirk, W9VES, *RF/Microwave Circuit Design for Wireless Applications*; ISBN 0-471-29818-2 John Wiley & Sons, Inc, 2000.

Dr. Ulrich L. Rohde studied electrical engineering and radio communications at the universities of Munich and Darmstadt, Germany. He holds a PhD in Electrical Engineering (1978) and a ScD (with honors, 1979) in Radio Communications, a Dr-Ing (2004), and several honorary doctorates.

He is president of Communications Consulting Corp, Chairman of Synergy Microwave Corp and a partner of Rohde & Schwarz, Munich, Germany. Previously, he was the President of Compact Software, Inc and Business Area Director for Radio Systems of RCA, Government Systems Division. He is a Professor of microwave circuit design and has held Visiting Professorships at several universities in the United States and Europe.

Dr Rohde holds several patents and has published more than 60 scientific

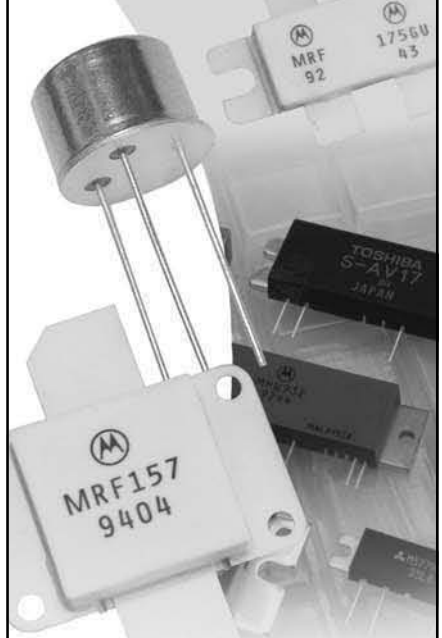
papers in professional journals. He contributed a chapter entitled "Oscillators and Frequency Synthesizers" to the Handbook of Microwave and Optical Components, second edition, contributed a chapter entitled "Frequency Synthesizers" to the Wiley Encyclopedia of Telecommunications and has written six books: Communications Receivers, (third edition); RF/Microwave Circuit Design for Wireless Applications; Microwave and Wireless Synthesizers: Theory and Design; Microwave Circuit Design Using Linear and Nonlinear Techniques (with co-authors George Vendelin and Anthony M. Pavio) Second Edition 2005; The Design of Modern Microwave Oscillators for Wireless Applications Theory and Optimization (with co-authors Ajay K. Poddar and Georg Boeck) May 2005; Communications Receivers: Principles and Design; and Digital PLL Frequency Synthesizers: Theory and Design.

Dr Rohde is a member of the following: Fellow member of the IEEE; an Invited Panel Member of the FCC spectrum Policy Task Force on Issues Related to the Commission's Spectrum Policies; ETA KAPPA NU Honor Society; Executive Association of the Graduate School of Business at Columbia University, New York; the Armed Forces Communications and Electronics Association; Fellow of the Radio Club of America and former Chairman of the Electrical and Computer Engineering Advisory Board at New Jersey Institute of Technology. He holds German call sign DJ2LR (since 1956), Swiss call sign HB9AWE, Falkland Islands VP8CRL and US N1UL. □□

From
MILLIWATTS
 to **KILOWATTS**sm

More Watts per Dollarsm

- Transistors
- Power Modules
- Semiconductors



ORDERS ONLY:
800-RF-PARTS • 800-737-2787

Se Habla Español • We Export

TECH HELP | ORDER | INFO: 760-744-0700

FAX: 760-744-1943 or 888-744-1943



An Address to Remember:
www.rfparts.com

E-mail:
 rfp@rfparts.com



The Quest for the Elusive TBWB4EQ (The Triband Wideband 4-Element Quad)

L.B. gives us the straight story on wideband quads!

By L. B. Cebik, W4RNL

Triband quads for 20, 15 and 10 meters have a long history—about as long as hams have used quads. A number of longer multiband quads have periodically appeared in the literature. In these notes, I shall be very interested in 4-element quads of planar design, that is, with the elements for each band on a vertically oriented support frame. These designs use the same spacing between elements for all bands.

In the course of our exploration, I shall examine beams in the 30- to 35-foot boom range. Our first stop will

be to examine a long-standing *ARRL Antenna Book* design to understand its limitations, especially its narrow operating bandwidth on at least one of the 3 bands that it covers. The results of this small study will form the basis for seeking out a design with a broader operating bandwidth on all bands. The first stop will be the 1983 design from W6PU, a design that has held persistent interest for two decades. The designer used the central pair of elements to form phase-fed dual drivers. My interest in this design covers two long-standing expectations of phase-fed dual driver quads: their gain and their operating bandwidth.

Next, I shall turn to designing a modified W6PU-quad that virtually anyone can replicate in model form. The goal will be to obtain full-band

coverage of 20, 15, and 10 meters, with adequate gain and front-to-back performance. I shall use a few techniques not easily available to the design originator in order to simplify the array and to overcome some of the problems with the original version. Finally, I shall set up a reasonably fair set of comparative beam designs to evaluate whether anyone should go to the effort of actually building a multiband wideband 4-element quad beam.

A Standard Triband 4-Element Quad Design

Many quad builders prefer to bypass the 3-element beam on their way up the ladder of performance. Odd numbers of elements tend to place the driver very close to the support mast and tower, resulting in

1434 High Mesa Dr
Knoxville, TN 38938
cebik@cebik.com

a conflict between electrical and mechanical requirements. An even number of elements places the most equally distant between the center two elements, freeing the builder from at least one potential interaction problem.

Traditionally, quad designers have used a somewhat arbitrary spacing of the elements. 4-element quads for multiband service often use equal spacing between all elements, with 8 feet and 10 feet being the most common values. A few designs have used a combination of these values, so that we can find 4-element triband designs with boom-lengths ranging from 24 feet to about 30 feet or so. The premise behind the spacing selection stems from the use of planar element assemblies. In terms of wavelengths, a fixed spacing between elements results in a different spacing for each band. For example, fixed 10 foot spacing between elements is about 0.14λ on 20, 0.21λ on 15, and 0.28λ on 10 meters.

The design of the quad then rests upon finding the element circumferences that will produce an acceptable combination of gain, front-to-back ratio, and feed-point impedance, all with satisfactory operating bandwidths. Prior to the 1990s, the design effort was largely empirical, a term meaning trial and error. Indeed, most existing quad designs in amateur literature have their roots in the pre-computer-modeling period of antenna design.

One very interesting design appears in *The ARRL Antenna Book* for editions prior to the 19th. It appears in the table on page 12-2 of the 18th

edition. The beam consists of 4 elements, each spaced 10 feet from the adjacent element. Hence, we have a total boom length of 30 feet, plus whatever end lengths are necessary to handle the support-arm structures. Fig 1 supplies a basic outline of the quad's electrical structure. Throughout, the design of this quad, and the others that we shall examine, presumes separate feed lines for each band, with closed driver loops for each inactive band.

Table 1 shows the element dimensions for the quad design. The antenna uses a direct feed-line connection on 20 and 15 meters. However, 10 meters requires a quarter-wavelength $75\text{-}\Omega$ matching section to transform its higher feed-point impedance (above $100\ \Omega$) down to the feed line's $50\text{-}\Omega$ characteristic impedance. The fixed element spacing creates a rising driver impedance as we move upwards through the HF bands. Although carefully choosing the element lengths can

alter the impedance to some extent, there are severe limits to the range of adjustment. Trying to lower the 10-meter impedance for a direct $50\text{-}\Omega$ feed tends to degrade the other performance parameters on that band.

In trying to model this antenna in NEC-4 using #12 AWG copper wire, I had to alter the published length of the 20-meter and the 10-meter drivers—both upward—in order to place the $50\text{-}\Omega$ SWR curves within the band limits. 15 meters required no adjustment in the model. In part, this situation results from the fact that the 15-meter dimensions result from interaction between the elements for that band and the elements for both of the other bands. The 10-meter and 20-meter elements interact mainly with only one other band. Key variables for those bands also include methods of assembly. Attaching elements to the support arms is subject to a number of variations, some of which result in the creation of small

Table 1
Dimensions of The ARRL Antenna Book 4-element, 30 foot-boom, triband quad.

Element	Space from Reflector in feet	Circumference in feet		
		20 Meters	15 Meters	10 Meters
Reflector		72.42	48.67	35.70
Driver	10.0	70.42 (70.80*)	47.33	34.70 (35.20*)
Dir. 1	20.0	69.08	46.33	33.60
Dir. 2	30.0	69.08	46.33	33.60

*Dimensions in parentheses indicate modeling changes of the driver circumference to set the $50\text{-}\Omega$ SWR curve within the band limits. 20 and 15 meters use direct $50\text{-}\Omega$ coax connections; 10 meters uses a $1/4\lambda$ $75\text{-}\Omega$ matching section to the $50\text{-}\Omega$ feedline.

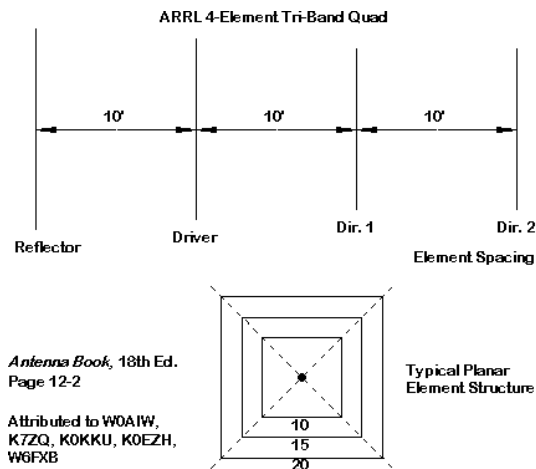


Fig 1

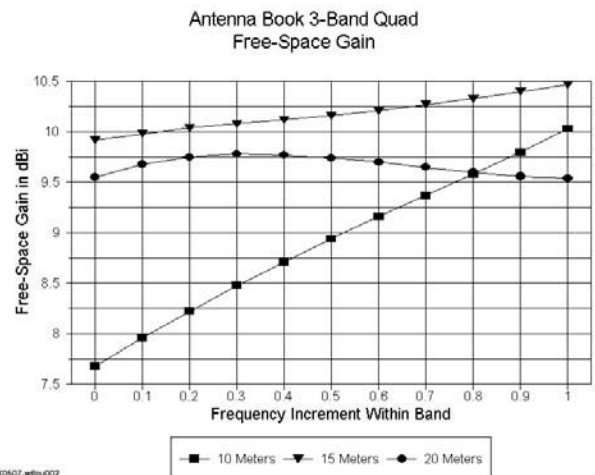


Fig 2

1-turn inductive loops at each corner. Together, they can have an effect upon the electrical length of a loop, with the most pronounced effect on the driver, where the relative current magnitude is highest. The fact that I had to increase both driver lengths—which make clean corners in the model—by similar amounts suggests that the empirically derived design may take such mounting loops into account.

I modeled this traditional design in free-space as simply a guide to its anticipated performance level. All other beam designs that we shall consider also use free-space models, thus allowing a direct comparison of performance among them. Fig 2 shows the modeled forward gain performance of the array. This and other performance graphs subdivide each amateur band into 10 parts to permit combined presentations. 10 meters covers the 28- to 29-MHz portion of the band.

To make sense of the graph, we should note a few benchmarks that emerge from monoband beams. A short-boom 3-element Yagi (about 16 feet on 20 meters) achieves a free-space gain of over 7 dBi, while a long boom version of the array (about 24 feet on 20 meters) is capable of just over 8 dBi. These values are approximate, since 3-element Yagis show a rising gain value across the operating bandwidth. An optimized 2-element monoband quad achieves 7 dBi or so. We may optimize 3-element models for the widest operating bandwidth and obtain just over 8.5 dBi or for maximum gain and reach about 9.1-dBi free-space gain.

An optimized 4-element monoband quad that uses #12 copper wire—like the other quads cited—is capable of just about 10 dBi maximum.¹

Since the boom length of the triband quad is considerably shorter than its monoband 4-element counterpart, we should not expect 4-element performance in the optimized monoband sense of the term. And we do not get it. However, we do obtain very respectable 20-meter performance in the 9.5-dBi range across the band. Helped by interactions with the surrounding elements for other bands and a longer boom as a percentage of a wavelength, the 15-meter gain performance does achieve the 10-dBi level. The 10-meter boom length is too long and thus shows a rising curve with a minimum value below 8 dBi. All in all, the quad design achieves quite good gain performance as a triband effort on a 30 foot boom.

Optimizing a monoband quad tends to bring the maximum 180° front-to-back ratio in close frequency-proximity to a desired gain level and the resonant feed-point impedance of the array. Hence, these values are usually in excess of 20 dB and sometimes as high as 40 dB, although such a high peak front-to-back value is a narrow-band phenomenon. Most optimized monoband designs strive for relatively equal band-edge values, and the exact band-edge front-to-back ratio will depend on the element diameter and the bandwidth of the passband as a function of its center frequency. A triband quad does not

have the luxury of such techniques, as Fig 3 will reveal.

Both 20 and 15 meters show very respectable front-to-back curves, with minimum values between 10 and 12 dB, both at the low end of the bands. 10 meters shows the most problematical curve, with extremely low values in the CW portion of the band, but much improved values higher up. The coincidence of the rising gain and front-to-back curves suggests that one might go some distance in further optimizing performance for 10 meters within the first MHz of the band. However, every change in the 10-meter loop dimensions will force a change in the adjacent 15-meter element, with consequences for the outer 20-meter element. Hence, optimizing the present 10-meter portion of the design—with the potential pitfalls of ruining the 15- or 20-meter performance—is a significant task. It falls outside our use of the design as a representative existing design for comparative purposes.

The 50-Ω SWR curves appear in Fig 4. Both 10 and 15 meters achieve less than 2:1 SWR across the bands. However, remember that the 10-meter driver includes a quarter-wavelength matching section that the model includes. Only the 20-meter SWR curve falls short of the mark, largely due to the fact that both the feed point resistance and reactance show large excursions. The resistance changes by 44 Ω across the band, while the reactance changes by 81 Ω. For comparison, the feed point resistance on 15 meters changes by just 6 Ω, while the reac-

¹Notes appear on page 27.

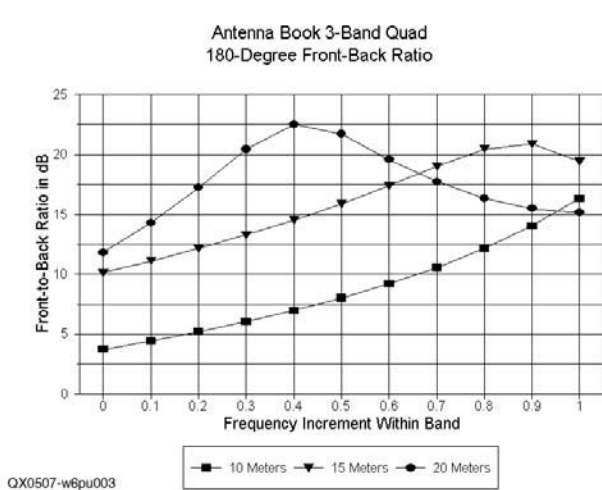


Fig 3

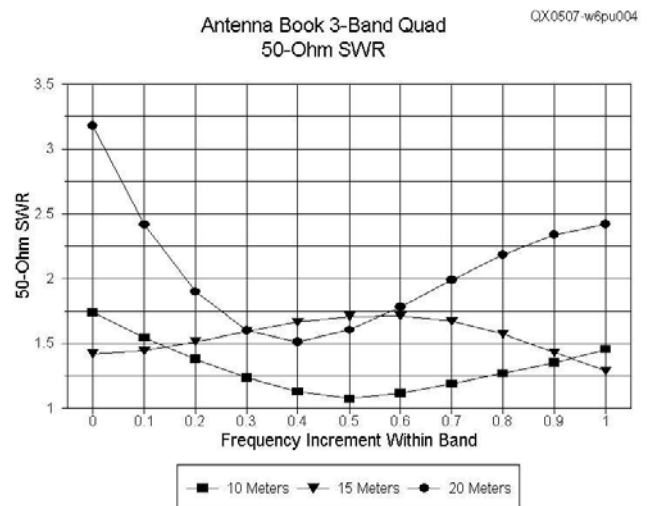


Fig 4

tance changes by 20 Ω. The 20-meter curve is a function of the fact that the loops for that band have no further lower-band loops with which to interact. Hence, they tend to show more normal monoband properties for the boom length and the element spacing than do the higher-band elements. Despite slight interactions with the 15-meter elements, the 20-meter elements display the narrow SWR bandwidth typical of monoband 20-meter quads on the same boom. The original tables for the ARRL quad design show separate dimensions for the CW and the SSB portions of the band.

Multiband quads have a few other idiosyncrasies that do not show up readily in tables. Pattern shape is one of them, and Fig 5 displays some of them. However, the ARRL quad design is remarkably free of extreme pattern distortion, and so the figures only modestly represent what we often see in more extreme forms. The pattern to the left shows a typical multiband quad fantail. The rear lobes on multiband quads often show considerable strength in rear quartering directions, resulting in worst-case front-to-back ratios that are considerably lower than the 180° front-to-back ratio. Inadequately designed LPDAs with too few elements for the frequency span covered tend to show a similar problem. It is likely that the fantail effect is a product of interactions with supposedly inert elements for other bands. Some have attributed the spread to the fact that there is a small vertically polarized component to the pattern, but this component does not result in forward beam-

widths significantly wider than those we achieve from Yagis of similar gain potential. With respect to the relatively modest fantail shown in Fig 5, the only function of the vertical radiation component is to reduce the deep side nulls that we might find for a Yagi.

The other pattern anomaly that accompanies multiband design is the appearance of extra lobes, as shown by the 15-meter pattern in Fig 5. In monoband designs, it is possible to suppress secondary or forward side lobes through at least 6-element arrays. However, multiband quads tend to show some extraneous lobes, even with only 3-4 elements per band. The most likely source of them is from the inactive elements for the other bands. As we increase loop size above about 1.5 λ or decrease it below about 0.75 λ, the radiation tends to move from the desired broadside orientation toward the loop edges. Even low-level, induced activity in

the supposedly inert loops can yield small lobes, such as the pair of side lobes shown in Fig 5.

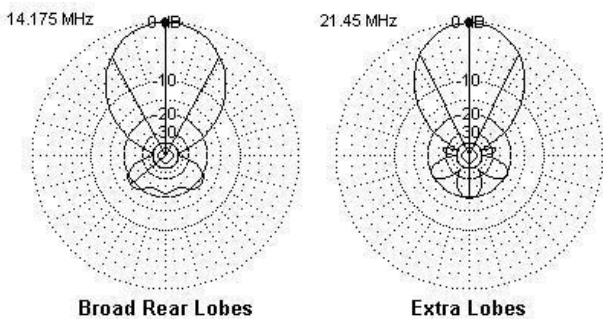
Nonetheless, the patterns of the ARRL quad show the anomalies only in small and relatively harmless ways. Moreover, the array shows very adequate levels of gain and front-to-back ratio. The 10-meter performance might withstand further optimizing, assuming one could achieve this goal without unduly disrupting the performance on 20 and 15 meters. Still, the task is one internal to the basic 4-element design itself.

We came to the ARRL 4-element, triband quad with the idea of using it as a comparator for reportedly improved designs. However, there are perhaps only two reasons for changing the basic design of the quad. One is to improve the operating bandwidth across 20 meters. The other is to see if we cannot achieve higher levels of gain and front-to-back ratio from a similar boom length. The next step in

Table 2
Dimensions of the W6PU dual-driver, 4-element, 33.5 foot-boom, triband quad.

Element	Space from Reflector in feet	Circumference in feet		
		20 Meters	15 Meters	10 Meters
Reflector		75.42*	50.30*	37.24*
Driver 1	13.0	71.75	47.83	35.92
Driver 2	21.5	68.17	45.42	34.08
Dir. 1	33.5	68.67	45.83	34.42

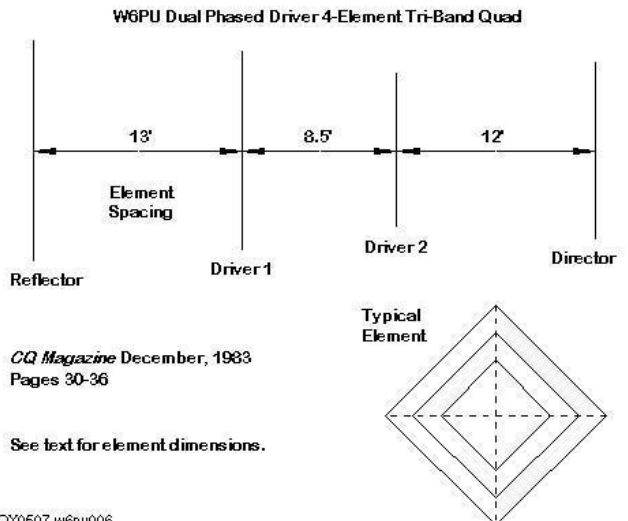
*From R. Martinez, W6PU, "The Evolution of the Four-Element Double-Driven Quad Antenna," *CQ*, Dec, 1983, pp. 30-36. Original specifications call for reflectors using the same circumference as the first driver, but with shorted transmission-line stubs and trimmer capacitors. The NEC-4 models use electrically equivalent full-size reflector loops, with the circumferences listed in the table.



Some Typical Multi-Band Quad Pattern Characteristics

CX0507-w6pu005

Fig 5



CX0507-w6pu006

Fig 6

our exploration is to review an old design that seems to promise both.

The Original W6PU Dual Driver 4-Element Triband Quad

In the December, 1983, issue of *CQ*, Robert Martinez, W6PU, presented "The Evolution of the Four-Element Double-Driven Quad Antenna" (pp. 30-36). The article is absolutely typical of the period relative to antenna design. Without the benefit of well-calibrated computer calculation of antenna performance potentials, the era was filled with countless writers who handled decibels without due care.² Perhaps the most important of the W6PU claims are an improvement of 5.5 to 6.0 dB in forward gain and a 30-dB front-to-back ratio. Since the author refers to 2-element and 4-element quads for 40 through 10 meters, it is unclear over what the new antenna showed the higher gain. However, we can model the W6PU 4-element, triband, dual-driver quad and see what we get. Since we have just reviewed a comparable model of a reasonably competent 4-element single-driver quad, we shall be able to tell if the builder effected any improvements by using dual drivers.

Fig 6 shows the general outlines of the W6PU quad. The total boom length is 33.5 feet (plus the usual end additions for hardware). Table 2 supplies the element loop circumferences used to construct the test model from the article description. The original reflector loop specifications called for

loops identical in circumference to the ones used for driver one. However, each reflector had a specified shorted transmission line stub with a trimmer capacitor across the short to tune the stub. See Table 3 for the values involved and Fig 7 for the layout given in the article. Unfortunately, the text gives the builder the alternative of using 300- Ω line or home-crafted lines spaced 1.5 inches apart. A stub made from #12 AWG copper wire and spaced 1.5 inches will have a characteristic impedance of about 435 Ω . Hence, for modeling purposes, it became impossible to know what sort of stub lengths and trimmer settings might have been used. The simpler method of proceeding was to use full size reflectors that are electrically equivalent to the stubbed and trimmed elements used in the original model. The values shown in Table 2 resulted in the best gain and front-to-back performance across the band—without altering the other element sizes.

Note that the driver closest to the

reflector is designated as driver one, while the one closer to the director is called driver two. This orientation is necessary to fully appreciate the sketch in Fig 8. The right-hand side shows the phase-line arrangement between drivers for the 20-meter band, which uses a single line—and the 10- and 15-meter bands, which use a split-line phasing system. The feed point, contrary to most phase-line systems used in horizontal arrays, is at or closer to the rear driver (driver 1). Table 4 provides data on the specified line lengths. The original article carefully notes the use of 50- Ω (RG-8A/U) line with a velocity factor of 0.66. The electrical lengths used in the model of the antenna are the equivalent lengths for a velocity factor of 1.0.

Modeling a multiband quad in *NEC* requires attention to a number of factors. First, the antenna wires require a bit more than minimal segmentation at the highest frequency. The model uses 7 segments per side or 28 segments per loop at 10 meters.

Table 3
Dimensions of the reflector stubs of the original W6PU quad.

Band	Stub Z (Ω)	Stub Length (feet)	Trimmer Capacitor (pF)
20	300	4.50	150
15	300	3.50	100
10	300	2.25	75

Note—article specifies 300- Ω or 1.5-inch wide stub line. Reflector circumference for each band is identical to the listed value for the first driver circumference in Table 2.

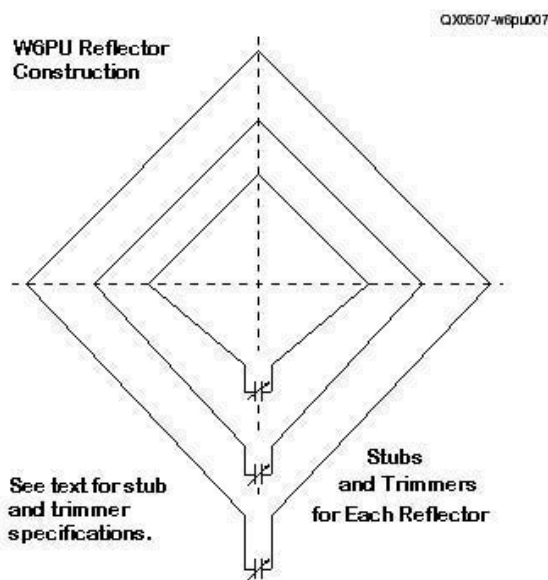


Fig 7

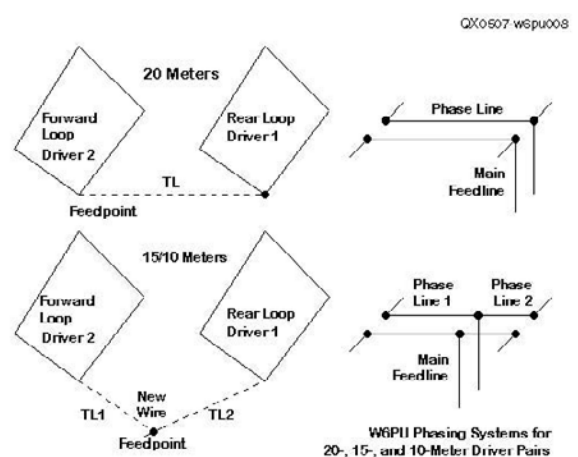


Fig 8

Since the segment length should be relatively constant throughout the assembly, the 15-meter elements used 11 segments per side and the 20-meter elements used 15 segments per side. Second, the split phase lines require a junction segment to use for the antenna feed point. The technique appears in the left-hand side of Fig 8. All wires are #12 AWG copper.

The structure is a diamond. Setting coordinates around the system involves calculating the support-arm length for each circumference loop. For square loops, the corner coordinates are each simply the circumference divided by 8, so that each side is $\frac{1}{4}$ of the circumference. For diamond loops, the arm length is the circumference divided by 4 square roots of 2 or 5.6569. To avoid having to make multiple adjustments to change any loop size, I used software (in this case, *NEC-Win Plus*) with variables. Fig 9 shows part of the set-up of the page on which I assigned variables. Fig 10 presents a portion of the page on which I set up the wires by using variables instead of constants. An alternative view of the same program page would show the numbers created by the assignment of variables. Changing a loop size thus requires only one revised entry in the model. Since *NEC-Win Plus* uses *NEC-2*, I cross-checked the results of each run using *NEC-4* software. The results are the same.

Running the model on each of the bands produced the free-space E-plane patterns shown in Fig 11. Each pattern represents my judgment of the best pattern on the band, with a record of the frequency at which it occurred. Besides the anticipated fantailed rear lobes on the upper two bands, they are all well behaved. The question is whether we achieved anything with these well-shaped patterns.

Fig 12 graphs the free space gain of the array across each of the bands, using the same graphing scale that we applied to the single-driver ARRL quad beam. The 10-meter gain curve is very similar to the one obtained from the ARRL quad. The 15-meter curve is similar in its evenness, but at a level that is below that we obtained from the single-driver beam. The 20-meter curve peaks at mid-band. It descends very slowly above the peak frequency, but drops precipitously at the low end of the band.

We can see the results for the 180° front-to-back values in Fig 13. The values are not significantly different overall from those obtained from the

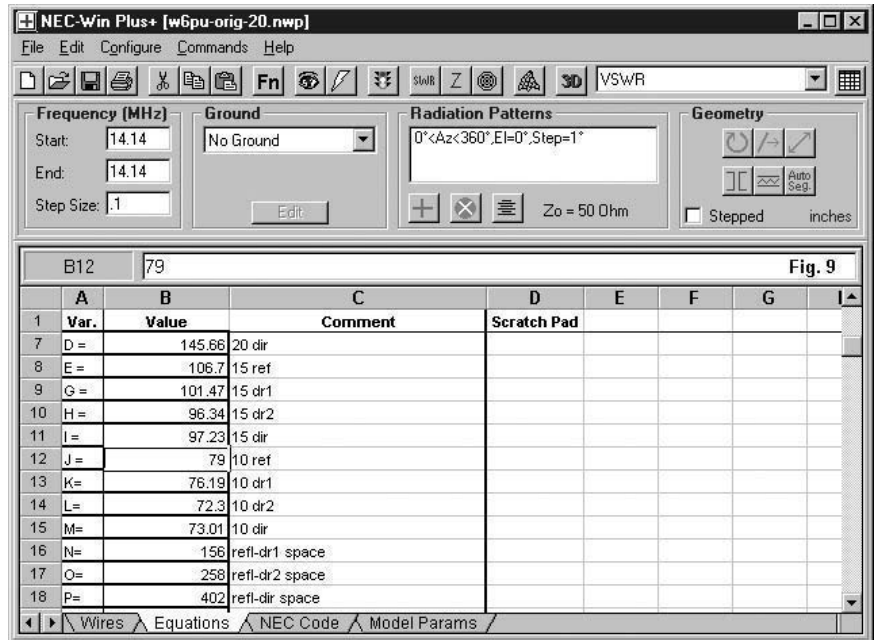


Fig 9—*NEC-Win Plus* screen for assignment of variables.

QX0507-w6pu009

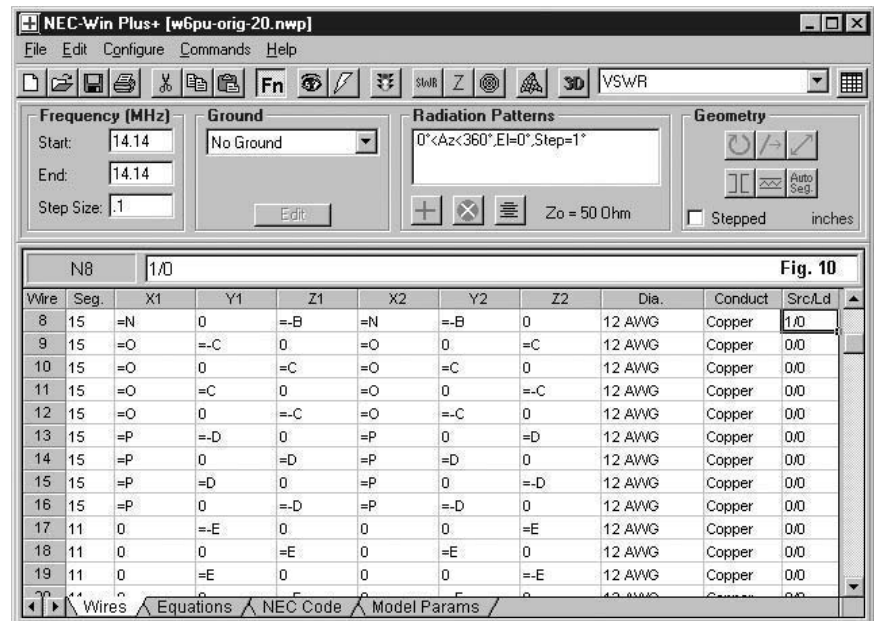
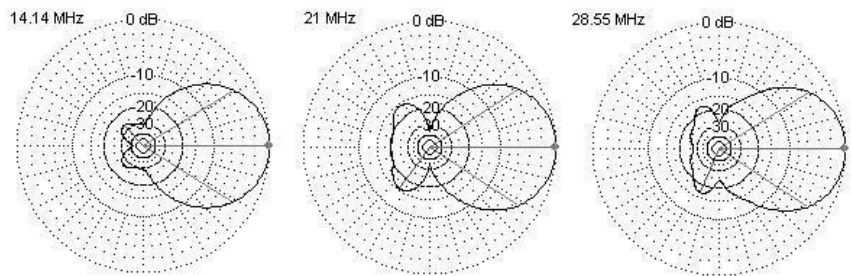


Fig 10—*NEC-Win Plus* screen using variables to define wire parameters.

QX0507-w6pu010

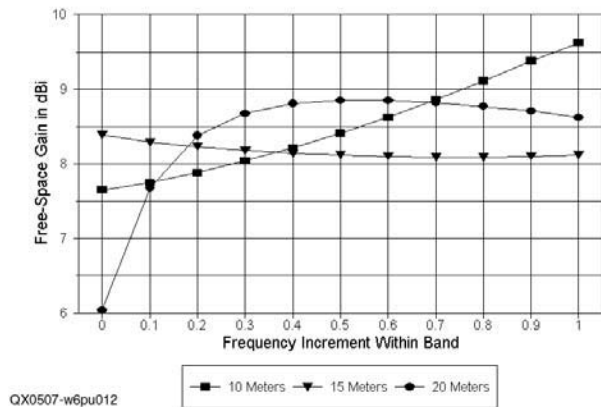


Original W6PU Dual-Driver 4-Element Tri-Band Quad
Best Free-Space E-Plane Patterns

QX0507-w6pu011

Fig 11

Original W6PU Phase-Fed Quad
Free-Space Gain



Original W6PU Phase-Fed Quad
180-Degree Front-Back Ratio

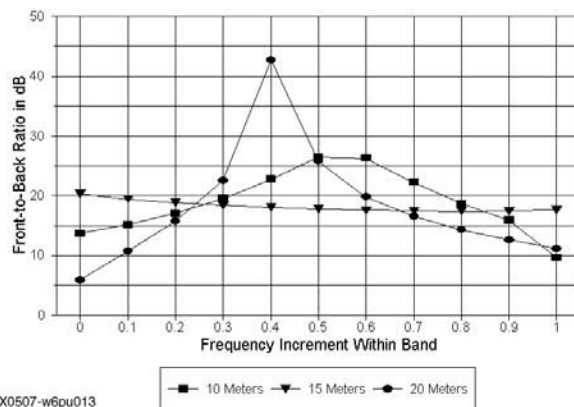


Fig 12

Fig 13

single-driver array. Perhaps the one major difference lies in the very high peak value on 20 meters near 14.14 MHz. The pattern shape in Fig 11 reveals that the antenna has almost no rear lobes at all—just enough to recognize the deep 180° dipole. Accompanying this remarkable front-to-back value is a severe decrease in the front-to-back ratio at the low end of the band, corresponding to the great decrease in forward gain in the same frequency region.

One might surmise that W6PU created the antenna to obtain a coincidence of maximum gain and maximum front-to-back ratio for a small portion of the 20-meter spectrum. 10 meters also shows a mid-band front-to-back ratio peak, but of much smaller proportions. 15 meters is flat. However, the array design using phase-fed drivers fails to produce any gain over the single driver quad explored earlier in these notes. Since we do not know the design of the quad against which he made his gain comparisons, any further conclusions than this one would be speculative.

We need not speculate about the feed-point impedances obtained with the model of the W6PU array. They are all too low to graph against a 50-Ω standard. All of the reported impedances have a very low reactive component, with the maximum range over the 3 bands going from $-j8 \Omega$ up to $+j11 \Omega$. However, the resistive component is problematical. On 10 meters, it runs from 9 to 20 Ω. On 15, the range is 9 to 11 Ω. On 20, it runs from 1.5 to 15.5 Ω. The diagrams all show a direct connection to a 50-Ω feed line. However, the model suggests that a 1:4 transformer would be necessary to achieve a 50-Ω impedance

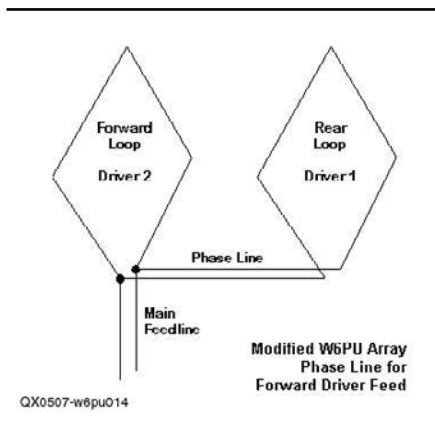


Fig 14

across even part of the bands. With such a transformer, 15 meters would show under 2:1 50-Ω SWR across the band. 10-meters might provide about 800 kHz of coverage, since the feed point resistance rises very slowly across the first half of the band and much more rapidly thereafter. On 20, the SWR would be satisfactory only over the upper or SSB portion of the band. Of course, this speculation assumes the use of a 1:4 transformer with high efficiency.

The number of times that the W6PU dual-driver array has been brought to my attention suggests that numerous antenna planners are using the beam as a potential foundation for their own antenna work. Yet, we are left with a quandary. If the dual-driver system aimed to increase gain over a single driver, it failed. If it aimed to produce a wider passband than the single driver array, it also failed.

In arrays using phase-fed dual drivers, the constraints of phase-feed-

ing the drivers make maximum gain and a wide passband virtually contradictory. It is possible to set the current magnitude and phase on the two elements so that they yield very high gain—over 7 dBi in free-space models of 2-element phased horizontal arrays—over a very narrow passband and at a very low impedance. It is also possible to set the driver current magnitudes and phases to achieve maximum front-to-back ratio, but only at a lesser gain, perhaps just below 6 dBi. The required current magnitudes and phases for a given pair of elements are very different for the two conditions. In phase-fed Yagi studies, I have used the high-gain setting with a director to achieve further gain and a very good front-to-back ratio—but only at the cost of a low feed-point impedance and a bandwidth only suited to the narrower 30-, 17- and 12-meter bands.³

Obtaining a wide operating bandwidth tends to require a set of current magnitude and phase conditions that fall in between those needed for the extremes of gain and of front-to-back ratio. The improvement in horizontal arrays using linear elements tends to be only marginal, usually to the front-to-back ratio over the entire passband, relative to Yagis with similar spacing and the same number of elements. The gain remains at or just under the levels achieved by a well-designed Yagi of the same boom length and the same number of elements.⁴

Since it is unlikely that the phase-fed dual driver system can achieve any gain advantage over the single-driver ARRL quad array, perhaps the rightful place for the W6PU array lies in providing full band cov-

erage with good gain and front-to-back values for all of the bands—including 20 meters. However, if we hope to achieve a wideband, 50-Ω feed system, the array will have to undergo considerable redesign.

A Modified W6PU Dual Driver 4-Element Triband Quad

Designing a simple two-driver log-cell Yagi begins with the design of the phased drivers. When we add parasitic elements to the driver set, we ordinarily do not disturb the drivers. Instead, we set the length and spacing of each parasitic element for a desired set of performance curves over the selected passband. Finally, we either accept the feed point conditions presented by the phased drivers, or we take the entire array through a number of iterations attempting to preserve the performance curve while attaining a desired feed-point impedance curve. In theory, designing a dual-driver monoband quad would follow the same scenario.

Our subject antenna, however, is not a monoband quad, but rather a triband quad with preset element spacing. Our goal is to discover if we can adapt the basic design to a reasonably high-performance array, using the ARRL quad as an initial measuring stick. As well, the goal is to find out if we can extend the passband so that we obtain full band coverage on 20 and 15 meters and full coverage from 28 to 29 MHz on 10 meters. The task has some limiting factors. First, the element spacing, even between drivers, varies from one band to the next as a function of a wavelength. Second, the interactions among the active elements and the passive ones may complicate not only the sizing of the parasitic loops, but as well, the phase line for the active band. Indeed, because changes in the phase line length on one band will affect the activity of the elements when passive, we have an additional variable that will affect the outcomes. Hence, we shall require a considerable number of iterations to assure that we attain the project goals.

Refer to Fig 5 for the general outline of the modified W6PU phased-driver array. The elements of that sketch do not change in the process of modification. However, we do change the phase-line scheme to a more conventional one that uses a single line between drivers for each band. As well, we feed the forward driver, as shown in Fig 14. These moves are for convenience of design and do not invalidate the use of split

lines to effect the desired phasing. The goal is to find a ratio of current magnitude on the drivers and a set of relative phase angles that will yield acceptable performance.

A phased pair of drivers requires relative current magnitudes and phase angles of certain orders for any given performance curve. The current magnitudes are normally close to but hardly ever precisely equal. The current phase angle between the two elements varies with the spacing, with the rear element showing a positive angle relative to the forward element. The wider the spacing, the larger the phase-difference required for a given result.

At the same time, we wish the feed point to exhibit an acceptable impedance. In our test case, the target is 50-Ω resistive, with slow variations of both resistance and reactance as we move away from the design frequency. For a system that uses a single line between the drivers, we may presume a constant voltage at the junction of the forward element and the phase-line end. The parallel connection forms a current divider. The forward element feed-point impedance sets the current level and phase angle for the forward element. However, the impedance on the phase-line side is determined by the impedance of the rear element, as transformed along the phase line. Hence, the phase-line characteristic impedance and length play a role in

determining what impedance appears at the junction. This impedance, in parallel with the forward element impedance, determines the current division. The transformation of the current and its phase angle working back toward the rear element determine the current magnitude and phase angle at that point. The parallel combination of the phase-line forward-end impedance and the forward element impedance yield the feed-point impedance of the array.⁵ If we use a split pair of phase lines, with a length forward to the front element and another length back to the rear element, we only complicate the situation by one more set of transformations along an added transmission line.

The presence of parasitic elements and of interactive undriven elements for inactive bands assures that the simple calculations will not yield usable results. Therefore, when all else fails, one uses the method of experimental iteration, also known as trial and error. By a series of trial phase-line lengths and characteristic impedances, accompanied by judicious re-sizing of some element circumferences, one can see trends in performance, as well as the limits of improvement made by further changes of the same type. The initial stage involved finding setting for the individual bands, followed by re-adjustments occasioned by the fact that changes to one band required ad-

Table 4
Phase-line lengths for each band for the W6PU quad.

Band	Line Route	Physical Length	Electrical Length	Feedpoint
20	Driver 2 to Driver 1	8.50'	12.88'	Driver 1
15	Driver 1 to Junction	7.17'	10.86'	Junction
	Driver 2 to Junction	14.58'	22.10'	Junction
10	Driver 1 to Junction	5.33'	8.08'	Junction
	Driver 2 to Junction	9.67'	14.65'	Junction

Note—All phase lines 50-Ω, VF 0.66 coaxial cables. Driver 1 is the element closest to the reflector—that is, the rear driver.

Table 5
Dimensions of the W6PU dual-driver, 4-element, 33.5 foot-boom, triband quad.

Element	Space from Reflector in feet	Circumference in feet		
		20 Meters	15 Meters	10 Meters
Reflector	—	73.07	50.30	37.24
Driver 1	13.0	72.12	49.97	36.06
Driver 2	21.5	67.41	46.20	33.00
Dir. 1	33.5	67.88	45.83	34.42

ditional changes to the other bands.

Table 5 provides the dimensions of the final model for the modified W6PU array. The most notable changes are the enlargement of the rear drivers and the shrinkage of the 20-meter and 10-meter forward drivers. The 15-meter forward driver is actually larger than in the original array. Changes to the circumferences of reflectors and directors tweak performance or the position of performance peaks within the passband.

A 50-Ω phase line proved satisfactory for all bands, but its length is not what we expect of a two-element phase-line. We are used to the trick of reversing the connections of a short phase line to accrue the impedance transformation of a longer line, for example, giving a half twist to a 45° line to effect a 135° line. Because early principles in amateur circles stressed the impedance transformation rather than the current transformation in the phase line, we have mislabeled the effect of the half twist. A 45° line with a half twist does not transform to 135°, but instead to -45°—or 315°, if counting always in a positive direction. Of course, the current transformation is only 45° if the rear element has an impedance that matches the characteristic impedance of the phase-line.

The spacing between the two drivers in our array does not permit the use of a very short line. Hence, we need to use longer lines without the twist for our phase lines. The shortest line must be at least 8.5 feet long, plus a small addition to clear the supporting mast for the array. On 20 meters and 15 meters, the required 50-Ω lines are considerably longer. In this exercise, I shall pass over the difficulties of physically controlling the route taken by the longer lines.

Table 6 presents the required line lengths for the phase lines for all 3 bands. On 10 meters, the 8.79-foot line may be too short for routing around the mast. Therefore, I have included its reversed counterpart, which is similar in length to the 20-meter line. The table also contains some other useful information, such as the spacing between drivers for each band measured as a function of a wavelength and in electrical degrees—both at the middle of each band. As well, I have shown the physical lengths of the lines assuming velocity factors of 0.66 and 0.80 as a rough guide to the actual line lengths a builder might encounter. Anyone contemplating building this or any other phased array is well advised not to trust the

published velocity factor values, but to measure the velocity factor of the actual material being used.

One more table completes the data necessary to understand something of the complexity of a multiband, dual-driver quad array. Table 7 provides information on the modeled mid-band differentials between the two drivers in terms of their current magnitudes and phase angles. The data may provide some appreciation of how element interactions complicate matters in triband phased arrays. The lines for 20 and 15 meters are considerably longer than we might expect for the spacing between drivers, while the 10-meter line is shorter. (These expectations are based on the erroneous rule of thumb that a spacing of 0.125-λ requires a phase line of 135 electrical degrees.) Indeed, the 15-meter line, under the influence of both the 10- and 20-meter inactive elements, is longer than 1/2 λ (180°).

The current ratios initially look to be well off of any ideal ratio, where something close to 1:1 might be expected. However, I experimented extensively with the 20-meter drivers and obtained peak performance with exactly equal currents and a phase difference of 110°. The improvement was exactly 0.01-dB increase in gain and 3 dB in front-to-back ratio. Since the front-to-back ratio at the center of 20 meters already exceeds 23 dB and since the added gain is not obtainable with a commonly available

transmission line, I concluded the tests.

The question that follows this foray into the design parameters for a multiband, phase-fed quad array is what we obtained for our efforts. In terms of free-space gain, Fig 15 provides the results. Relative to the original W6PU design, we obtain higher gain across each of the three bands. 20 meters shows a smooth gain curve, with no major drop-off at either band edge. 10 meters shows the cross-band rise that we saw in the original design, but at a high average level. 15-meter gain is flat across the band and slightly greater than in the original design.

If we compare array gain with the ARRL quad with which we started this investigation, we find the 20-meter results to be very comparable, with the ARRL single-driver quad having an average 0.1-dB advantage. However, the ARRL quad shows an average advantage of about 1.3 dB over the dual-driven array on 15 meters. The 10-meter gain curve largely offsets that advantage, since the ARRL version is much steeper. It has about a full dB less gain at the low end of the band and only just exceeds the modified W6PU array at the top end. In essence, this result establishes that a phase-fed quad array has no particular gain advantage over a more conventional single-driver array of about the same boom length and using the same number of elements.

Table 6
Phase-line lengths for each band for the modified W6PU quad.

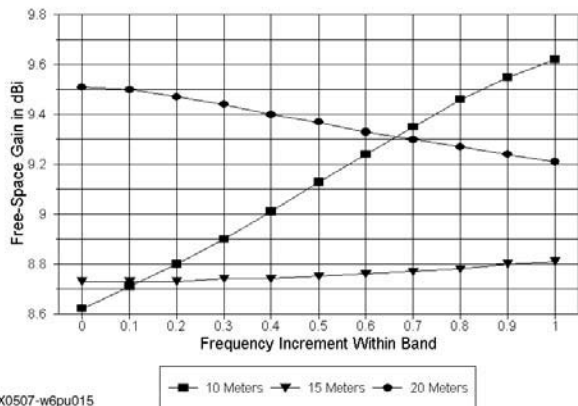
Band	Driver Spacing Wavelengths	Line Electrical Degrees	Physical Length Length feet	VF=	
				.66	.80
20 (14.175)	0.1225	44.10	31.25'	20.63'	25.00'
15 (21.225)	0.1834	66.02	25.83'	17.05'	20.67'
10 (28.5)	0.2463	88.67	13.33'	8.79'	10.67'
10 (alt)*	0.2463	88.67	30.59'	20.19'	24.47'

Note—all lines are 50-Ω without reversal, except 10 (alt)*, which uses a reversed 50-Ω line. For all lines, the route is from driver 1 (rear) to driver 2 (forward), with the feed point at driver 2.

Table 7
Current phasing data.

Freq. MHz	Differentials Between Rear Driver and Forward Driver		Line Length Degrees
	Current Magnitude Ratio Rear-to-Forward	Relative Current Phase Rear (Forward = 1.0)	
14.175	1.365:1	103.2	162.1
21.225	0.779:1	131.3	200.7
28.5	0.856:1	150.3	139.1

Modified W6PU Phase-Fed Quad
Free-Space Gain



Modified W6PU Phase-Fed Quad
180-Degree Front-Back Ratio

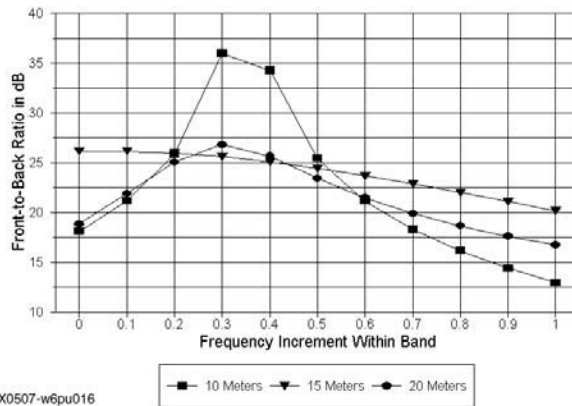


Fig 15

Fig 16

The 180° front-to-back ratio results appear in Fig 16. The original W6PU array has a very sharply peaked 20-meter front-to-back curve with very poor values at the low end of the band. In contrast, the ARRL quad 20-meter front-to-back curve almost parallels the modified array curve, although the latter has somewhat better low-end values. On 15 meters, the modified array shows a value above 20 dB all across the band. The original W6PU array was several dB lower at all points in a parallel curve. The ARRL front-to-back curve rises from 10 dB to 22 dB across the band, in contrast to the smooth results for the modified phase-fed design.

On 10 meters, the modified and original W6PU designs again show parallel curves. However, the modified design manages to increase the front-to-back ratio by at least 3 dB everywhere in the band. Unfortunately, the ARRL array requires significant improvement in its 10-meter front-to-back performance, with a curve that runs from 4 dB at the low end of the band to only 14 dB at 29 MHz. Although the gain differentials among the designs may be operationally moot in most cases, the modified phase-fed array has superior performance in the front-to-back category over both of the other arrays.

Since the motivation for this design exercise was to determine if phase-feeding a quad array could improve the operating bandwidth, especially on 20 meters, we should examine Fig 17. The graph settles the question immediately. On 20 and 15 meters, the 50-Ω SWR curve is 1.5:1 or lower everywhere on each band. Although the 10-meter SWR

Modified W6PU Phase-Fed Quad
50-Ohm SWR

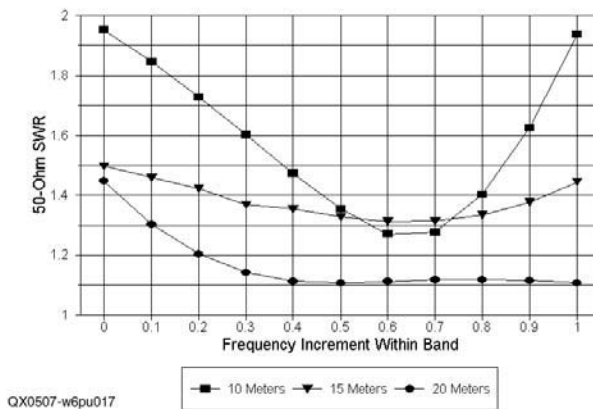
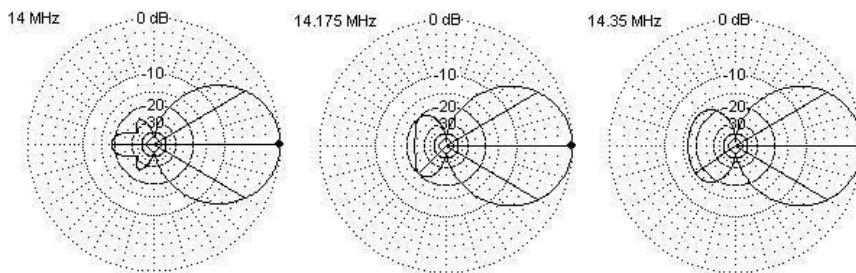


Fig 17



Modeled 20-Meter Free-Space Azimuth Patterns
Modified W6PU Quad Array

Fig 18

curve remains below 2:1 across the first MHz of the band, it does not match the corresponding 10-meter SWR curve of the ARRL quad. However, that single-drive quad does not match the phase-fed array on either

20 or 15 meters, with 20 meters being very deficient in coverage.

As I indicated early on in the investigation, multiband quads require attention not only to levels of performance, but to pattern shape as well.

Therefore, I am including some modeled free-space E-plane patterns that will closely resemble the azimuth patterns one might achieve with such an antenna at least 1λ above real ground. Fig 18 samples the 20-meter patterns at the band edges and in the middle of the band. Perhaps the only way to describe these patterns, relative to our expectations from a comparable monoband Yagi, is that they are clean and well-behaved.

In Fig 19, we find the corresponding patterns for 15 meters. The forward lobes are once more clean. The rear lobes show a minor tendency toward fan-tailing as we increase the frequency within the band, so that the worst-case front-to-back ratio is about 15 dB at the high end of the band. Compared to many multiband quad designs, the 10-meter patterns in Fig 20 are quite free from anticipated abnormalities. The rear lobes, while not as diminutive as we might like from a monoband Yagi, are free from quartering sidelobes that would yield a ratio of under 20 dB. From 28.5 MHz to 29 MHz, the forward lobe barely shows small bulges, indicating an incipient but undeveloped secondary forward lobe.

All-in-all, then, the modified W6PU phase-fed driver multiband quad in principle offers reasonably good performance on all three of the wide upper HF amateur bands. It is broadband in its full coverage of each band, and its gain and front-to-back levels are very respectable for quad arrays with a 33.5 foot boom. The modified version overcomes the shortcomings that appeared in models of the original W6PU design, while generally equaling or bettering the performance curves for the ARRL design (except for 15-meter gain).

In the final analysis—and apart from prejudices for or against quads—the design leaves us with a final question: how does the anticipated phase-fed quad performance stack up over and against the performance of a comparable multiband Yagi design?

The Modified Phase-Fed Quad vs. Two Multi-Band Yagis

The modified W6PU phase-fed quad uses 12 elements in 4 groups of three on a 33.5 foot boom. To evaluate its performance fairly, we need to compare the figures that appear in the graphs (Fig 15, 16 and 17) with those from an array with which the quad might be competitive as a design of similar complexity, similar coverage and similar size. Hence, monoband quads and

Yagis are not suitable comparators in the evaluation. The potential gain figures for the monoband antennas, cited at the beginning of this study, serve only to reveal to what extent the multiband quad (or other multiband antennas) achieves (or fails to achieve) monoband performance.

A more suitable comparator for a

first-order competitive comparison would be a multiband Yagi having a similar boom length to the one used in the quad, something in the range from 30 to 35 feet. Over the years, I have developed models of at least two possible designs. Although the models have roots in the measurement of dimensions of actual antennas, they

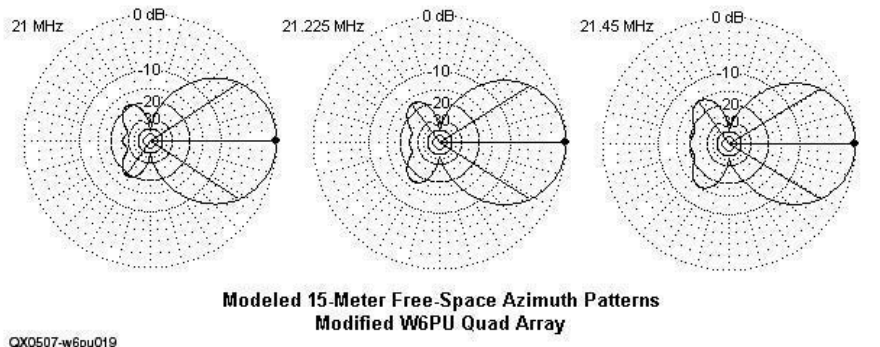


Fig 19

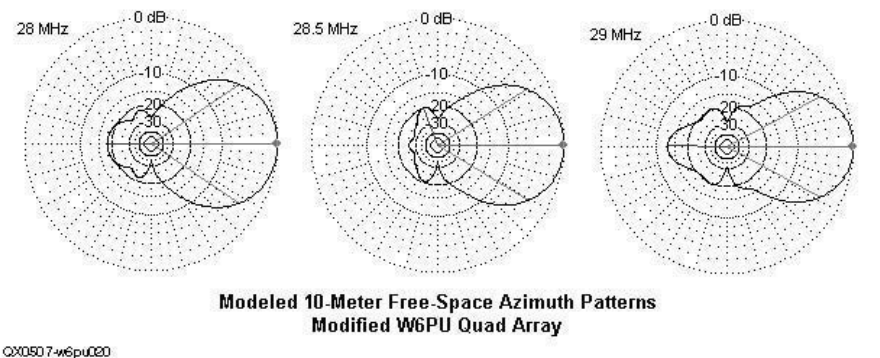
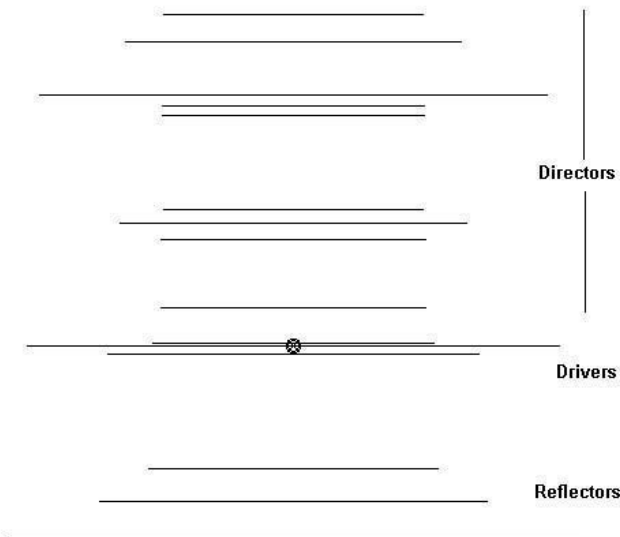


Fig 20

Table 8
General dimensions of a 15-element, triband Yagi with master and two slaved drivers.

El. #	Function	Length (feet)	Diameter (inches)	Distance from Reflector (feet)
1	20-m reflector	34.50	0.625	
2	15-m reflector	23.33	0.50	2.17
3	10-m reflector	17.50	0.40	4.17
4	15-m slaved driver	22.33	0.50	11.09
5	20-m master driver	32.17	0.625	11.60
6	10-m slaved driver	16.97	0.40	11.79
7	10-m director 1	16.00	0.40	13.92
8	10-m director 2	15.92	0.40	18.00
9	15-m director 1	20.92	0.50	19.00
10	10-m director 3	15.58	0.40	19.83
11	10-m director 4	15.83	0.40	25.50
12	10-m director 5	15.83	0.40	26.08
13	20-m director 1	30.67	0.625	26.75
14	15-m director 2	20.33	0.50	30.00
15	10-m director 6	15.67	0.40	31.58

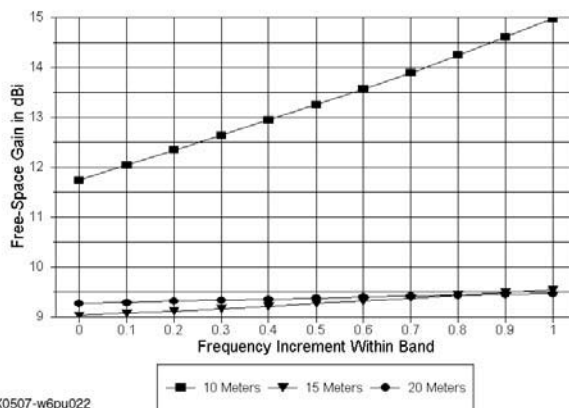
QX0507-w6pu021



15-Element Tri-Band Yagi Using a Master and 2 Slaved Drivers

Fig 21

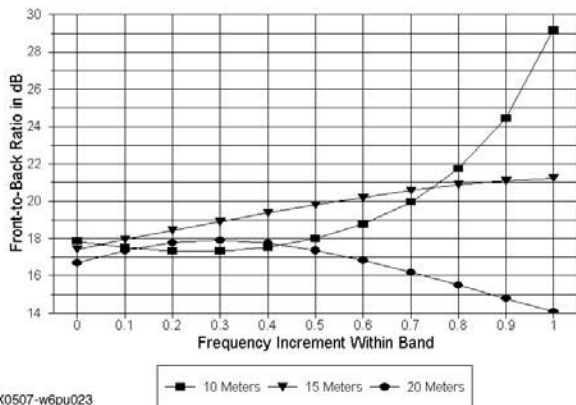
Tri-Band Yagi: Master-Slaved Drivers
Free-Space Gain



QX0507-w6pu022

Fig 22

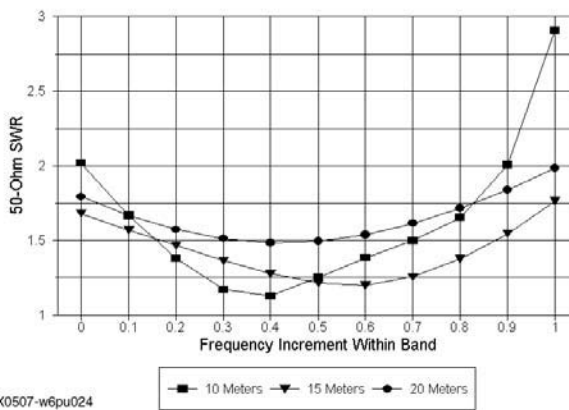
Tri-Band Yagi: Master-Slaved Drivers
180-Degree Front-Back Ratio



QX0507-w6pu023

Fig 23

Tri-Band Yagi: Master-Slaved Drivers
50-Ohm SWR



QX0507-w6pu024

Fig 24

are not models of the antennas themselves. Instead, they are modeling idealizations, using uniform-diameter elements, in contrast to the normal stepped-diameter element structures used in upper-HF horizontal arrays. Hence, the element lengths do not coincide with those of actual antennas. As well, both models use complex feeding systems so that the user requires only one feed point and cable. All such systems depend for the impedance transformations on not only the element lengths and spacing, but as well on the element diameter. The idealization of the model to uniform-diameter elements requires alter-

tations in the feed structure to simulate the actual one. As a consequence, the performance curves that emerge from the models may differ in detail from those obtained with real antennas of roughly similar outlines. These cautions result in a disclaimer: for true models of any antenna, commercial or otherwise, one needs to consult the maker or the maker's literature.

In addition, various antenna makers use different methods and test setups for obtaining performance results that eventually appear in one or another form of print. The modeling results that I shall present stem from simple free-space models. Hence, they

may not coincide with numbers that may appear for similar-looking antennas. As well, makers modify and improve designs with time, and the models used here may be dated relative to their roots.

Nevertheless, we may use these idealized models for a limited purpose: to gather basic data on the potential performance of multiband Yagis in the 30 to 35-foot category. We shall limit the use of the data to seeing how the modified quad design stacks up with these modeled Yagis. The comparison may tell us whether the quad design is roughly competitive, vastly superior, or embarrass-

ingly inferior. If one needs finer shades of evaluation, one must build all of the arrays and test them on a rated range.

One question that the evaluation will not tell us is whether the quad enjoys in fact its reputation as a band opener and closer. Such a study involves more than the basic modeled performance of the antenna, since it likely depends on propagation phenomena as well as on radiation pattern phenomena. Consequently, these notes will remain silent on that perennial issue in the Yagi-vs.-quad discussion.

A 15-element tri-band Yagi using a master driver and two slaved drivers: The first of our multiband Yagis uses a boom just over 31.5 feet long, plus such end extensions as may be needed to mount the element-to-boom hardware. The general outline appears in Fig 21, with the model dimensions shown in Table 8. The design uses 3 20-meter elements, 4 15-meter elements and 8 10-meter elements. This type of listing is conventional and based on the length of the elements. However, as in all multiband Yagi designs, the elements for inactive bands relative to one being used are active to some degree.

20-meter elements are particularly troublesome to 10-meter operation, since they can be not only active, but may control 10-meter performance. The length of a 20-meter element as it approaches a full wavelength on 10 meters tends to be long in terms of what the 10-meter portion of the array requires, even from a full-wave element. The effect is to drag the performance curves lower in frequency, preventing full high-band coverage. The normal compensation is to add a 10-meter director immediately to the driver side of the 20-meter director. As well, one usually needs to place a further 10-meter director on the other side of the 20-meter director. Although less of a burden in this respect, similar treatment usually accompanies the placement of 15-meter directors, as these elements can also affect 10-meter performance. Signs of such design maneuvers appear in Fig 21.

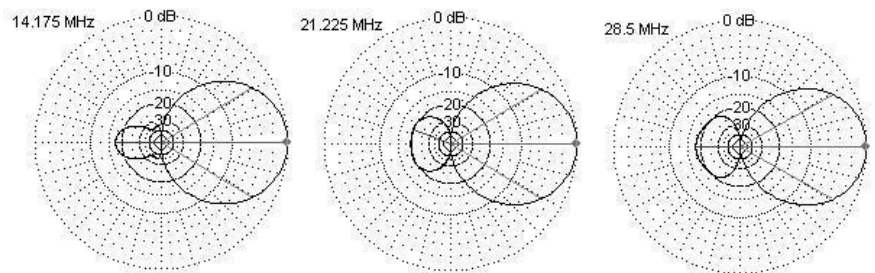
A second reason for surrounding lower-band directors with high-band directors is the fact that in developing a design, directors for different bands—especially for 10 and 20 meters—seem to “want” to be in the same place. The design at hand does not use traps to resolve the placement issue. Instead, the fore-and-aft high-band director treatment settles the issue.

The driver section of the antenna employs a master 20-meter driver. Closely spaced slaved drivers for 15 meters and 10 meters require no connection to the master driver to perform their function. Such systems depend upon the mutual coupling between elements—all of which are highly dependent upon element length and spacing of the slaved drivers relative to the master driver—to provide the higher-band energy for the array and to show a suitable impedance at the master driver on all three bands.

Such a design is capable of high levels of performance on all three upper-HF bands. Fig 22 shows the modeled free-space gain of the ar-

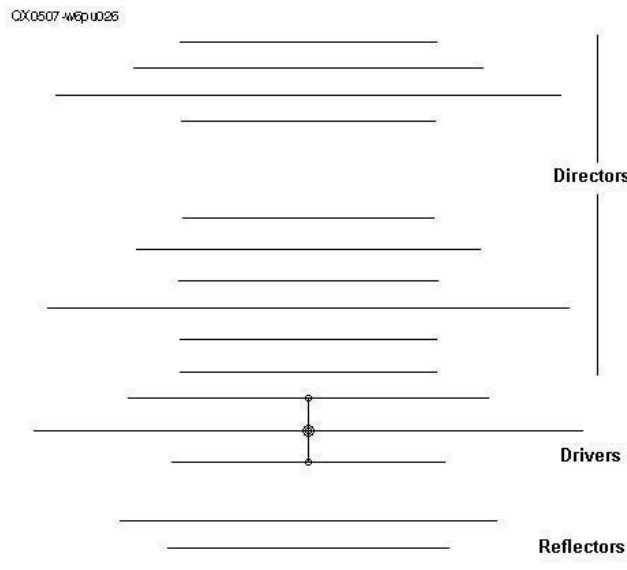
ray. The values for 20 and 15 meters form smooth curves and range from just above 9 dBi to about 9.5 dBi. The boom length is long for 10 meters and is filled with directors that increase gain in addition to compensating for interactions with elements for other bands. Hence, 10-meter gain is considerably higher than for the lower bands, ranging from about 11.7 dBi to nearly 15 dBi across the first MHz of the band.

Fig 23 shows the modeled 180° front-to-back performance of the array. From monoband beams, we expect to see values above 20 dB everywhere within the band covered. Although the front-to-back ratio of a tri-band beam may peak over the 20-dB marker



15-Element Tri-Band Yagi Using a Master and 2 Slaved Drivers
Representative Free-Space E-Plane Patterns

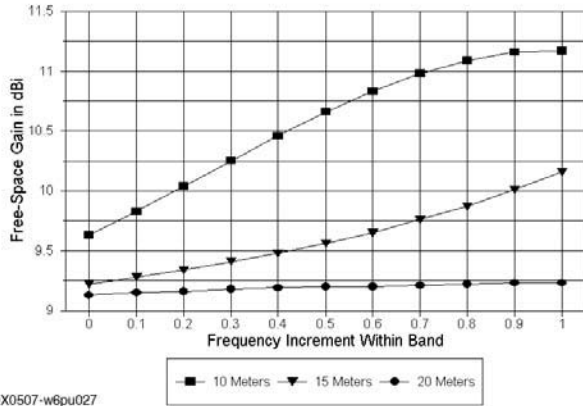
Fig 25



16-Element Tri-Band Yagi Using 3 Directly Coupled Drivers

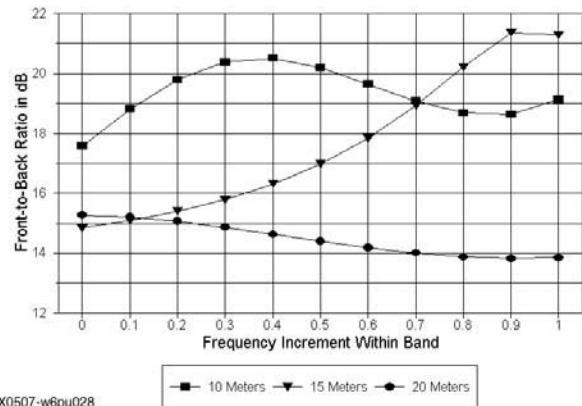
Fig 26

Tri-Band Yagi: Direct-Coupled Drivers
Free-Space Gain



QX0507-w6pu027

Tri-Band Yagi: Direct-Coupled Drivers
180-Degree Front-Back Ratio



QX0507-w6pu028

Fig 27

Fig 28

level, the average front-to-back ratio averages in the range between 17 and 20 dB. In the test model, the 20-meter ratio drops to just above 14 dB at the high end of the band, while the 10-meter ratio appears headed for a sharp peak just beyond 29 MHz. Nonetheless, the curves are important also for what they do not show: the extremely low values at one or another band edge that often attach to some conventional multiband quad designs. For example, the lowest value on 20 meters—where the array uses 3 elements—is well above what we might obtain from a 2-element driver-reflector quad design.

The 50-Ω SWR performance appears in Fig 24. On 20 and 15 meters, the array achieves an SWR well below the conventional standard of 2:1 at the antenna feed point. The antenna also manages to cover all but the last 100 kHz of the 10-meters, as defined in terms of its first MHz. Some improvement in the 10-meter curve may be possible by judicious adjustments to the length and spacing of the 10-meter slaved driver relative to the master 20-meter driver. However, my experience with 2-band antennas using the same type of driving system suggests that without beneficial element interactions that broaden an operating curve, reduced coverage is natural. The means taken to isolate 10-meter gain and front-to-back performance from problematical interactions with lower-band elements also limits the SWR passband. All multiband antennas ultimately demand compromises and decisions as to which properties receive priority.

Multiband Yagi designers are as

Table 9
General dimensions of a 16-element, triband Yagi with directly coupled drivers.

El. #	Function	Length (feet)	Diameter (inches)	Distance from Reflector (feet)
1	20-m reflector	34.68	0.70	
2	10-m reflector	17.29	0.55	1.64
3	15-m reflector	23.24	0.625	3.28
4	10-m driver	16.77	0.55	6.89
5	20-m driver	33.74	0.70	8.86
6	15-m driver	22.16	0.625	10.83
7	10-m director 1	15.73	0.55	12.47
8	10-m director 2	15.73	0.55	14.44
9	20-m director 1	32.17	0.70	16.40
10	10-m director 3	15.99	0.55	18.04
11	15-m director 1	21.27	0.625	20.01
12	10-m director 4	15.47	0.55	21.98
13	10-m director 5	15.66	0.55	27.89
14	20-m director 2	31.17	0.70	29.53
14	15-m director 2	21.58	0.625	31.17
15	10-m director 6	15.73	0.55	32.81

concerned with pattern shape as with the basic performance numbers. Fig 25 provides a sample pattern from each band—taken at the band-center frequency—to create a quick check on this property. In all cases, the patterns are clean, that is, typical Yagi patterns for the level of gain and front-to-back ratio.

A 16-element triband Yagi using directly coupled drivers: A single multiband Yagi design might be an aberration from the norm, so I am including a second tribander using a boom nearly 33 feet long. It employs 16 elements: 4 for 20 meters, 4 for 15 meters, and 8 for 10 meters. Let one think that the design is a clone of the 15-element Yagi, a comparison of Fig 26 with Fig 21 will reveal that the element placement is quite different throughout. What this array shares

in common with the first one are two major design features. One is the use of surrounding 10-meter directors for the 20- and 15-meter directors. The other is the general progression of elements, which is a factor controlled by the frequencies covered more than a simple decision of the designer.

The 16-element array differs from the 15-element Yagi in several important ways. The 4th 20-meter element changes the relationships among all of the directors, allowing a wider spacing between the 10-meter directors and the lower-band directors. As well, the array places the 10-meter driver behind the 20-meter driver, with the 15-meter driver in front. The result is a slight reduction in 10-meter gain and an enhancement of 15-meter gain, relative to what would be possible had one reversed the drivers.

The positions of the drivers also result from the feed system, which directly couples energy from the master driver's feed point to each of the other two drivers via a low-impedance transmission line. This system uses close driver spacing, but not as close as in the master-slaved driver system. Nonetheless, the higher-band drivers receive both direct energy and mutually coupled energy from the 20-meter driver. Hence, the higher-band driver lengths and spacing are critical to the success of the feed system. Table 9 provides the dimensions of the model that uses uniform-diameter elements. Compared to the 15-element array, the 16-element Yagi uses much fatter elements, especially on the upper bands.

The gain that we obtain from the model of the 16-element array appears in Fig 27. The 10-meter gain shows the steeply rising curve common to most multiband designs, but at a somewhat lower level than for the 15-element design. In contrast, the 15-meter curve is slightly higher. 20-meter gain levels are comparable within about 0.2 dB.

Fig 28 shows the modeled 180° front-to-back ratio results. Overall, the front-to-back ratio fluctuates within the 14 to 22 dB range. No sharp peaks appear in the graph, although one might exist between 21.36 and 21.45 MHz in the last tenth of the 15-meter band.

The advantages of the directly coupled drivers—used by more than one maker these days—appear in Fig 29. Although the graph indicates a few 50-Ω SWR values above 1.5:1, the curve shapes strongly suggest that with judicious adjustment of the drivers, all of the curves would settle in with band-edge values well below 1.5:1. To go with the performance curves, the 16-element array patterns all classify as clean and well behaved, as revealed by the samples in Fig 30.

The comparison and conclusion: The two multiband Yagi designs, as modeled here, are sufficiently similar to form a basis for evaluating whether the modified W6PU phase-fed quad array is competitive. By competitive, I simply mean that it is capable of sufficient performance to warrant a move from abstract modeling design to planning a physical implementation. A review of the performance curves for all three antennas is necessary for detailed evaluation, but we can gain something of value by summarizing the average performance figures. Table 10 provides the averaged data for free-space gain, 180° front-

to-back ratio, worst-case front-to-back ratio, and 50-Ω SWR. The insertion of the worst-case figure provides for the tendency of the quad to show a fantail rear lobe structure on some bands, such as 15 meters.

Clearly, the Yagis win the gain contest on 10 meters by a wide margin, due to the ability to add the extra directors on a 30-35-foot boom. On 15 meters, the Yagis hold a slight gain margin—about 0.5 dB—but 20 meters

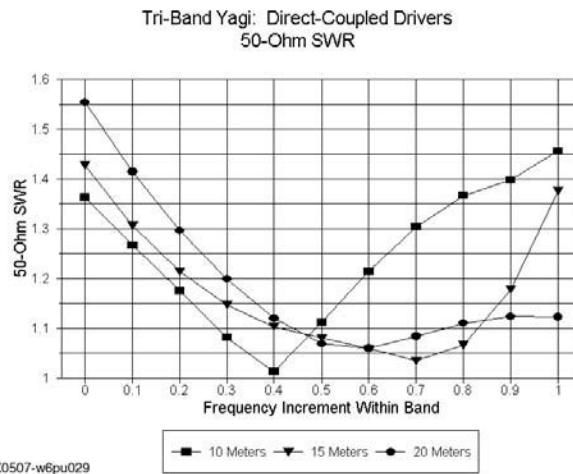


Fig 29

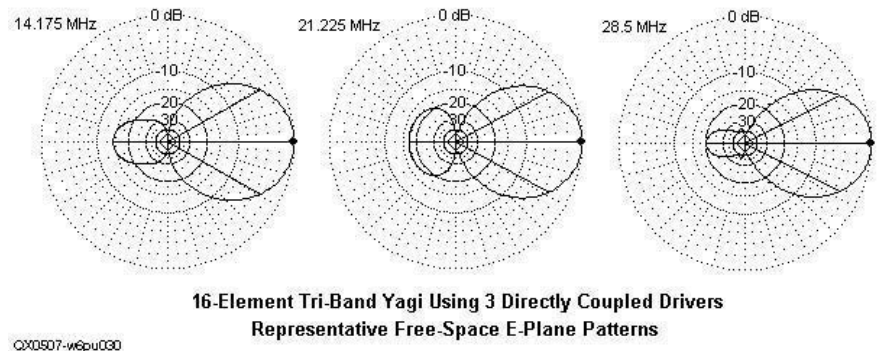


Fig 30

Table 10
Some average values of performance parameters by bands—modified W6PU quad array and 2 triband Yagis

Band	Free-Space Gain dBi	180°/Worst-Case Front-to-Back Ratio dB	50-Ω SWR
<i>Modified W6PU 4-element phase-fed Quad</i>			
10	9.13	22.17 / 18.28	1.59
15	8.76	23.94 / 16.95	1.38
20	9.37	21.48 / 19.74	1.17
<i>15-element, master with two slaved drivers, tri-band Yagi</i>			
10	13.29	19.97 / 18.68	1.64
15	9.27	19.62 / 19.18	1.43
20	9.37	16.56 / 16.56	1.66
<i>16-element, directly coupled drivers, triband Yagi</i>			
10	10.55	19.32 / 19.32	1.25
15	9.61	17.64 / 17.17	1.18
20	9.19	14.47 / 14.47	1.20

is a dead heat. In the 180° front-to-back category, the quad is superior by a margin that ranges from slight—that is, a fraction of a dB—to a margin that might be operationally significant—5 dB. When it comes to worst-case front-to-back ratios, the field is split, with each antenna in the table taking top honors once. All of the arrays cover all bands with less than 2:1 50-Ω SWR, with the exception for one Yagi of the top 100 kHz of the first MHz of 10 meters.

Although it is dangerous to make decisions based on such summary figures, the averages do indicate that the phase-fed four-element quad is sufficiently competitive with triband Yagis of similar boom length to rank as neither vastly superior nor embarrassingly inferior. Hence, quad aficionados might be attracted to the design or to some offshoot of it. A myriad of mechanical features that may influence such a decision go uncovered in this study. Certainly, quad hardware is readily available. However, even some seemingly minor construction details can affect performance. For example, the creation of loops at the fastening points of the loops to the support arms can detune a loop from its modeled dimensions. In addition, one would need to carefully handle the long phasing lines between the drivers. For many operators contemplating a new antenna in the size range that we have been considering, one final fact may prove decisive. A quad design of the sort investigated here is a home-brew effort, whereas the Yagi models have commercial counterparts that require only assembly in accord with detailed instructions.

This investigation began with an evaluation of the ARRL quad as a well-designed single-driver quad in order to establish two things: whether it has limited band coverage and whether the use of phase-fed dual drivers would provide any gain or band-coverage advantages over a single-driver quad. The initial modeling of the most prominent dual-driver 4-element quad developed by W6PU failed to provide the promised 50-Ω feed-point impedance, although the general design showed promise in other operating categories. Some judicious redesign of the phasing system and the element dimensions yielded a promising design with full-band coverage on 20 through 10 meters. However, the exercise laid to rest the old claim that driver-phasing significantly increases array gain. The truer func-

tion of driver phasing is to obtain a wider operating bandwidth while sustaining other performance figures, such as the front-to-back ratio.

Our final question was whether or not the resulting quad design is electrically competitive with multiband Yagis of similar boom length. The general answer is affirmative, although specific properties of one or another type of array may tip the balance. Since all multiband arrays are filled with compromises occasioned by element interaction, the quad is neither decisively superior nor decisively inferior to comparable Yagi designs from a strictly electrical perspective.

About the intangibles that form both the quad and the Yagi mystiques, I must close with a prudent “no comment.”

Notes

¹See L. B. Cebik, *Cubical Quad Notes*, Vol. 2, *antenneX*, 2001, for background on the optimized monoband quads used as benchmarks.

²Without casting a single aspersion on the antenna that W6PU created, we may note that he gives the basic quad loop a 2 to 2.5 dB advantage over the dipole. (The actual advantage when using the same element wire-diameter is 1.0 to 1.1 dB.) He attributes a much lower radiation elevation angle to the quad over a Yagi, when both are mounted at the same height. (The effective height of a quad is about two-thirds of the distance upward from the lowest point to the highest, a net increase in effective height that fails to lower the radiation angle significantly relative to the Yagi.) W6PU gives the diamond shaped quad loop a gain advantage over the square loop. (The differential is negligible in electrical terms, although some builders prefer the diamond for its support of feed cables along its arms and its ability to withstand winter weather.) Finally, he tends to add up all of the small gains to reach a value for his antenna that is their simple sum.

If any problematical tendency has remained from the early 1980s in antenna

work, it is the temptation to sum up the theoretic gains from individual modifications to a basic antenna and then to claim that the gain of the new antenna is that sum. In most instances, the new antenna will not achieve the performance level of the claims derived from simple summing. In some cases, a basic modification will dominate the performance, negating the gains of other modifications. In other cases, modifications will cancel each other rather than re-enforcing each other. The only way to have confidence in performance levels is to create the entire new antenna structure and then to test it. Accurate modeling is one route to testing antenna ideas before building and, equally important, before making claims about the design.

³For fuller information on phase-fed horizontal arrays, see the 4-part series “Some Notes on Two-Element Horizontal Phased Arrays,” in *The National Contest Journal*, beginning in Nov/Dec, 2001 and concluding in May/June, 2002.

⁴For further background on antennas using phase-fed driver cells and linear elements, see L. B. Cebik, “Some Aspects of Long-Boom, Monoband Log-Cell Yagi Design,” *QEX*, Jul/Aug, 2001, pp. 11-22.

⁵See L. B. Cebik, “Modeling and Understanding Small Beams: Part 5, The ZL Special,” *Communications Quarterly*, Winter, 1997, pp. 72-90, for some of the equations relevant to an analysis of action along an array phase line.

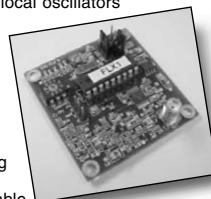
Licensed since 1954, L. B. Cebik, W4RNL, is a prolific writer on the subject of antennas. Since retiring from teaching at the University of Tennessee, LB has hosted a Web site (www.cebik.com) discussing antennas—both theoretical and practical. He has written more than 15 books, including the ARRL course on antenna modeling. Serving both as a technical and an educational ARRL advisor, he's also been inducted into both the QRP and QCWA Halls of Fame. LB can be reached at 1434 High Mesa Dr, Knoxville, TN 38938 or at cebik@cebik.com. □□

Flash Crystal Frequency Synthesizer

- **Clean, Stable RF Signal Source** – Great for local oscillators and lab test equipment applications!
- **Several Models Available** – Covering from 7 MHz up to 148 MHz
- **Can Store Up to 10 Frequencies** – Board-mounted mini rotary dip switch for frequency selection
- **Completely Re-Programmable** – Program the 10 frequencies using any PC running *Hyperterminal* (included in *Windows* operating systems)
- **Economical** – A fraction of the cost of comparable lab-grade RF signal synthesizers
- **Outputs Approximately 5 mW (+7 dBm)** – Female SMA RF output connector
- **Fully Assembled, Tested, and Ready to Go!** – Just \$80 (plus \$4.30 S/H in US)
- **Super Compact** – Measures less than 2 by 2 inches!
- **Power Requirements** – 8 to 15V dc at approximately 55 mA

For Further Details, Visit Our Web site for the Owners Manual

Expanded Spectrum Systems • 6807 Oakdale Dr • Tampa, FL 33610
813-620-0062 • Fax 813-623-6142 • www.expandedspectrumsystems.com



HC-49 Crystals

- Frequencies: 3535, 3560, 7030, 7038, 7040, 7042, 7058, 7122, 7190, 7195, 10106, 10125, 10700, 14057, 14058, 14060, 21060, 24906, 28060, 28238, 28258 kHz
- Specs: +/-100 ppm, 18 pf

Cylindrical Crystals

- Frequencies: 3560, 7030, 7038, 7040, 7042, 7190, 10106, 10125, 14025, 14200, 14285, 18096, 21026, 21060, 24906, 28060 kHz.
- Specs: +/-100 ppm, 18 pf, 3x8 mm. (3560 crystal: 3x10 mm)

Ground System Configurations for Vertical Antennas

Once you decide on a vertical antenna design, you next need to define the ground system. This paper will help you decide what's right for you.

By Al Christman, K3LC

Abstract

All hams want to get the most “bang for their buck” when building an antenna. This article compares the performance of vertical-monopole antennas when they are installed over a variety of ground systems. The first group of antennas has just a single vertical element or radiator, but two-element cardioid arrays and four-element square arrays will also be reviewed in the future. The ground systems examined here all utilize buried wires that are arranged in many different configurations. Computer analysis indicates that, for a given total length of wire, some configurations perform much better than others.

Introduction

Vertically-polarized antennas are widely used on the low bands, and the question often arises concerning how to achieve the most gain for a specified amount of wire in the ground system. We are all familiar with the classical AM-broadcast-style ground system using buried radials, but is it possible to do better? Using *EZNEC4*,¹ I will attempt to answer this question. For simplicity, all simulations were performed on the 80-meter DX phone band at a frequency of 3.8 MHz. Average soil, with a conductivity of 0.005 Siemens/meter and a dielectric constant of 13, will be used in the computer model. In each case the radiator has a physical height of

0.25λ , or about 64.71 feet. All conductors are made of # 12 AWG copper. The wire segment-lengths are tapered in accordance with the most conservative *NEC* guidelines. The shortest segments, such as the one containing the feed-point at the base of the monopole, have a length of six inches. The ground wires all begin at the base of the vertical element (at zero height) and the inner segment of each wire slopes downward so that its outer end is at the “final” depth in the soil, normally 3 inches.

Single Vertical Element with Symmetrical Radial Ground System

The first 18 ground systems each incorporate uniformly spaced equal-length radials. The number of radials varies from 30 to 240, and the length of the radials spans the range from 0.125λ to 1.0λ . Fig 1 illustrates a typical system (model # 5) utilizing 60

Grove City College
100 Campus Dr
Grove City, PA 16127-2104

¹Several versions of *EZNEC* antenna-modeling software are available from Roy Lewallen, W7EL, PO Box 6658, Beaverton, OR 97007 or www.eznec.com.

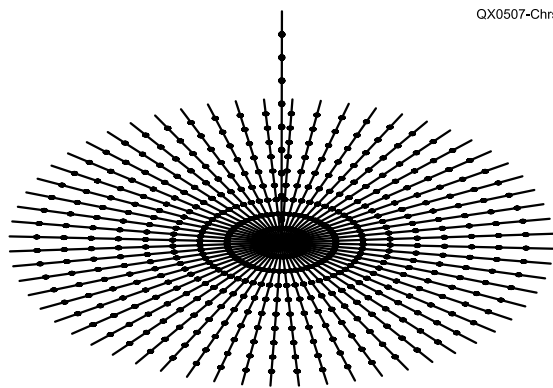


Fig 1—EZNEC representation of a quarter-wave vertical element with a symmetrical ground system utilizing 60 quarter-wave radials uniformly spaced 6° apart. Both the monopole and the radials utilize tapered segment lengths.

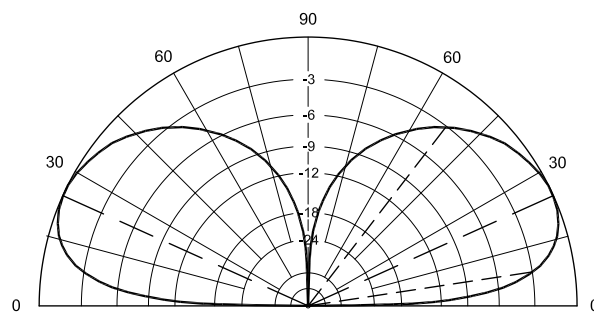


Fig 2—Elevation-plane radiation pattern for the antenna shown in Fig 1. The peak gain is 0.45 dBi at 24° take-off angle.

buried 0.25λ radials, and Fig 2 displays the elevation-plane radiation pattern for this antenna. Single-vertical antennas using symmetrical ground systems such as these will generate azimuthal-plane radiation patterns that are circular, or omni-directional. Table 1 lists the number and length of the radials, the peak gain and corresponding take-off angle (TOA) at which maximum gain occurs, the feed-point impedance and the total length of wire required for each ground system. In the main part of the table, the antennas are listed in order of increasing radial-length and number of radials. As expected, doubling the number of radials always yields more gain, but the improvement becomes progressively smaller each time more radials are added. For eighth-wave radials, 60 is probably sufficient, because installing more produces only a small amount of additional gain.

The magnitude of the input resistance behaves in a very interesting manner. As long as only 0.125λ or 0.25λ radials are used, an antenna with more gain also has a lower input resistance. For a ground screen composed of 240 quarter-wave radials, the feed-point resistance is just $37.6\ \Omega$, the lowest value in the entire table. When half-wave radials are used, however, the input resistance climbs above the $40\text{-}\Omega$ level, although once again it decreases monotonically as more radials are added and the gain rises higher. A switch to full-wave radials again boosts the feed-point resistance, even though the gain is now greater than ever before. Notice that the maximum gain varies significantly, from -0.25 dBi to $+2.33$ dBi, as does the total length of wire in the ground sys-

Table 1

Performance data for ground systems composed of uniform-length, symmetrically-spaced radials. The ground systems are listed in order of increasing radial-length and number of radials.

Model number	Number of radials	Length (λ)	Gain (dBi)	Takeoff angle (deg)	Input impedance (Ω)	Total length of wire (λ)
1	60	0.125	-0.25	24	$45.44+j18.62$	7.5
2	120	0.125	-0.21	24	$44.79+j17.48$	15
3	240	0.125	-0.19	24	$44.49+j17.0$	30
4	30	0.25	0.15	25	$44.15+j26.07$	7.5
5	60	0.25	0.45	24	$40.45+j23.72$	15
6	120	0.25	0.58	24	$38.50+j22.02$	30
7	240	0.25	0.63	25	$37.60+j21.13$	60
8	30	0.5	0.46	25	$46.65+j26.91$	15
9	60	0.5	1.03	26	$43.85+j26.02$	30
10	120	0.5	1.39	25	$42.05+j25.91$	60
11	240	0.5	1.56	26	$40.85+j26.07$	120
12	30	1.0	0.58	24	$46.25+j26.74$	30
13	60	1.0	1.30	25	$43.25+j25.50$	60
14	120	1.0	1.92	26	$41.52+j24.99$	120
15	240	1.0	2.33	26	$40.49+j25.02$	240
6	120	0.25	0.58	24	$38.50+j22.02$	30
16	120	0.25(a)	0.61	25	$38.44+j22.24$	31.6
17	120	0.25(b)	0.63	24	$38.57+j22.46$	32.3
18	120	0.25(c)	0.64	24	$38.56+j22.53$	33.9

Notes

- A circular perimeter wire connects the outer ends of all the radials together. This extra wire contributes another $1.6\ \lambda$ to the overall length of wire required for the ground system.
- A 5-foot ground rod is added at the outer end of each of the radials. The extra length of these rods increases the overall length of wire required for the ground system by $2.3\ \lambda$.
- A circular perimeter wire is added, along with a 5-foot ground rod at the outer end of each radial. Together, these modifications add an extra $3.9\ \lambda$ to the total length of wire required for the ground system.

tem, from a low of just $7.5\ \lambda$ all the way up to $240\ \lambda$. There are slight variations in the take-off angle at which the peak gain occurs, but this angle always hovers near 25° .

The lower portion of Table 1 was included to show what happens when a perimeter wire and/or ground rods are added to a radial ground system.

The results for ground-system model # 6 (120 0.25λ radials) are repeated for comparison purposes, followed by new models # 16 (perimeter wire added), # 17 (ground rods added), and # 18 (both perimeter wire and ground rods added). In every case, the peak gain rises only slightly, so it is likely that adding either ground rods or a

perimeter wire (or both) to a radial ground-screen is not worthwhile, especially when viewed in terms of the amount of extra work they entail. Table 2 contains the same information as Table 1, but here the antennas are listed in order of increasing gain, without regard to the number or length of the radials. Note that only those antennas using ground systems with half-wave or full-wave radials are able to achieve a gain of more than 1.0 dBi.

If one is limited to radials no longer than 0.25λ , then a very large number must be utilized to even approach the one-decibel gain figure (a ground screen with 240 $0.25\text{-}\lambda$ radials yields a gain of 0.63 dBi). Table 3 again repeats much of the data from Table 1, but now the order of entry has been changed so that the overall length of wire in the ground system takes priority. When two ground systems both utilize the same total length of wire, they are listed in order of increasing gain. If two ground systems both have the same gain and the same total wire-length, they are listed in order of increasing radial-length.

Consider the case where only 7.5λ of wire can be dedicated to the ground system. From Table 3, using 30 quarter-wave radials instead of 60 eighth-wave radials produces 0.4 dBi of extra gain. If a maximum of 15λ of wire is available, 30 half-wave radials work best, although 60 quarter-wave radials yield only 0.01 dB less gain, and take up less space. For 30λ of wire, 60 half-wave radials are definitely superior to either 120 quarter-wave radials or 30 full-wave radials. At the $60\text{-}\lambda$ level, 120 half-wave radials produce a bit more gain than 60 full-wave wires, and require only a fraction of the acreage. Notice that, for total wire lengths ranging anywhere from 15 to 60λ , half-wave radials generated the most gain. For those who are willing to install 120λ of wire (more than 31,000 feet at 3.8 MHz), 120 full-wave radials do a better job than 240 half-wave wires.

Single Vertical Element with "Incomplete" Radial Ground System

Is it possible to arrange the radials in such a way as to produce a directional radiation pattern of some kind, using only a single vertical element? Let's see what happens if we confine all the radials to an arc which spans just 180° of azimuth, instead of the full 360° . Fig 3 shows a vertical antenna (model # 19)

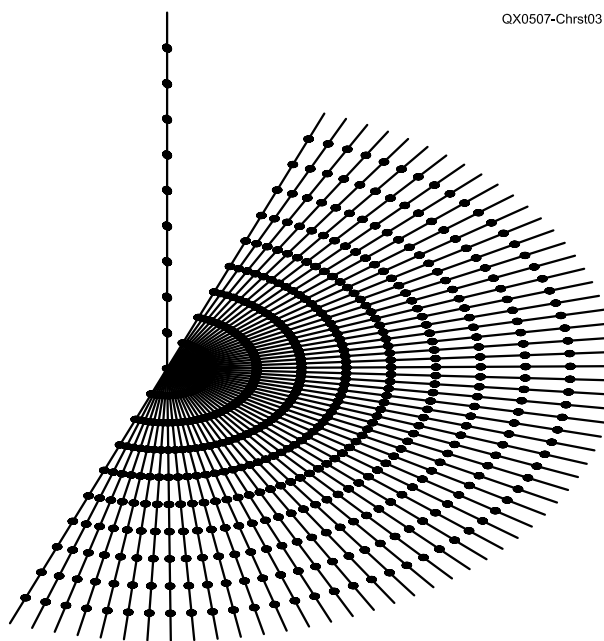


Fig 3—EZNEC representation of a quarter-wave vertical element with an incomplete radial ground system using 61 quarter-wave radials spaced 3° apart. All of the radials are concentrated in the sector to the east of the monopole, extending over an azimuthal range from 0 to 180° . Both the monopole and the radials utilize tapered segment lengths.

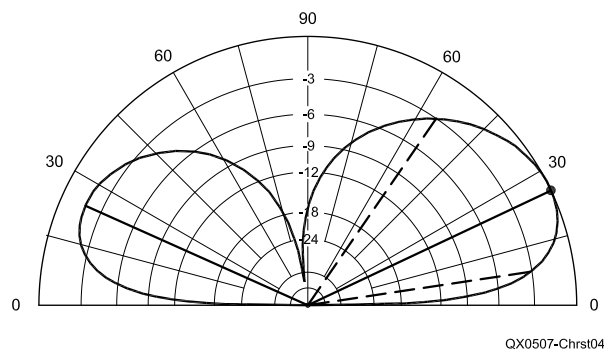


Fig 4—Elevation-plane radiation pattern for the antenna shown in Fig 3. The peak gain is 0.35 dBi at 25° take-off angle. The front-to-back ratio is 1.67 dB and the front-to-side ratio is 0.70 dB.

Table 2
Performance data for ground systems composed of uniform-length, symmetrically-spaced radials. The ground systems are listed in order of increasing antenna gain. Those using a perimeter wire and/or ground rods have been omitted for simplicity.

Model number	Number & length (λ) of radials		Gain and takeoff angle (dBi & deg)		Input impedance (Ω)	Total length of wire (λ)
1	60	0.125	-0.25	24	$45.44 + j18.62$	7.5
2	120	0.125	-0.21	24	$44.79 + j17.48$	15
3	240	0.125	-0.19	24	$44.49 + j17.0$	30
4	30	0.25	0.15	25	$44.15 + j26.07$	7.5
5	60	0.25	0.45	24	$40.45 + j23.72$	15
8	30	0.5	0.46	25	$46.65 + j26.91$	15
6	120	0.25	0.58	24	$38.50 + j22.02$	30
12	30	1.0	0.58	24	$46.25 + j26.74$	30
7	240	0.25	0.63	25	$37.60 + j21.13$	60
9	60	0.5	1.03	26	$43.85 + j26.02$	30
13	60	1.0	1.30	25	$43.25 + j25.50$	60
10	120	0.5	1.39	25	$42.05 + j25.91$	60
11	240	0.5	1.56	26	$40.85 + j26.07$	120
14	120	1.0	1.92	26	$41.52 + j24.99$	120
15	240	1.0	2.33	26	$40.49 + j25.02$	240

whose radials are concentrated entirely in the eastern sector, extending from due north through east to due south. This ground system utilizes 61 quarter-wave radials uniformly-spaced 3° apart in azimuth. Such an arrangement might be contemplated by an operator who doesn't need coverage in all compass directions, or who doesn't have room for a complete 360° ground system. Fig 4 is a plot of the elevation-plane radiation pattern, with the front of the "beam" to the right (due east).

This design yields very little front-to-back or front-to-side ratio, even though there are no radials at all to the west of the vertical element. Table 4 lists the important performance data for the six antennas with 180° ground systems that were examined in this section. In all cases, the peak gain measurement was taken at an azimuth angle of 90°, which bisects the radial-ground screen. Notice that the front-to-back ratio (F/B) and front-to-side ratio (F/S) of these antennas are quite low, less than 3 dB in all cases. For the operator who was hoping for a quick-and-easy "beam" antenna, this is bad news. But, for the ham with a small backyard, or one who is forced by circumstances to place the vertical element at one edge of their property, the good news is that he/she can still make contacts off the "back" of the antenna, even though there are no radials at all in that direction. However, comparing Table 4 with Table 3, it can be seen that, for any particular total length of wire, it is usually possible to get a bit more gain in all directions by installing a complete radial ground screen that covers all 360° of azimuth.

What if we further confine the radials to just 90° of azimuth, instead of 180° as above? Will this work better? Fig 5 illustrates an antenna (model # 25) whose radial ground system is limited exclusively to the northeast quadrant, using 31 quarter-wave radials. For the operator with a really small lot, this allows the antenna to be placed in one of the corners, and maximizes the length of the radials. Fig 6 shows the elevation-plane radiation pattern for this antenna, with the front of the beam to the right (northeast, or an azimuth angle of 45°). The performance data for antennas with six different 90° ground systems is compiled in Table 5. It shows that antennas with single-quadrant radial ground systems provide only a small amount of directivity, with F/B and F/S remaining below 3 dB (as was true earlier with the 180° ground systems). Com-

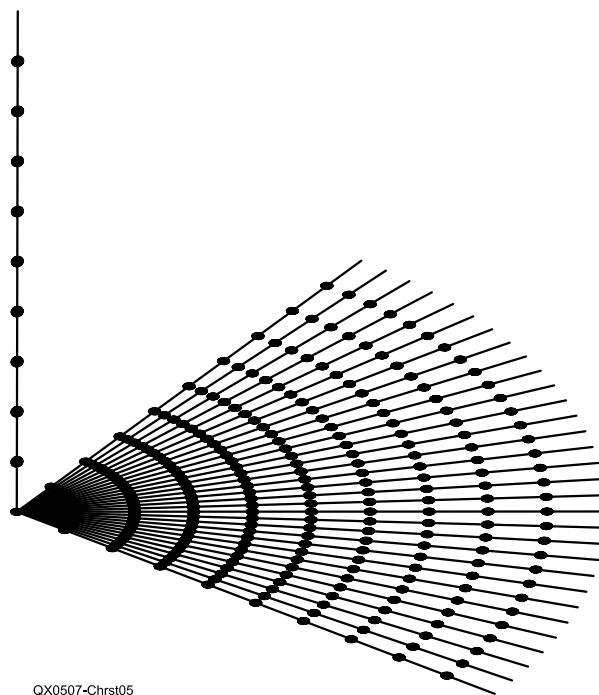


Fig 5—EZNEC representation of a quarter-wave vertical element with an incomplete radial ground system using 31 quarter-wave radials spaced 3° apart. All of the radials are concentrated in the quadrant to the northeast of the monopole, extending over an azimuthal range from 0 to 90°. Both the monopole and the radials utilize tapered segment lengths.

QX0507-Chrst05

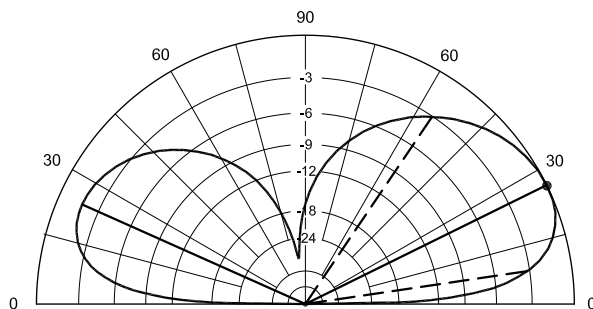


Fig 6—Elevation-plane radiation pattern for the antenna shown in Fig 5. The peak gain is -0.37 dBi at 26° take-off angle. The front-to-back ratio is 1.76 dB and the front-to-side ratio is 0.90 dB.

QX0507-Chrst06

Table 3

Performance data for ground systems composed of uniform-length, symmetrically-spaced radials. The ground systems are listed in order of increasing total wire-length. Again, those utilizing a perimeter wire and/or ground rods have been omitted.

Model number	Number & length (λ) of radials		Gain and takeoff angle (dBi & deg)		Spacing between tips of radials (λ)	Total length of wire (λ)
1	60	0.125	-0.25	24	0.013	7.5
4	30	0.25	0.15	25	0.052	7.5
2	120	0.125	-0.21	24	0.007	15
5	60	0.25	0.45	24	0.026	15
8	30	0.5	0.46	25	0.105	15
3	240	0.125	-0.19	24	0.003	30
6	120	0.25	0.58	24	0.013	30
12	30	1.0	0.58	24	0.209	30
9	60	0.5	1.03	26	0.052	30
7	240	0.25	0.63	25	0.007	60
13	60	1.0	1.30	25	0.105	60
10	120	0.5	1.39	25	0.026	60
11	240	0.5	1.56	26	0.013	120
14	120	1.0	1.92	26	0.052	120
15	240	1.0	2.33	26	0.026	240

paring these results with those in Table 3 reveals that the maximum gain is always less than what could be achieved simply by utilizing a complete radial ground system with the same total length of wire.

To summarize, the use of an incomplete radial ground screen is probably not advisable, since its peak gain is generally lower than the omnidirectional gain produced by a symmetrical system of comparable total wire length. Nevertheless, some operators may desire the modest F/B and F/S achievable with these ground-screens, or perhaps circumstances may force them to place the vertical radiator at the edge or corner of the yard.

Single Vertical Element with Asymmetrical Radial Ground System

Thus far, our computer analysis indicates that it may not be such a good idea to simply omit ground radials in certain azimuthal sectors. So, what if we start out with a completely symmetrical radial ground system, and then augment it in some directions, perhaps by utilizing more radials, or longer radials, or both? Fig 7 is an EZNEC drawing of a vertical antenna (model # 33) whose ground system includes 121 half-wave radials evenly dispersed (1.5° apart) over the eastern 180° azimuthal sector, in conjunction with 29 quarter-wave radials spaced uniformly (6° apart) throughout the western arc. The elevation-plane radiation pattern is displayed in Fig 8, with the nose of the beam to the right (due east, or 90° azimuth). Again, there is very little directivity.

Table 6 lists the important data for the four antennas with asymmetrical ground systems which were examined in this section, given in order of increasing total wire length. The western sector always had 29 quarter-wave radials, evenly-spaced at 6° intervals, while the number or length of the radials in the eastern sector was progressively increased. As the eastern half of the ground system was continuously filled with more wire, the peak gain rose steadily. With a reasonable number of radials directed to the west, however, both F/B and F/S remained quite low, as we might expect, considering the outcome of the earlier computer simulations. To compare these results with those for the completely symmetrical ground systems described initially, we must interpolate between the values given in Table 3, since the total wire lengths are not the same. We find that here,

model # 34 (which utilizes one-wave-length radials) is competitive, when judged in terms of peak gain versus total length of buried wire. However, the remaining three asymmetrical-radial ground systems are inferior to the conventional design.

To continue, let's create some antennas which have ground radials in all four quadrants, but with an augmented number and/or length of ra-

dials in just a single quadrant (the northeast sector in these examples). Fig 9 shows an antenna (model # 36) with 31 half-wave radials (spaced 3° apart) in the northeast quadrant and 89 quarter-wave radials (also spaced 3° apart) dispersed uniformly throughout the remaining three azimuthal quadrants. Fig 10 is the elevation-plane radiation pattern for the antenna, with the front of the

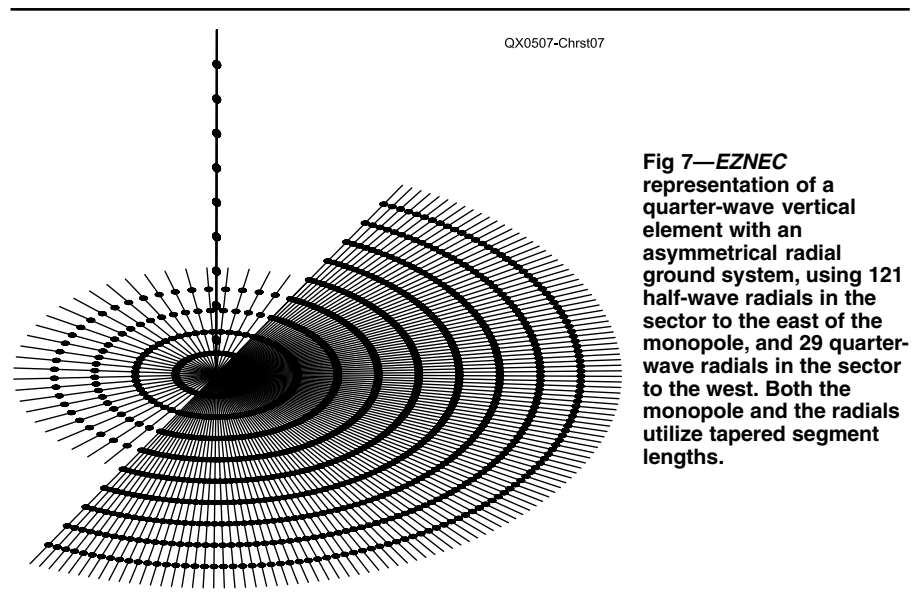


Fig 7—EZNEC representation of a quarter-wave vertical element with an asymmetrical radial ground system, using 121 half-wave radials in the sector to the east of the monopole, and 29 quarter-wave radials in the sector to the west. Both the monopole and the radials utilize tapered segment lengths.

Table 4
Performance data for incomplete radial ground systems. The radials span an azimuthal range of 180° instead of the normal 360°. The ground systems are listed in order of increasing total length of wire.

Model number	Number & length (λ) of radials		Peak gain and takeoff angle (dBi & deg)		F/B (dB)	F/S (dB)	Total length of wire (λ)
19	61	0.25	0.35	25	1.67	0.70	15.25
20	121	0.25	0.44	26	1.73	0.72	30.25
21	61	0.5	0.78	26	1.65	0.66	30.5
22	121	0.5	0.92	26	1.71	0.65	60.5
23	61	1.0	1.42	26	2.42	1.00	61
24	121	1.0	1.84	28	2.78	1.14	121

Table 5
Performance data for incomplete radial ground systems. The radials span an azimuthal range of 90° instead of the normal 360°. The ground systems are listed in order of increasing length of radials and number of radials.

Model number	Number & length (λ) of radials		Peak gain and takeoff angle (dBi & deg)		F/B (dB)	F/S (dB)	Total length of wire (λ)
25	31	0.25	-0.37	26	1.76	0.90	7.75
26	31	0.5	0.01	26	1.70	1.17	15.5
27	31	1.0	0.64	26	2.42	1.82	31
28	91	0.25	-0.24	26	1.88	0.93	22.75
29	91	0.5	0.17	26	1.72	1.18	45.5
30	91	1.0	1.13	29	2.80	2.11	91

beam to the right (northeast, or 45° azimuth). As can be seen, this particular design has almost no front-to-back ratio at all. Table 7 summarizes the performance information for the four antennas under review in this section, with the data listed in order of increasing total wire length. The 270° sector that extends from northwest to southwest to southeast always has 89 radials (uniformly spaced at 3° intervals) whose length is either 0.125 or 0.25 λ . The northeast quadrant usually contains 31 radials, except in the final case, where the number was raised to 91; the length of these radials varies from 0.25 to 1.0 λ . As expected, the peak gain increases as more wire is added to the ground system, but the F/B and F/S are always quite low. If we compare this table with Table 3 (where the radial ground systems are totally symmetrical), we find a mixed bag of results. For models # 35 and 36, a conventional ground system with symmetrical radials can provide more gain using less wire, but the reverse is true for models # 37 and 38, which are now actually superior to comparable antennas using traditional symmetrical radial-ground systems. Notice that both of these “superior” ground systems utilize 31 or more one-wavelength radials in the augmented quadrant.

In summary, an asymmetrical radial-ground screen may be just the ticket if you’re looking for a bit of extra gain in a specific direction, or have a backyard with an unusual shape. But, as the tables show, some configurations are more desirable than others, so exercise caution. The limited amount of computer simulation reviewed here indicates that a sector containing very long (one wavelength or more) radials may prove to be advantageous.

Single Vertical Element with Mesh-type Ground System

Now let’s examine some antennas which utilize a mesh or grid-type ground-screen, rather than radials. Fig 11 shows an antenna (model # 39) with a mesh-style ground system in which each small square within the grid has a side-length of 3 feet (0.0116 λ) while the overall ground-screen measures approximately 0.5 λ on each side. Fig 12 is the elevation-plane radiation pattern when viewed through a corner of the ground-grid (northeast is to the right). Table 8 gives the results for the two mesh-style ground systems that were modeled. Notice that a square ground-screen is not symmetrical with respect

to azimuth angle. In other words, the ground screen looks different when viewed through a corner than it does when viewed through one of the sides. As a result, two values will be quoted for the gain of each antenna. The larger ground-screen utilizes more than twice as much wire as the smaller one, and provides about 0.4 dB of additional gain.

Mesh-type ground systems were not studied extensively because they are inferior to conventional radial-ground systems of equal size. First consider model # 6 (with 120 uniformly-spaced quarter-wave radials) which uses 30 λ of wire to produce

0.58 dBi of gain in all directions, versus model # 39, which uses 50% more wire (45 λ) to achieve virtually the same performance on a similarly sized plot of land. Further, model # 10 (with 120 symmetrically disposed half-wave radials) uses 60 λ of wire to generate 1.39 dBi of omni-directional gain, while model # 40 requires 106 λ of wire to yield a peak gain of only 1.03 dBi, and occupies a similar amount of acreage.

Before completely abandoning mesh-style ground systems, I decided to change the position of the vertical monopole, moving it first to the middle of one edge of the ground-

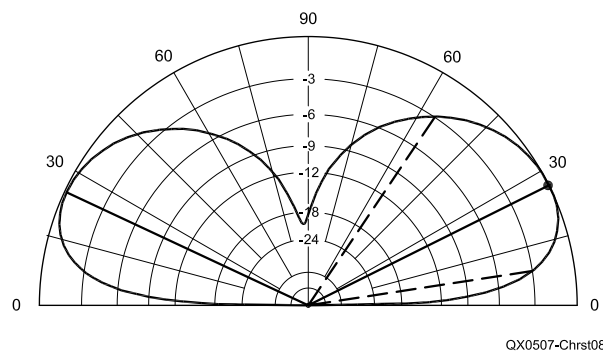


Fig 8—Elevation-plane radiation pattern for the antenna shown in Fig 7. The peak gain is 1.14 dBi at 26° take-off angle. The front-to-back ratio is 0.29 dB and the front-to-side ratio is 0.09 dB.

QX0507-Chrst09

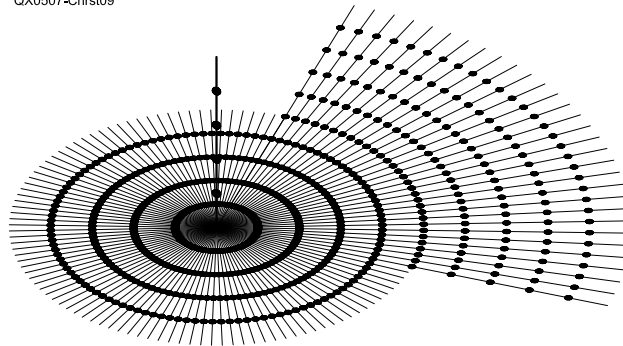
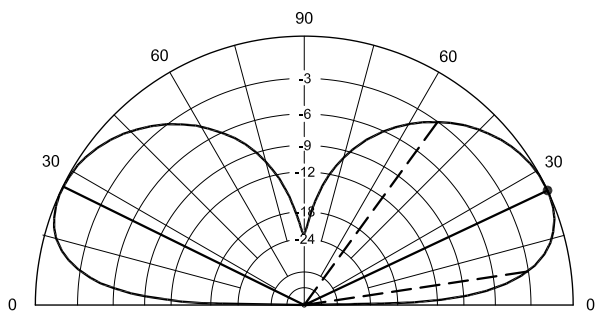


Fig 9—EZNEC representation of a quarter-wave vertical element with an asymmetrical radial ground system, using 31 half-wave radials in the northeast quadrant, and 89 quarter-wave radials spread over the remaining 3 quadrants. Both the monopole and the radials utilize tapered segment lengths.

Table 6

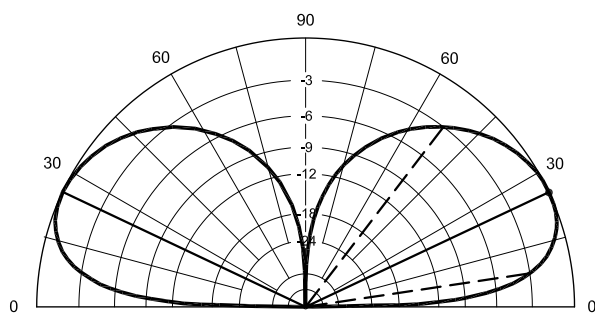
Performance data for asymmetrical radial ground systems. The radials in the eastern 180° sector are different in length and/or spacing from those in the western 180° sector, which always utilizes 29 0.25- λ radials spaced 6° apart. The ground systems are listed in order of increasing total length of wire.

Model number	Number & length (λ) of radials (eastern)		Peak gain and takeoff angle (dBi & deg)		F/B (dB)	F/S (dB)	Total length of wire (λ)
31	61	0.25	0.60	25	0.16	0.08	22.5
32	121	0.25	0.67	25	0.25	0.12	37.5
33	121	0.5	1.14	26	0.29	0.09	67.75
34	121	1.0	2.07	27	1.36	0.59	128.25



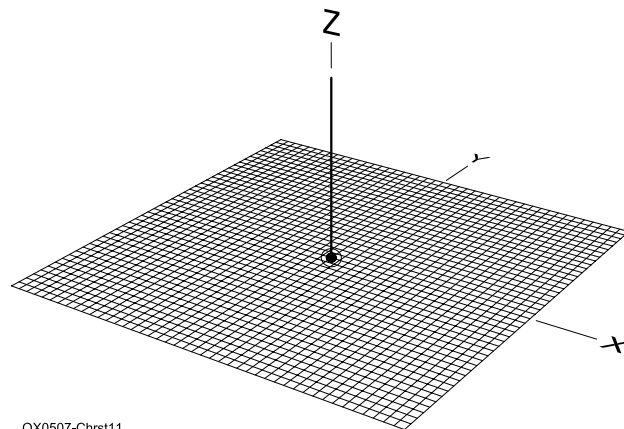
QX0507-Chrst10

Fig 10—Elevation-plane radiation pattern for the antenna shown in Fig 9. The peak gain is 0.94 dBi at 26° take-off angle. The front-to-back ratio is 0.01 dB and the front-to-side ratio is 0.28 dB.



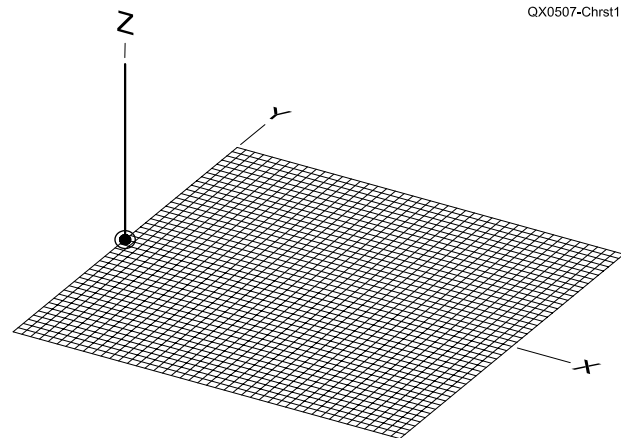
QX0507-Chrst12

Fig 12—Elevation-plane radiation pattern for the antenna shown in Fig 11. The peak gain, off the corners of the ground system, is 0.62 dBi at 25° take-off angle. The gain off the sides of the ground-screen is 0.57 dBi at the same elevation angle.



QX0507-Chrst11

Fig 11—EZNEC representation of a quarter-wave vertical element with a mesh- or grid-type of ground-screen. Each small square within the mesh is 3 feet on a side, while the overall ground-screen has side-lengths of about 0.5 λ . In this drawing, the wire-segmentation dots have been omitted for clarity.



QX0507-Chrst13

Fig 13—EZNEC representation of a quarter-wave vertical element with a mesh- or grid-type of ground-screen. Each small square within the mesh is 3 feet on a side, while the overall ground-screen has side-lengths of about 0.5 λ . In this drawing, the wire-segmentation dots have been omitted for clarity. Note that the vertical monopole has been placed at the center of the left (western) edge of the ground-screen.

screen, and then into one of the corners. These two scenarios are shown in Fig 13 (model # 41) and Fig 14 (model # 42) respectively. In both cases the small squares are 3 feet on a side, while the overall ground-screen is about 0.5 λ per side (same ground-screen as model # 39). Note that model # 41 achieves its maximum gain firing due east, while # 42 fires northeast. Table 9 gives the results. The outcome is extremely poor when the vertical radiator is positioned in a corner of the ground-grid, following the trend that was seen earlier with incomplete single-quadrant radial ground systems. Once again, a conventional symmetrical radial-ground system, using much less wire (see Table 3), works better than either of these mesh-style designs.

Table 7

Performance data for asymmetrical radial ground systems. The radials in the north-eastern 90° quadrant are different in length and/or spacing from those in the remaining 270° sector. The ground systems are listed in order of increasing total length of wire. NE = northeast quadrant, R = remaining 270° sector, including northwest, southwest and southeast quadrants.

Model number	Number of radials	Length (λ)	Peak gain and takeoff angle (dBi & deg)	F/B (dB)	F/S (dB)	Total length of wire (λ)
35	NE 31	0.25	0.25 25	0.42	0.26	18.88
	R 89	0.125				
36	NE 31	0.5	0.94 25	0.01	0.28	37.75
	R 89	0.25				
37	NE 31	1.0	1.58 25	0.73	0.94	53.25
	R 89	0.25				
38	NE 91	1.0	1.97 28	1.07	1.21	113.25
	R 89	0.25				

Single Vertical Element with Parallel-wire Ground System

Instead of arranging the ground wires in a mesh configuration, let's position them parallel to each other, as shown in Fig 15 (model # 43). Here the ground screen includes two "bus wires," each a quarter-wave long, extending directly north and south of the vertical monopole, to which are attached a total of 45 quarter-wave wires. All 45 of these parallel wires extend directly eastward from the two bus wires, and are spaced 3 feet (0.0116 λ) apart. Note that there are no ground wires located to the west

of the vertical element. The principal elevation-plane radiation pattern, as displayed in Fig 16, exhibits a small amount of directivity (east is to the right). Table 10 lists the performance data for the three antennas with incomplete parallel-wire ground-screens that were studied. The only variable was the length of the 45 parallel wires. In all cases the maximum F/B and F/S are less than 3 dB, and the peak gain values are well below those obtainable from classical symmetrical-radial ground systems (as shown in Table 3). By this time we have come to expect that antennas with incomplete ground

systems will not generate much gain, and this hypothesis has been confirmed yet again.

Now let's extend the parallel wires to both the east and west sides of the vertical monopole, as illustrated in Fig 17 (model # 46). Table 11 shows what happens when we utilize complete ground systems by extending the 45 parallel wires an equal distance to both the east and west of the vertical monopole. In a series of steps, the overall length of these wires is increased from 0.5 to 2 λ . Since these ground-screens are now symmetrical to the east and west, the gain is the same in both directions, leading to zero F/B. As can be seen, the F/S is also quite low. Comparison with Table 3 reveals that a traditional symmetrical-radial ground system, with a similar total length of wire, can easily generate more gain than any of these parallel-wire ground-screens.

Table 8

Performance data for mesh- or grid-type ground systems. Each ground screen is composed of many small squares of wire. The ground systems are listed in order of increasing total length of wire.

Model number	Ground screen square (ft/side)	Dimensions overall (λ /side)	Corner Side	Peak gain and takeoff angle (dBi & deg)	Total length of wire (λ)
39	3	0.5	Corner	0.62 25	45
			Side	0.57 25	
40	5	1.0	Corner	1.03 26	106
			Side	0.96 26	

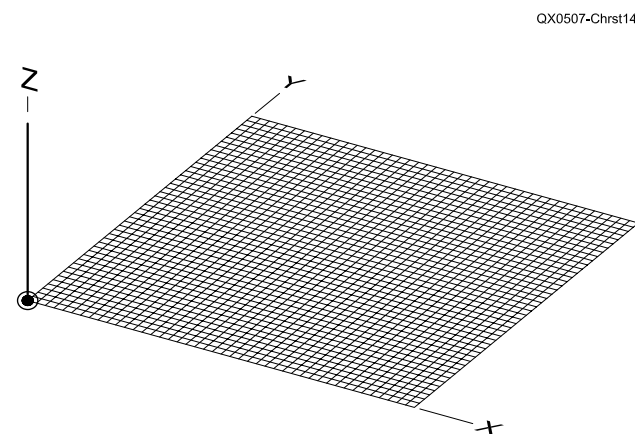
Table 9

Performance data for mesh- or grid-type ground systems in which the vertical monopole is located away from the center of the ground-grid. In each case the ground screen is composed of many small "squares" of wire that are 3 feet on a side, while the overall ground system is about 0.5 λ on a side.

Model number	Location of vertical monopole on ground screen	Peak gain and takeoff angle (dBi & deg)	F/B (dB)	F/S (dB)	Total length of wire (λ)
41	western edge	0.35 27	1.54	0.96	45
42	southwest corner	-0.55 27	1.74	1.18	45

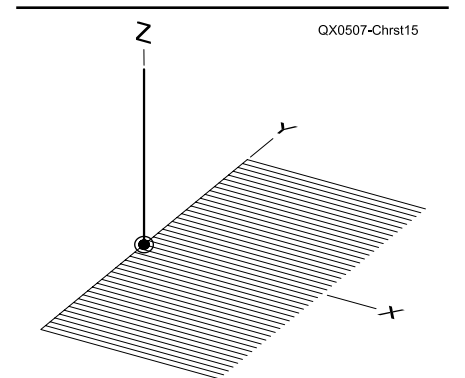
Single Vertical Element with Hybrid Ground System

I decided to see what would happen if I simulated a ground system that was a combination of both conventional radials and parallel wires, as shown in Fig 18 (model # 49). I began with a classical ground-system using 120 quarter-wave radials, all symmetrically spaced around the base of the vertical monopole. Then I removed the 59 radials that lay to the west of the vertical element. This left 61 radials, forming an incomplete



QX0507-Chrst14

Fig 14—EZNEC representation of a quarter-wave vertical element with a mesh- or grid-type of ground-screen. Each small square within the mesh is 3 feet on a side, while the overall ground-screen has side-lengths of about 0.5 λ . In this drawing, the wire-segmentation dots have been omitted for clarity. Note that the vertical monopole has been placed at the front-left (south-western) corner of the ground-screen.



QX0507-Chrst15

Fig 15—EZNEC representation of a quarter-wave vertical element with an incomplete parallel-wire ground screen. There are two quarter-wave bus wires extending directly to the north and south from the base of the monopole. To these wires are attached 45 parallel wires, which extend in an easterly direction. These 45 wires are spaced 3 feet apart, and their length is 0.25 λ . In this drawing, the wire-segmentation dots have been omitted for clarity. Note that the vertical monopole is located at mid-point of the left (west) edge of the ground-screen.

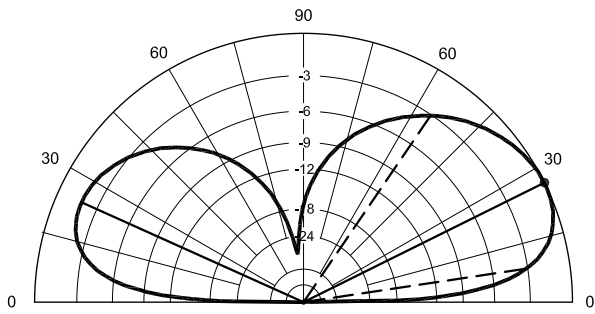
ground system whose maximum north-south dimension was 0.5λ , but only 0.25λ from east to west.

Next, I added a set of 61 parallel wires, each a quarter-wave long, with their spacing adjusted so they would all fit within the existing ground-system dimensions of 0.5λ north-south by 0.25λ east-west. This spacing turned out to be 2.16 feet, or about 0.0084λ . To finish the model, I joined each parallel wire to its corresponding radial and trimmed off the ends, as necessary, to remove any excess. Only the due north and due south

Table 10

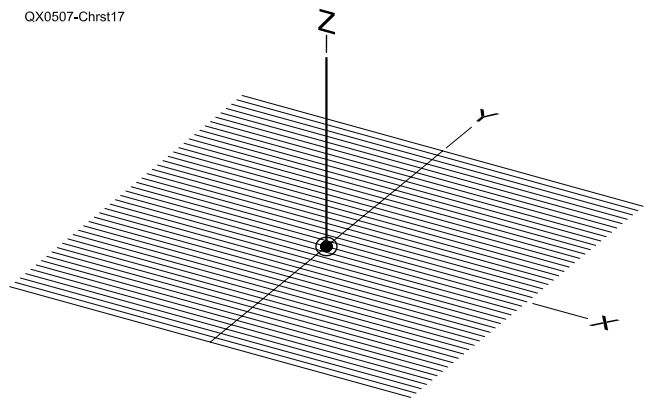
Performance data for unidirectional parallel-wire ground systems, in which the vertical monopole is located at the center of the western edge of the ground-screen. The north-south dimension of the screen is held constant at 0.5λ , and there are 45 parallel wires, spaced 3 feet apart, running east-west. The ground systems are listed in order of total wire length.

Model number	Length of the 45 parallel wires (λ)	Peak gain and takeoff angle (dBi & deg)		F/B (dB)	F/S (dB)	Total length of wire (λ)
43	0.25	-0.74	26	1.60	0.83	11.75
44	0.5	-0.36	26	1.54	1.27	23
45	1.0	0.15	28	2.14	1.78	45.5



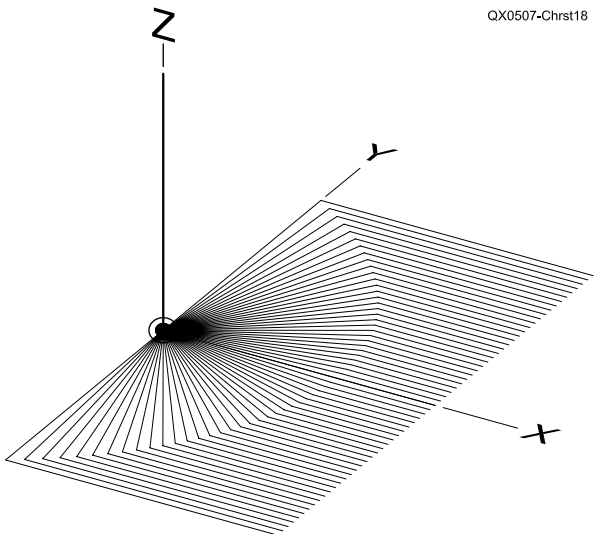
QX0507-Chrst16

Fig 16—Elevation-plane radiation pattern for the antenna shown in Fig 15. The peak gain, directly east, is -0.74 dBi at 26° take-off angle. The front-to-back ratio is 1.60 dB and the front-to-side ratio is 0.83 dB.



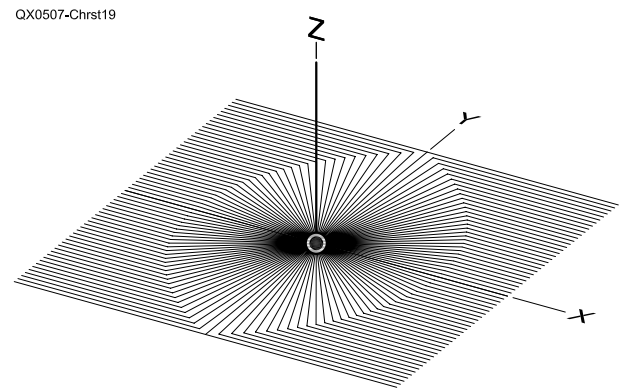
QX0507-Chrst17

Fig 17—EZNEC representation of a quarter-wave vertical element with a symmetrical parallel-wire ground-screen. There are two quarter-wave bus wires extending directly to the north and south from the base of the monopole. To these wires are attached 45 parallel wires, which extend toward both the east and the west. These 45 wires are spaced 3 feet apart, and their end-to-end length is 0.5λ . In this drawing, the wire-segmentation dots have been omitted for clarity.



QX0507-Chrst18

Fig 18—EZNEC representation of a quarter-wave vertical element with an incomplete hybrid ground-screen. There are 61 wires that begin as true radials, but eventually they bend to form a set of parallel wires (spaced 2.16 feet apart) that are oriented in an east-west fashion. The overall dimensions of the ground-screen are 0.5λ from north to south and 0.25λ from east to west. Notice that the vertical element is positioned in the middle of the western edge of the ground-screen. In this drawing, the wire-segmentation dots have been omitted for the sake of clarity.



QX0507-Chrst19

Fig 19—EZNEC representation of a quarter-wave vertical monopole with a complete hybrid ground-screen. There are 120 true radials that eventually bend to form two sets of parallel wires (spaced 2.16 feet apart) that are oriented in an east-west manner. The overall dimensions of the ground-screen are 0.5λ by 0.5λ , and the vertical element is positioned in the middle of the ground-screen. The wire-segmentation dots have been omitted for clarity.

radials (and the northern-most and southern-most parallel wires) remained at their original lengths, while all the other wires had to be truncated to some extent.

Table 12 lists the results of this series of tests, in which the east-west dimension of the ground-screen was expanded in a series of steps from 0.25 to 1.0 λ . This was accomplished simply by lengthening the 61 parallel wires, while the total north-south dimension of the ground system was held constant at 0.5 λ . The peak gain increases as the ground wires are made longer, but all of these systems yield only a modest amount of rejection to the back and sides. Comparing the data from this table with that of Table 3 (and using interpolation), we find that a traditional radial-ground system can always provide a bit more gain from the same total length of wire.

To finish this section, I added 61 bent ground wires that extend to the west of the vertical monopole for a distance of 0.25 λ , as illustrated in Fig 19 (model # 52). Now the antenna has a complete hybrid ground system. I kept the western portion of the ground-screen constant as shown in the figure, but once again I varied the overall length of the east wires, as was done previously. Table 13 displays the outcome of this procedure. Since model # 52 has a ground-screen that is symmetrical to the east and west, it has no front-to-back ratio. Surprisingly, model # 53, which has an extended ground-screen to the east, actually produces more gain to the west (!) resulting in a negative F/B. When we look back at Table 3, we find (as usual) that these antennas with hybrid ground-screens yield less gain than a classical ground system with symmetrical radials.

Conclusions

For a vertical antenna utilizing just a single element, it appears that a conventional ground system, composed of equal-length uniformly-spaced radials, can provide the most gain for a given total length of wire. However, computer simulation indicates that some combinations of radial length and number of radials are far superior to others. The only exception to this general rule was found for selected examples of asymmetrical radial-ground systems in which the radials in one azimuthal sector were extended to at least one wavelength. The use of perimeter wires (which join the outer tips of adjacent radials together) and/or ground rods at the tips

Table 11

Performance data for symmetrical parallel-wire ground systems, in which the vertical monopole is located at the center of the ground-screen. The north-south dimension of the screen is held constant at 0.5 λ , and there are 45 parallel wires, spaced 3 feet apart, running east-west. The ground systems are listed in order of total wire length. Since these ground-screens are symmetrical, there is zero front-to-back ratio.

Model number	End-to-end Length of the 45 parallel wires (λ)	Peak gain and takeoff angle (dBi & deg)		F/S (dB)	Total length of wire (λ)
46	0.5	-0.58	25	0.24	23
47	1.0	0.17	26	1.13	45.5
48	2.0	0.60	27	1.54	90.5

Table 12

Performance data for incomplete hybrid ground systems, in which the vertical monopole is located at the center of the western edge of the ground-screen. The north-south dimension of the screen is held constant at 0.5 λ , and there are a total of 61 ground wires. Each wire begins in a radial fashion, and then bends so that it extends east-west. The ground systems are listed in order of increasing total wire length.

Model number	East to west dimension of the ground screen (λ)	Peak gain and takeoff angle (dBi & deg)		F/B (dB)	F/S (dB)	Total length of wire (λ)
49	0.25	0.58	26	1.78	0.84	23
50	0.5	0.82	26	1.68	1.27	38.25
51	1.0	1.34	29	2.29	1.79	68.75

Table 13

Performance data for complete hybrid ground systems, in which there are ground wires both to the east and the west of the vertical monopole. The north-south dimension of the screen is held constant at 0.5 λ , while the "east" dimension of the screen is varied. Each wire begins in a radial fashion, and then bends so that it extends east-west. The ground systems are listed in order of increasing total wire length.

Model number	East to west dimension of the ground screen (λ)	Peak gain and takeoff angle (dBi & deg)		F/B (dB)	F/S (dB)	Total length of wire (λ)
52	0.25	0.71	24	0	0.19	45.5
53*	0.5	1.09	26	-0.03	0.63	60.75
54	1.0	1.57	27	0.56	1.12	91.25

*This ground screen is highly unusual in that it exhibits more gain toward the west, where the ground-wires are shorter, than it does toward the east, where the ground-wires are longer. For this reason, the F/B is negative!

of radials, appears to be unnecessary, because they add very little gain. Incomplete ground-screens, in which one or more azimuthal sectors contain no radials at all, are certainly usable and can provide modest F/B and F/S. However, a complete ground system is generally preferable. Configurations such as meshes appear to be noncompetitive in terms of gain, when compared to ground-screens utilizing radials.

Al Christman, K3LC, has a PhD in electrical and computer engineering from Ohio University and is currently serving as a professor in the EE department of Grove City College in Western Pennsylvania. First licensed as WA3WZD in 1974, Al is an active DXer with honor-roll status on 20-meter SSB. You can contact Al at Grove City College, 100 Campus Dr, Grove City, PA 16127-2104. □□

A Blind Automatic Frequency Control Algorithm for Single Sideband

The author provides an effective method of autotuning and AFC functionality for SSB reception.

By Gary A. Geissinger, WA0SPM

Abstract

The state of the art in Amateur Radio single-sideband, suppressed-carrier (SSB) communications is advancing along several lines. Highly stable, well-calibrated transceivers, such as the ICOM IC-7800, are now becoming available to the amateur operator. These require no frequency adjustment during a QSO when similar quality rigs are on both ends of an HF link. Another trend is toward low cost QRP transceivers. With low cost sometimes comes the penalty of poor frequency stability and accuracy. Since maximum intelligibility occurs when transmit and receive fre-

quencies are matched, the receiving operator is sometimes forced to “chase” the signal as there are changes in temperature or supply voltage. It is interesting to note that rigs at both ends of the price / performance spectrum rely on software for functionality. The automatic frequency control approach presented here is applicable to any transceiver that contains reasonable computing horsepower.

SSB automatic frequency control (AFC) has been around for years on commercial radio circuits using a transmitted pilot carrier or tone. As the receiver and transmitter drift apart the tuning error is detected and compensated for in the receiver. While this approach is perfectly fine on commercial channels, it is unacceptable in the ham bands; all we need are more carriers to contend with...especially on 40 meters!

After I did my research on this topic and wrote the first draft of this article, I found out about a previous article in *QEX* on this topic. It is an excellent article written by Robert Dick that appeared in the Jan/Feb 1999 issue of *QEX*. While both articles use DSP to look at the spectral content of SSB voice signals, the mathematical algorithms are different and are derived differently. If you decide to give this a try, it might be fun to code up both algorithms and compare them. The moral of the story is that when you do research on communications—check *QEX* first!

Blind Optimization

The algorithm presented here is “blind”; that is, it depends on the statistics of the data rather than the explicit knowledge of an error through the use of a reference channel or sig-

DigitalGlobe Incorporated
1601 Dry Creek Dr, Suite 260
Longmont, CO 80501
ggeissinger@digitalglobe.com

nal. For CW, RTTY, PSK31, and other digital modulation formats that can be transmitted using a SSB transmitter there is no need for a blind optimization. The signals themselves provide the necessary reference information. Good examples are the automatic tuning feature in the ICOM IC-7800 and the AFC feature present in most PSK31 demodulators. Voice modulation doesn't provide a reference signal per se; additional processing is required to obtain the information required for AFC functionality.

Vowels—The Necessary Modulation Needed for AFC

A number of different types of sounds are created while speaking. These include vowels, consonants, breath sounds, then of course there is the silence between words. The algorithm described here depends upon vowel sounds and consonants that are

voiced. Vowel sounds are those continuous sounds that originate with the vocal cords and then are filtered by the vocal tract. The fundamental frequency is set by the vocal cords. The shape and adjustment of the vocal tract determines which vowel is spoken by altering the amplitude of the various harmonics.

The fundamental frequencies that are generated by an adult speaker fall into six overlapping ranges depending upon the physical properties of the larynx and vocal cords. As a general rule the spoken voice is at a frequency that is roughly twice that of the lowest fundamental possible for a given speaker. Using this and a tolerance of 50% to account for differences in individual voices, the spoken vowel fundamental frequency ranges are listed in Table 1.

Both even and odd harmonics are present at the larynx. The amplitude

of the harmonics decreases at a rate of about 12 dB per octave. The harmonics are present up to 4000 Hz, after which their amplitudes are severely attenuated.¹ Fig 1 gives an example of a male voice with a 160 Hz fundamental with no formant filtering.

In this example all of the harmonics are present at the larynx with a smoothly decreasing amplitude contour. The formant filters present in the human vocal tract alter this contour to produce different vowels sounds. A better example of the input signals of interest is shown in Fig 2 that gives the spectral analysis of a 155 Hz "ah" vowel in a bass-baritone voice.

While the harmonic sequence of the 155 Hz "ah" vowel is very similar to the analytical example in Fig 1, the primary difference between the two figures lies in the relative amplitudes of the vari-

¹Notes appear on page 44.

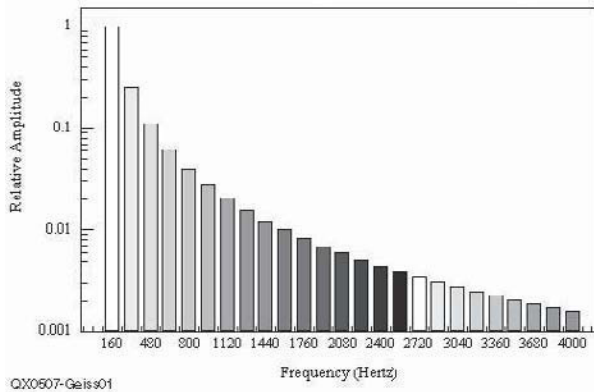


Fig 1—Harmonic series for a 160 Hz fundamental.

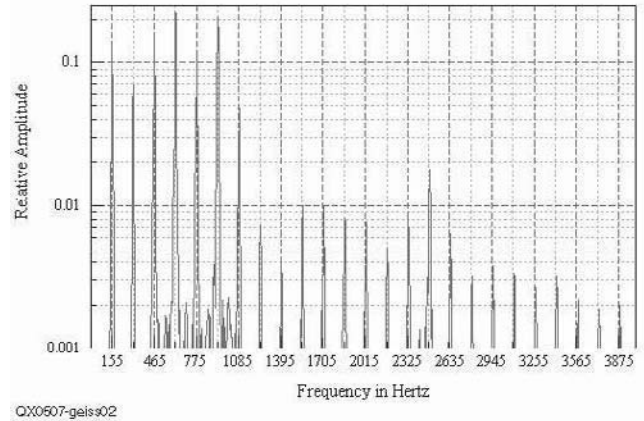


Fig 2—155 Hz "ah" Vowel.

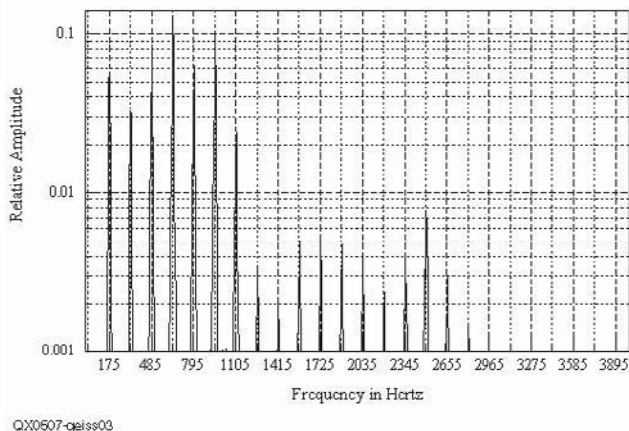


Fig 3—155 Hz "ah" Vowel with +20 Hz tuning error.

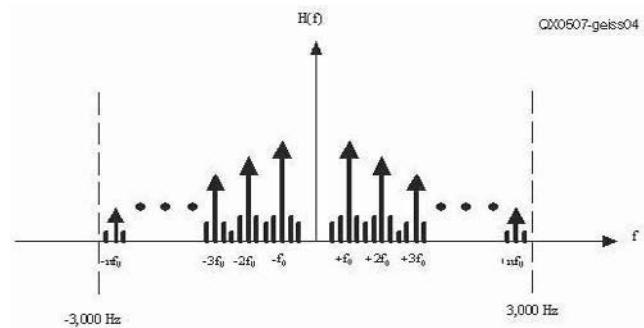


Fig 4—Fourier transform of vowel with side lobes.

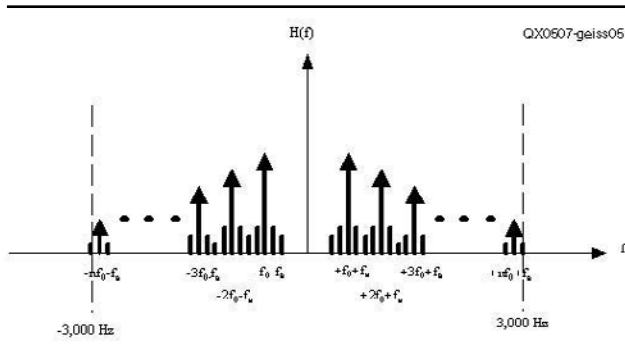


Fig 5—Vowel with side lobes subject to a tuning error.

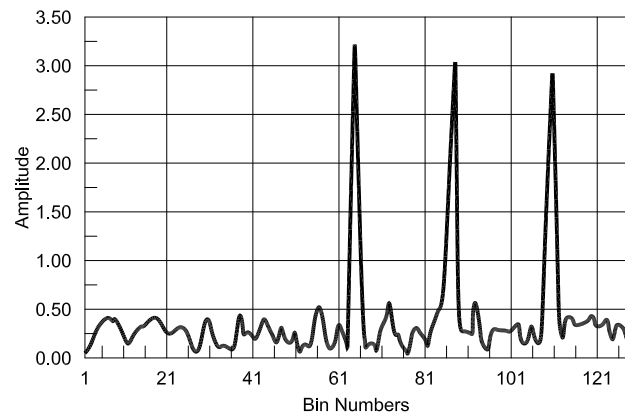


Fig 7—123.45 Hz vowel in frequency domain.

ous harmonics. In this figure there is some extraneous low amplitude noise from about 450 Hz to 1000 Hz. This was caused by a noise source present in the room during data acquisition and therefore should be ignored.

A Tuning Error Considered

SSB transmitters and receivers translate the modulation to the RF channel frequency and back through the process of mixing. This process moves the fundamental and harmonics as an ensemble; their relative spacing in frequency terms remains intact. Fig 3 shows an “ah” vowel at 155 Hz that has been received with a +20 Hz tuning error.

The invariant structure of the fundamental and harmonics is the key to the blind AFC algorithm...well, maybe not the fundamental. Most SSB communications occur with an audio passband from 300 Hz to 3,000 Hz. For many hams the fundamental is filtered out leaving only the harmonics in the transmitted sideband signal.

The Blind AFC Algorithm

The approach taken here is based on the application of digital signal processing techniques. As a result, all of the algorithms described here operate on

sampled data. No modification of the radio was required during the development and test; the audio output from the receiver was sampled and converted to digital words by an A/D converter and then processed by the DSP system. The tuning errors could then be corrected using the computer control interface present in the receiver or transceiver. Clearly a radio manufactured using this approach could embed all of the required circuitry and firmware directly into the radio. Many details in the DSP realization have been omitted for clarity. Describing processing steps such as moving between complex and real representations doesn't aid in understanding the basic algorithm. One additional comment: Numerous algorithms for each step were tested. The ones described here are the easiest to visualize and yield adequate performance.

Step One—Conversion to Frequency Domain

The receiver audio that is sampled by an A/D converter yields a time series of discrete signal amplitudes. Various sample rates, A/D resolutions, and windowing functions were tried in a process that could be the topic of an article by itself. A brief description of the system engineering aspects of those

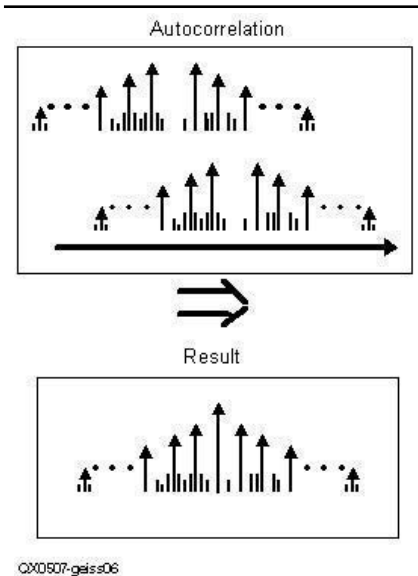


Fig 6—Example of vowel autocorrelation.

parameters is presented later. Since the AFC algorithm is interested in frequency errors, it is necessary to change the signals from time domain to the frequency domain. In this case a Discrete Fourier Transform in the form of the Fast Fourier Transform (FFT) algorithm was selected to perform the transformation. The FFT routine is used as a part of later computations as well. Keep in mind that other algorithms may be more efficient in practice, since the entire sampled bandwidth is not necessarily needed for the AFC algorithm. The result of an FFT is shown in Fig 4. The fundamental frequency and harmonics are notated on the figure. If a tuning error is present, it can be seen in the Fourier Transform as well.

Step Two—Determine the Fundamental Frequency

From the comparison of Figs 4 and 5 it is clear that the fundamental frequency can be recovered from the data even if it is not present or has been displaced by a tuning error. The fundamental frequency exists in the spacing between the energy maxima in the frequency domain. This makes some samples in the frequency domain correlated with others—this is called autocorrelation. Computing the autocorrelation can be very useful in identifying periodic signals^{2,3} and their characteristics. Keep in mind that the periodic signal in this case is in the frequency domain (the fundamental and its harmonics). An autocorrelation is defined by:

$$z(k) = \sum_{i=1}^n g(i)g(k+i) \quad (\text{Eq 1})$$

The spectral lines slide across each other as the index i changes. The only significant products present in the result are from multiplying two spectral lines together. Fig 6 diagrams this process.

It is inefficient to compute auto-correlations in this way—FFTs are generally used instead. Brigham outlines a method of computing correlations using only forward FFTs:⁴

$$\text{AutoCorr}(g, g)_j = \text{FFT}(G_K G_K^*)^* \quad (\text{Eq 2})$$

Consider a 123.45 Hz target vowel that has a -32.45 Hz offset as shown in Fig 7. The harmonic structure is evident in the sample, but the harmonics are shifted by the offset frequency. In addition, the noise amplitude is significant. After the sample sets are passed through the autocorrelation function, the noise amplitude drops markedly. As can be seen in Fig 8A, in addition to the reduction in noise, the fundamental harmonics start cleanly at the correct frequency. As expected, the autocorrelation removes the offset.

The harmonic structure is evident in the sample, but the harmonics are shifted by the offset frequency (bin number). As can be seen in Fig 8B, in addition to the reduction in noise, the harmonics start cleanly at the 0 frequency (bin 2049). The autocorrelation removes the offset as expected.

The placement of the second peak yields the fundamental frequency of the vowel with reasonable precision. Better numerical precision is gained if regression analysis is performed on the ensemble of peaks present in the autocorrelation. Armed with the vowel center frequency it is now possible to find the tuning error.

Other algorithms for finding the vowel fundamental were tried as well. Iterative techniques, in which one searches for the correct vowel frequency by “sliding dot products” using a reference vowel simulator worked well too; however, they were very slow. Only by constraining the search by the (guessed at) frequency range of the speaker did the processes run at a reasonable rate.

Step Three—Determination of the Tuning Error

Several possible algorithms immediately come to mind. Now that the fundamental frequency is known, one can simply compare the frequency domain peaks of the original data with those found in the autocorrelation; after some computation, taking differences will yield the tuning error.

Rather than performing the com-

parison in an inelegant fashion as described above, the correlation process was employed:

$$\text{Corr}(g, h)_j \Leftrightarrow G_K H_K^* \quad (\text{Eq 3})$$

An iterative approach also seemed like a possibility. A set of simulated data at the correct frequency was generated, with the offset (tuning error) frequency adjustable as a parameter. The correlation was then computed and maximized using a gradient search. A gradient algorithm provides a means to find the maximum of the curve. The gradient algorithm used to find a function maximum is:

$$x_{i+1} = x_i + g f'(x_i) \quad (\text{Eq 4})$$

where g is the “gain” or a constant used to prevent over-estimation of the function maximum.⁵

In the final version of the test software, the gradient search was used to “fine tune” the results from one of the first two algorithms.

System Engineering Aspects of the Design

The algorithms developed here are based on digital signal processing techniques using sampled data. The selection of the sampling interval, number of samples per ensemble, quantization

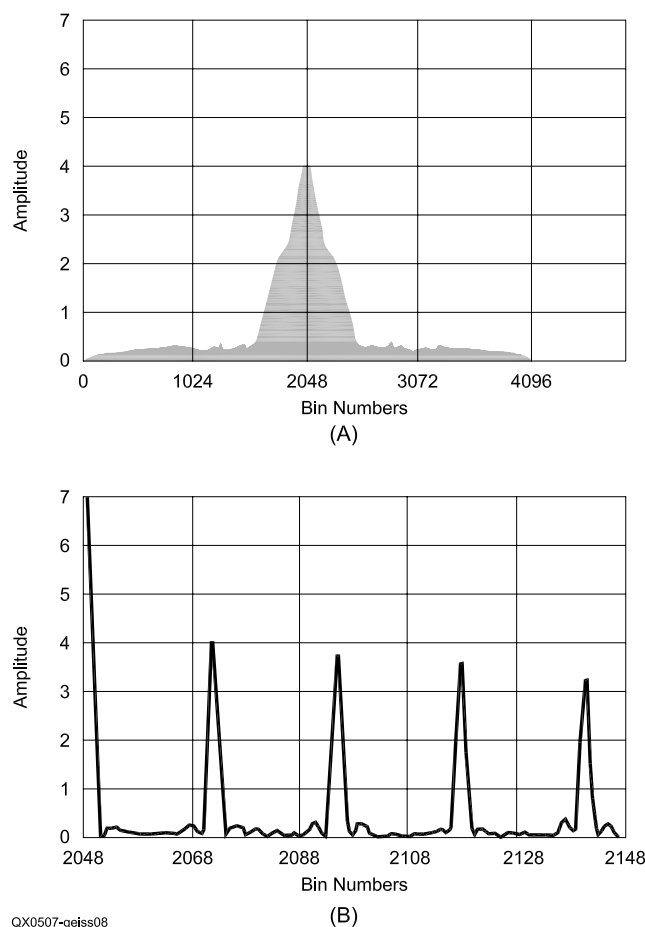


Fig 8—Autocorrelation of 123.45 Hz vowel in frequency domain.

Table 1—Spoken Vowel Fundamental Frequency Ranges

Voice Range	Classification	Frequency Range
Highest Female	Soprano	246.94-493.88 Hz
Most Probable Female	Mezzo-Soprano	207.65-415.30 Hz
Lowest Female	Contralto	185.00-370.00 Hz
Highest Male	Tenor	146.93-293.66 Hz
Most Probable Male	Baritone	92.50-185.00 Hz
Lowest Male	Bass	87.31-174.62 Hz

level, and numerical precision are driven by a number of factors. Each factor is described separately.

The length of vowels in time drives the total time span allowed for a data ensemble. The algorithms here are batch processes assuming that vowels are stationary for the duration of an ensemble. The exact duration of vowels depends upon the speaker, the language being spoken, and the dialog content. The assumption is that vowels will have a duration of between $\frac{1}{5}$ and $\frac{1}{20}$ of a second. This limits the time duration of a data ensemble to $\frac{1}{5}$ of a second or less.

Another constraint on the number of samples in an ensemble is the frequency resolution of the Fast Fourier Transform (FFT) algorithm itself. The goal is to keep the combined tuning error under 20 Hz. This implies that the bin spacing of the FFT should be less than 20 Hz with adequate margin.

Tight frequency resolution requirements tend to drive toward FFT based computations with a large number of bins. The computational capability of a typical personal computer (PC) must also be considered. Large numbers of complex computations, such as FFTs, can seriously affect the throughput of a PC. This limitation forces the FFT to have a minimum number of bins to meet the given frequency resolution requirement.

Since the highest frequency present at the output of a SSB demodulator is about 3 kHz, by the Nyquist theorem, the sample rate must be greater than 6 kHz. Unfortunately, the IF amplifiers, detectors, and audio amplification stages in an HF receiver have signifi-

cant noise contribution up to approximately 8 kHz. This would imply that it would be prudent to sample the receiver audio at a rate higher than 16 kHz so that high frequency noise does not alias into the analysis passband. Standard PC sound boards allow for sampling at 8 kHz, 11.025 kHz, 22.050 kHz, and 44.100 kHz.

The linear quantization levels available on a PC are 8 and 16 bits. The hardware floating point mathematics in a

PC is based on the IEEE-754 standard. The precision for a floating point computation ranges from single precision with a 23 bit mantissa to extended precision with a 63 bit mantissa. The selected floating-point resolution must be capable of supporting the multiplication of quantized data without a resultant loss of precision due to truncation.

The system level requirements led to a point design with characteristics as specified in Table 2.

Table 2—Point Design Based on System Specifications

Sample Rate	22,050 Hz
Ensemble Size	4,096 Samples
Quantization Level:	16 Bits Linear
Mathematical Precision:	IEEE-754 Extended Precision

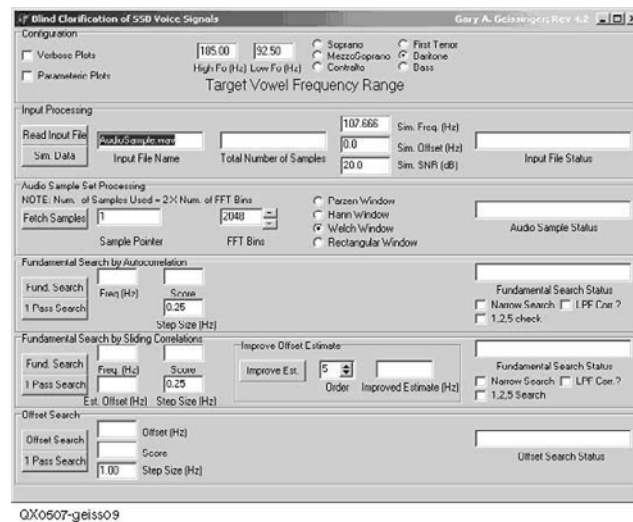


Fig 9— Program control panel.

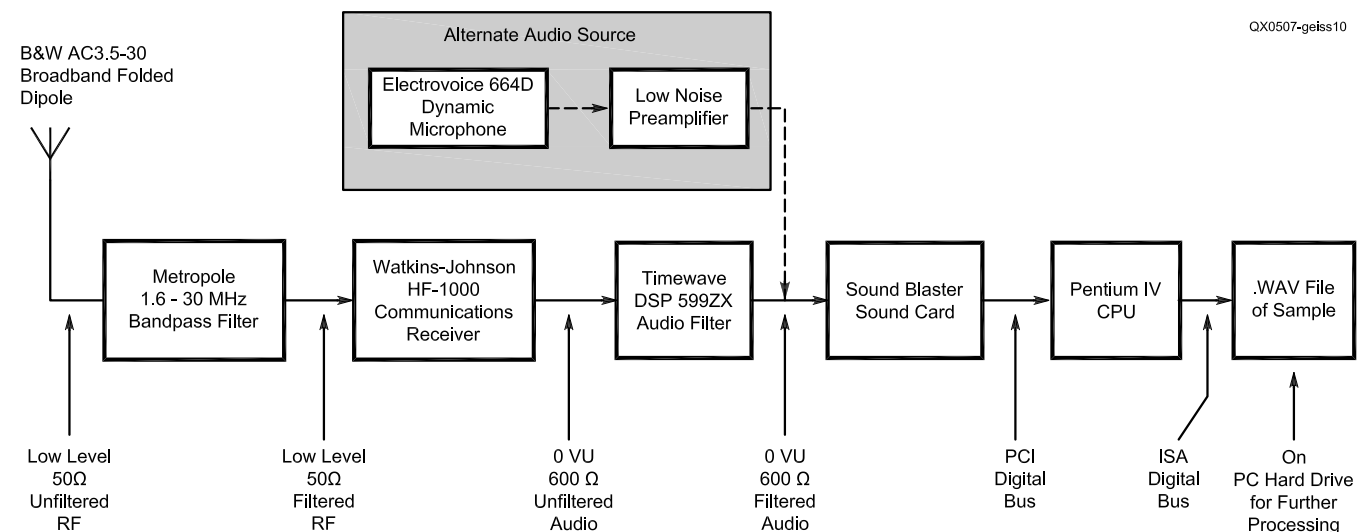


Fig 10—Data acquisition setup.

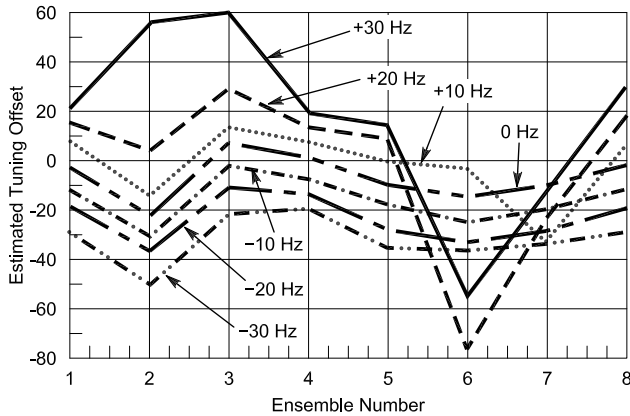


Fig 11—The quick brown fox...with various offsets.

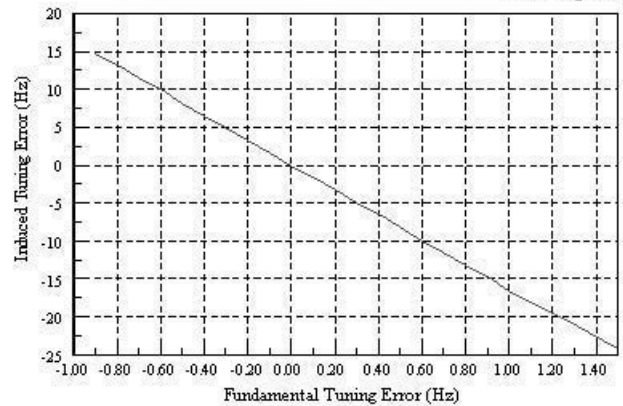


Fig 12—Errors in tuning error computation as a function of fundamental error.

The sample rate of 22,050 Hz along with an ensemble size of 4096 indicates that an ensemble will require 186 ms to collect, which is less than the $\frac{1}{5}$ second assumed duration of a vowel. The frequency resolution of FFTs using 4096 points is 5.383 Hz, less than the requirement of 20 Hz.

Using the maximum available quantization level of 16 bits was a reasonable choice, but it forced the requirement that the multiplication of two 16-bit values should not be truncated. The use of IEEE-754 extended precision with its 63 bit mantissas easily met this requirement.

The PC compiler chosen was Borland Delphi 6.0. A computer program was written to verify that extended precision was indeed 63 bits using a computation of machine epsilon in Delphi 6.0.

The final application program GUI shown in Fig 9 is not particularly user friendly, but it gives many processing options.

The Test Setup

Fig 10 shows the data acquisition test setup. Initial testing was simply done with a microphone. Then testing proceeded to using commercial AM and SW broadcast stations as signal sources. The final tests involved using an ICOM IC-756 PRO transceiver to generate the signal. White noise was added to the receive signal to test the performance of the algorithm as a function of signal to noise ratio.

Data Rejection is Crucial

As you can imagine, a technique such as this yields good results only a fraction of the time. This should make sense, as vowels are not the only sounds present in speech. In addition, vowels that change frequency during

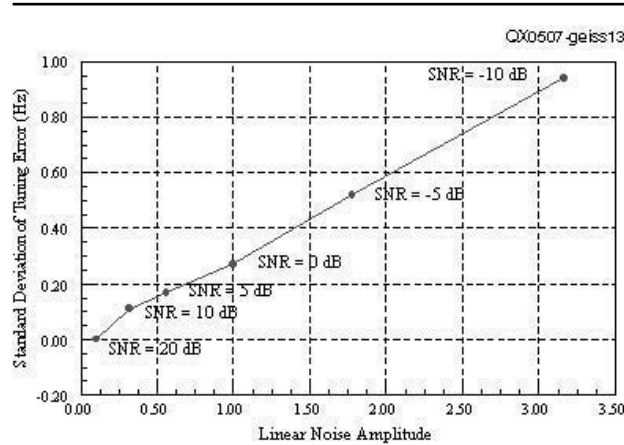


Fig 13—Effect of SNR on algorithm performance.

speech can give unpredictable results. Those effects as well as QRM and QRN force the need for consistent data qualification.

Several approaches were taken. First, it is assumed that the user has initially tuned the receiver to within about 50 to 80 Hz. Errors that exceed this amount are therefore inconsistent and can be ignored. The errors should trend; that is, when receivers and transmitters drift they have consistent long-term tendencies. In this case long term is on the order of a second or two. Finally, tests are required for signal to noise ratio and signal to interference ratio.

As seen in the test setup, an adaptive audio filter is present. This was used to remove heterodyne interference. A commercial DSP application implementing the AFC algorithm would do this internally.

Results Obtained

Fig 11 shows a typical result. This is a female speaker (my daughter) say-

ing, "The quick brown fox jumped over the lazy dog's back." The voice sample was recorded and played back with various tuning offsets between the transmitter and receiver. The AFC output was not used to tune the receiver; that way the algorithm performance could be examined. The SNR ratio was set at 10 dB using the IC-756 PRO as the signal source.

The algorithm actually did pretty well except for around data ensembles 6 and 7 where the wrong harmonic was picked during computation. Additional filtering probably could correct problems like this.

Fig 12 shows how the errors in finding the vowel fundamental change the computed tuning error result. The sensitivity is quite high.

Finally, the signal to noise performance was examined. Fig 13 demonstrates that QRN is not a strong factor in the AFC algorithm's performance.

Final Comments

Other effects were noted such as er-

rors in AFC computation due to rising or falling vowel inflection. Some languages tend to prolong vowels, others shorten vowels. This means that the AFC algorithm performance varies with selection of spoken language! An interesting pathological case was observed using a local AM radio station as a signal source. One of their sports personalities has a dual peak in his vowel fundamentals. I suspect that he suffered some sort of throat injury during his long career in the NFL.

Keep in mind that this algorithm is designed for voice communication; instantaneous tuning errors of 10 or 15 Hz are not of concern. If this algorithm were used for music or tones, then better performance would be required. Fortunately the tones would be "vowels only" in many cases which

should yield good performance ... unless one is listening to a drum solo!

Notes

- ¹A. H. Benade. *Fundamentals of Musical Acoustics*. New York, Oxford University Press, 1976.
- ²M. J. Hinich. *Detecting a Hidden Periodic Signal When Its Period is Unknown*. IEEE Transactions on Acoustics, Speech, and Signal Processing, Vol. ASSP-30, No. 5, Oct 1982.
- ³S. D. Stearns, R. A. David. *Signal Processing Algorithms*. Englewood Cliffs, Prentice-Hall, Inc., 1988.
- ⁴E. O. Brigham. *The Fast Fourier Transform and Its Applications*. Englewood Cliffs, Prentice-Hall Inc., 1988.
- ⁵E. K. P. Chong, S. H. Zak. *An Introduction to Optimization*. New York, John Wiley and Sons, Inc., 1996.

Gary Geissinger, WAØSPM, is an Extra class operator. He received his

Novice license in 1968 and became WNØSPM, moving to WAØSPM with his Technician class license.

He is the chief electrical engineer for DigitalGlobe Inc, an imaging and information company. During the evening he is a member of the graduate faculty of the University of Colorado at Denver and teaches senior and graduate level hardware and software classes. He is a member of IEEE, The Association of Old Crows and the ARRL.

He received an MSEE and two other degrees from the University of Colorado.

Although his favorite activity is working 6 meter SSB, he is also interested in DSP applications and operating digital modes on 20 meters when 6 isn't open. □□



Join the effort in developing Spread Spectrum Communications for the amateur radio service. Join TAPR and become part of the largest packet radio group in the world. TAPR is a non-profit amateur radio organization that develops new communications technology, provides useful/affordable kits, and promotes the advancement of the amateur art through publications, meetings, and standards. Membership includes a subscription to the *TAPR Packet Status Register* quarterly newsletter, which provides up-to-date news and user/technical information. Annual membership \$20 worldwide.



TAPR CD-ROM

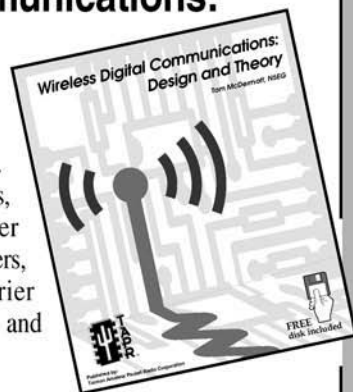
Over 600 Megs of Data in ISO 9660 format. TAPR Software Library: 40 megs of software on BBSs, Satellites, Switches, TNCs, Terminals, TCP/IP, and more!

150Megs of APRS Software and Maps. RealAudio Files.

Quicktime Movies. Mail Archives from TAPR's SIGs, and much, much more!

Wireless Digital Communications: Design and Theory

Finally a book covering a broad spectrum of wireless digital subjects in one place, written by Tom McDermott, N5EG. Topics include: DSP-based modem filters, forward-error-correcting codes, carrier transmission types, data codes, data slicers, clock recovery, matched filters, carrier recovery, propagation channel models, and much more! Includes a disk!



Tucson Amateur Packet Radio

8987-309 E Tanque Verde Rd #337 • Tucson, Arizona • 85749-9399

Office: (972) 671-8277 • Fax (972) 671-8716 • Internet: tapr@tapr.org www.tapr.org

Non-Profit Research and Development Corporation

A 47-GHz LNA

MMIC Experiences on the 6-millimeter Band

By Silvano Ricci, IØLVA
and
Daniele Moretti, IWØFGR

Daniele, IWØFGR, and I thought that we needed to improve our stations by increasing the receiver and transmitter performance with an increase in output power and a reduction in receiver NF. We reached this conclusion after some intense activity on the 10-GHz and 24-GHz bands and a shy attempt on the 47-GHz band with no contacts and with just two transverters based on a sub-harmonic mixer design.

Tackling such high frequencies is

not easy, and difficulties increase exponentially for the following reasons:

- Lack of suitable materials and components
- Lack of knowledge of the involved technologies, which differ greatly from those used by the majority of operators (on HF)
- Lack of equipment necessary for calibration and measurement

We needed to start by looking for the necessary active devices available on

the market, which could be used by us hams. We found that as the frequency increases, the availability of discrete active devices such as transistors (in both packaged and die forms) decreases. Instead, MMICs (Microwave Monolithic Integrate Circuits) are becoming more and more commonplace, as they are in the lower-frequency bands. For example, the ERA and MAR MMICs from Mini-Circuits Labs. Yet, there are certain difficult problems that need to be overcome to succeed in the millimeter-wave bands. The products present on the market have the following drawbacks for use in ham bands :

- The working frequency ranges for which these devices are optimized are about 10-20% of the center frequency and cover (rightly) the fre-

Silvano Ricci, IØLVA
Via Crocetta, 40
00010 S. Polo dei Cavalieri
Rome, Italy
silvano.ricci@transport.alstom.com
i0lva@katamail.com

Daniele Moretti, IWØFGR
Circ Cornelia 293 pal 5
Rome, Italy
danielemoretti@tiscali.it

quency bands of the telecom and military markets. The 10-GHz and 24-GHz ham bands are the most fortunate, but it is not so for the 6-mm band (47 GHz) or higher frequencies (77 GHz).

The MMICs on the market that can guarantee interesting performance are all in the die form, which means we have no choice but to tackle new technologies and their specific requirements (wire bonding, epoxy attach, handling and storage of die MMICs).

Before going any further with our experiences and realizations it is important to explain some of the technical problems and technologies that we had to face.

Handling of MMICs

MMIC Storage

Die MMICs are usually shipped in special containers, such as GEL-PAK trays (visit www.gelpak.com) or Wafflepack trays (visit www.ictray.com). These should be stored in a temperature- and humidity-controlled area, preferably under a dry-nitrogen flux. The latter aspect is important in GaAs MMICs if their surface is not passivated with NSi₄, since hydrogen molecules that are adsorbed into GaAs tend to change its electrical characteristics and modify the devices' functional characteristics.

GEL-PAK is in any case not recommended for long-term storage (typically greater than 1 year) due to pos-

sible chemical interactions between gel and the backside metallization of the die which can bring problems in attaching the device. In case it is necessary to store chips for a long time, it is better to have them delivered in Wafflepack trays.

All of this is very complicated for us hams, and for the majority of us practically impossible.

"It's so small! How do I pick it up?" Well the answer is easy: A pair of clean stainless tweezers are sufficient. Take care to pick up the die in a correct way, to avoid chipping the upper edge of the die (see Fig 1). We recommend buying tweezers from Dumont (visit www.etweezers.com/) or Fontax.

ESD

High-frequency GaAs devices are, for obvious reasons, usually not designed with on-chip ESD protection circuitry. Due to their reduced geometry sizes, MMICs are very sensitive to ESD degradation or failure. It is necessary to observe the same rules used for Class 0 silicon devices.

Assemblies with die MMICs

Die Attachment— General Guidelines

There are two methods for attaching a die to a substrate or a metal base (see Fig 1A). The choice is generally determined mainly by the devices' thermal-dissipation requirements, though attaching the die to a metal

base is the best solution to simultaneously achieve a good RF ground and thermal cooling. The two methods are conductive die attachment and eutectic die attachment.

The general guidelines are:

- Low-power devices can be attached with a silver-loaded epoxy.
- Medium-power devices can be attached with a silver-loaded organic adhesive (30-60W/mK, millikelvins) or epoxy (2-3W/mK), but this should be limited to devices mounted in low-temperature environments.

The recommended method is suitable for both medium and high-power devices. They should be attached with eutectic solder, such as (80/20 Au/Sn).

It is possible to attach low-power devices directly onto substrate materials (see Fig 1B), but take care to provide a low RF ground inductance under the die chip and avoid non-TEM propagation modes or spurious oscillations will result. This can be accomplished by including via-holes through the substrate (see drawings).

Epoxy Die Attachment

Epoxy die attachment is the standard industrial method. It has lower production costs with good reliability of the finished product. From a physical point of view, epoxy attachment is based on Van der Waals interaction rather than atomic or molecular in-

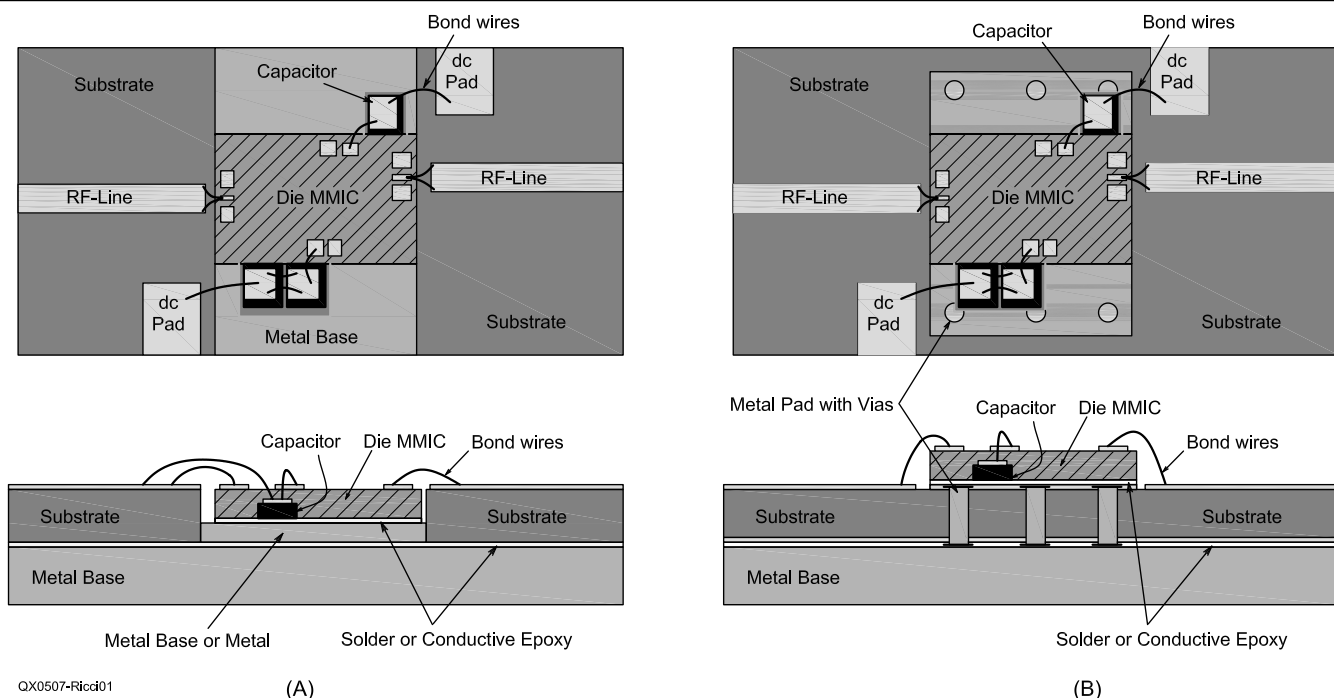


Fig 1—Die installation on metal (A) or substrate (B).

teraction. Epoxy is therefore an adhesive paste composed of two components, silver or gold grains filled epoxy and a hardener, mixed together and deposited in liquid form on the surfaces which are to be attached. The epoxy Curing times depend on temperature. It can be done at room temperature, but it is generally better to do it in a ventilated oven at, for example, 90°C and will take about an hour and a half.

Conductive epoxy can be bought as:

- One-component epoxy (hardener is shipped premixed with epoxy). This is a ready-to-use product, but to

slow polymerization, it must be stored at low temperatures (−40°C), but even in these conditions, its average useful life (pot-life) is approximately 6 months;

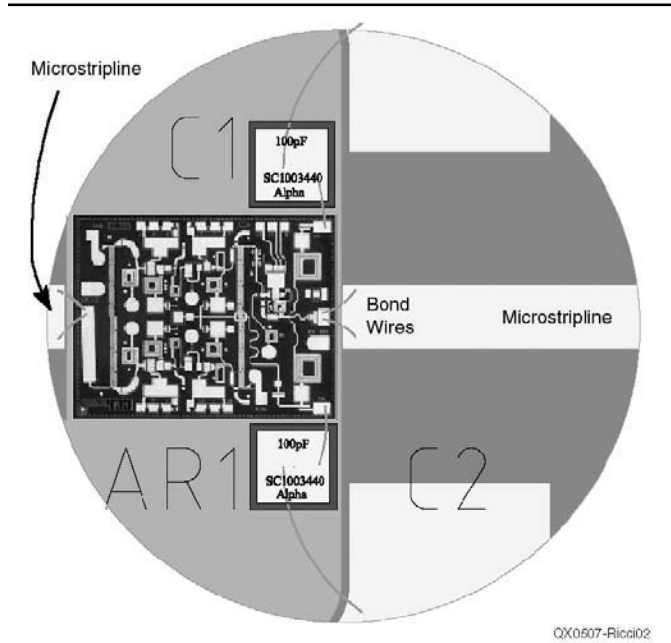
- Two-component epoxy, which must be mixed prior to use. The mixing procedure and ratios are indicated by the manufacturer, and they must be performed in a clean, dry environment. The unmixed components can be stored at room temperature, with an average storage lifetime of one year.

To achieve a good attachment, it is imperative to clean the dispensing

equipment and metal-base chip carriers (metal or substrate) with isopropyl alcohol to eliminate possible contaminants. The epoxy can be applied manually, with a needle.

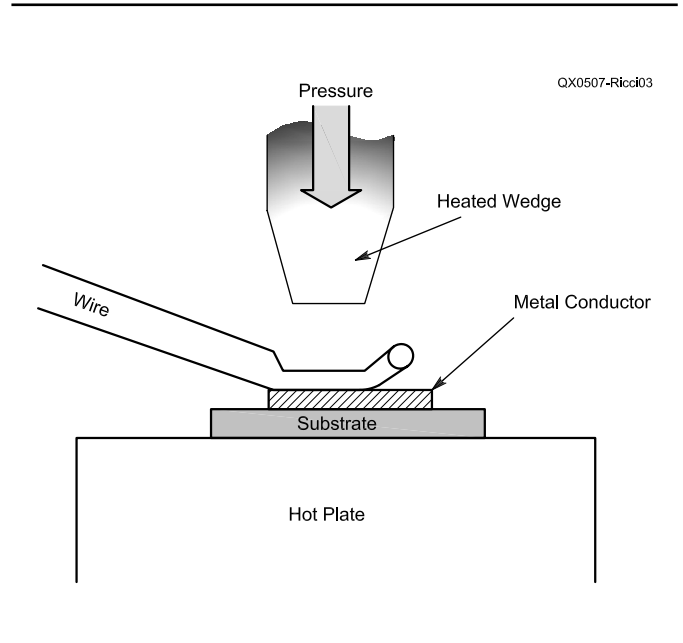
It is very important to minimize the thickness of the epoxy layer. First, to keep thermal resistances low. (Take care to avoid air bubbles and gaps!) Second, to avoid short circuits caused by the conductive epoxy overflowing the top of the chip or flowing between the chip, substrate and RF lines.

Learn to make the epoxy drop just a little larger than the chip lead, resulting in a narrow fillet around the



QX0507-Ricci02

Fig 2—A MMIC with external parts mounted on a circular substrate.

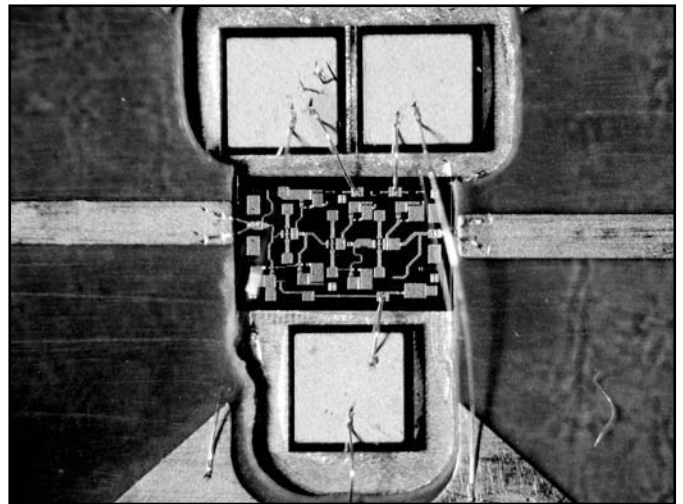


QX0507-Ricci03

Fig 3—Thermocompression wedge bonding.



(A)



(B)

Fig 4—At A, divergent wires connect to the microstripline as noted in the text. At B, a photo of properly mounted MMICS as described in the text.

contact! Position the chip directly at its final position and press it slightly, making sure not to damage the top surface of the die. Chips have delicate components, such as air-bridges, and spiral inductors, which are damaged very easily.

Here are some references for epoxies:

- EPO-TEK H20E from EPOXY TECHNOLOGY; www.epotek.com
- ABLEBOND 84-1LMI from ABLESTIK; www.ablestik.com
- DM6030HR from DIEMAT; www.diemat.com

QMI5030 from the former DEXTER ELECTRONIC MATERIALS (www.dexelec.com); as of August 2003, Dexter was bought by LOCTITE (www.loctite.com).

Eutectic Die Attach

We won't cover this topic section in this article. But maybe next time, when we do some high-power MMIC assemblies!

Bonding

Classic (SnPb) tin-lead soldering is not possible with die MMICs because of incompatibility between SnPb and gold (gold is present on the chip pads and microstrip) and because MMIC dimensions are much smaller (typical dimensions are $\frac{1}{2}$ mm²) than with other chips. Needless to say, with these very small dimensions it is fundamental to observe everything through a microscope! Other bonding materials and techniques are therefore necessary.

Bond wires

The bond wires used to connect the MMIC to the microstrip lines on the external substrates are usually pure gold, 18 μ m to 25 μ m in diameter, which have an inductance in the order of 0.6 nH/mm to 0.8 nH/mm. MMIC designs account for the inductance effect of bonding wires in the

final chip performance, so it is desirable to strictly adhere to the MMIC designers recommended mounting specifications.

The best way to achieve the electric transition from the coplanar-with-ground structure to the microstrip structure is by using two divergent bond wires as shown in the Fig 4A. This can only be conveniently accomplished with 18 μ m-thick wire and by thermosonic wedge-bonding as described in the next paragraph.

This pair of bond wires must be no longer than 200 μ m in order have an overall inductance value ranging from 0.2 nH to 0.4 nH.

Bonding Processes

The two main types of bonding processes are:

1. Ultrasonic bonding (very popular in laboratories);

2. Thermocompression bonding (the preferred industrial method) is subdivided into:

A. Thermocompression wedge bonding (see Fig 3)

B. Thermocompression ball bonding

Ultrasonic bonding uses ultrasonic energy (typically 60-100 kHz) to increase the plasticity of metals to be bonded. The ultrasonic system of a wire bonding machine consists of two parts: the ultrasonic generator and the ultrasonic transducer. Here is the bonding sequence: First, under the application of force by the wedge tip, a certain amount of deformation occurs in the lattice structure of the bond wire and/or bond surface. Next is a cleaning phase. Ultrasonic energy (with amplitude vibrations of 1-5 μ m, much smaller than the bond-wire diameter) makes the wire and wedge move together, creating friction at a constant pressure on the wire and bond interface surface. Shortly, the wire deforms and heats so that welding occurs. (Welding occurs by

the diffusion of the wire and bond surface-lattice dislocations.)

Thermocompression uses a combination of heat and pressure to connect the wire between the die bond pad and the microstripline on the external substrate. No melting between metals occurs as the bond comes about by the interaction of atomic forces between the wire and the metal pad.

Thermocompression Wedge Bonding uses a hard heated wedge-bonding tip made of tungsten carbide together with a wire spooler equipped with a wire clamp. The wire is pressed on the bond pad with a controlled force, typically 20 to 22 grams. This process requires a precise alignment of tool force, work stage and tip temperatures.

Thermocompression Ball-Bonding instead has the wire fed through a capillary in the tip, which is heated to a high temperature (300-400°C). A hydrogen flame or spark discharge is produced at the end of the tool to melt the end of the wire and form a small ball. The tool then moves over the bond pad of the die and presses vertically (force is around 30 to 50 grams) the ball on the pad to realize bonding. The tip is moved to the new location (external substrate) and wire is again pressed (no ball is formed in this case) to achieve the new bond and thereafter cut.

Bonding process control should be completed to validate the die attach process control over time (repeatability) by *pull testing*. Pull-testing may be destructive or non-destructive depending on the test method, but we shall not discuss that here.

Substrate Materials for Microwave

Choice of the appropriate microwave substrate material takes into account many factors such as :

- frequency of operation;
- cost;
- thickness;

Table 1—Characteristics of Thermocompression Bonding Techniques

Characteristic	Wedge-Bonding	Ball-Bonding
Footprint	Very small, 1.5 to 2 times wire diameter	Large, 3 to 5 times wire diameter
Length	Shortest possible	Longer, wire starts off vertically
Wire Size Capability	$\geq 18 \mu$ m	$\geq 18 \mu$ m
Speed	SLOW 2 separate alignments necessary; wire needs to be moved exactly under tool end.	FAST omnidirectional movement of tip; wire is fed directly under tool end.

Table 2—Microwave Circuit Materials

Minimum Substrate (mm)	Copper Available Thickness (μm)	Thickness - unplated (μm)	ε @ 10 GHz	Loss Tan @ 10 GHz	Dimensional Stability
Rogers RO4003	127 ±10	17-70	3.38 ±0.05	0.0027	Good
Rogers RO5870	127 Tol. ?	13-35	2.33 ±0.02	0.02	Poor
Rogers RO5880	127 Tol. ?	13-35	2.20 ±0.02	0.02	Poor
Taconic TLY 3	127 Tol. ?	17-35	2.33 ±0.02	<0.02	Fair

- size/Dk;
- dimensional stability.

There is a drawback though. Duroid, though its electric properties are superior to other materials at these frequencies, is unfortunately not the best choice for thermosonic bonding. It is a soft material and the temperatures that are reached in the microstrip region tend to detach the copper strip from the substrate. A harder material would perform better.

Our experiments

At 47 GHz, it is convenient to use Teflon-based copper-laminated dielectric materials (ε>> 2.3, with a flash of gold on the copper of approximately 3 μm to avoid oxidization) 5 mils thick (127 mm). This is not only an electrical necessity (microstrip propagation requires that the height of the dielectric material be many times smaller than the electric wavelength) but also a mechanical necessity. MMICs are usually about 100-127 μm thick, which means that the RF pads of the MMIC are at nearly the same height as the RF microstrip lines. This simplifies bonding, which would otherwise require a “deep-access” bonding tool. It also ensures that the bond wires remain as short as possible, minimizing their total inductance, which turns out to be an electrical requirement, as well.

In this case, a 50 Ω microstrip line is approximately 350 μm wide, while on the MMIC the RF pads are usually about 70 μm wide and usually are coplanar with ground lines.

The MMICs meet the following conditions for proper mounting and performance (see Fig 4):

- The low-power MMICs were glued with conductive epoxy (like H20E EPO-TEK) on top of a conductive mechanical holder.
- There are two 50-Ω microstrip lines for the input and output, each at least two electrical wavelengths (in microstrip) to allow for tuning. Tuning was accomplished by moving shorting bars made of copper (with a gold finish). A gold-loaded conduc-

Table 3—Measured Results for a Single CHA2094B

Parameter	Prototype 1	Prototype 2
Gain	14.3 dB	13.8 dB
NF	5.30 dB	4.78 dB

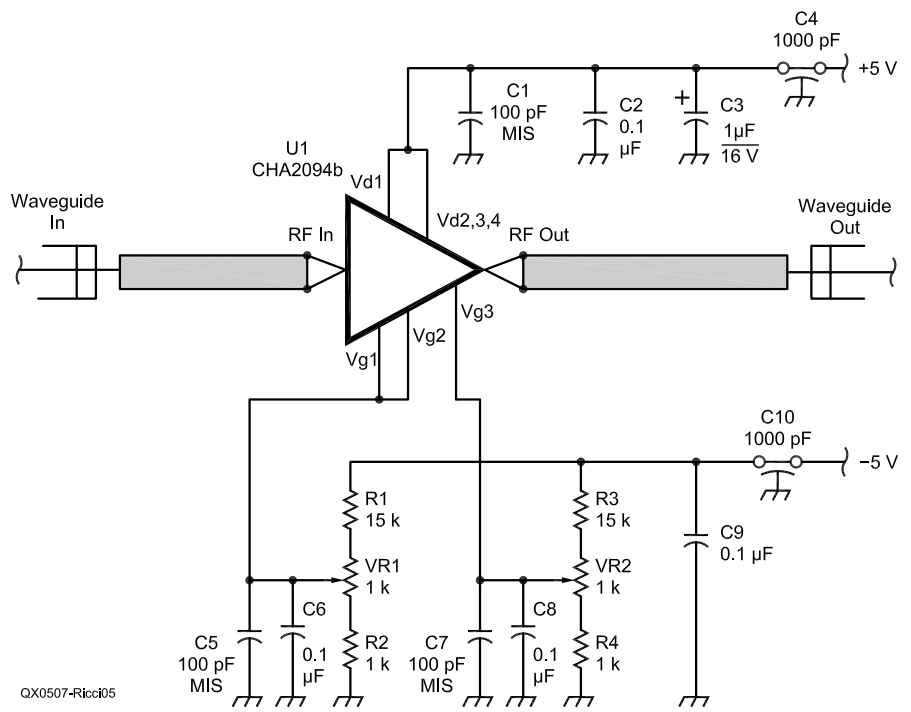


Fig 5—A schematic of the single-MMIC circuit.

tive epoxy, such as H81E (from EPO-TEK) can be used, but it is very expensive! The microstrip lines were glued with a conductive epoxy (such as H20E) to the mechanical holder or at the bottom of the cavity. It is better to obtain some 5 mil 5880 or 5870 Duroid (ROGERS Corp.) that has one side with coated with ½-ounce ED copper and the other side with thick (60 or 90 mil) ED copper. Vendors can provide their dielectric material in such form upon request. This solution is apparently costly, but it does not require a me-

chanical holder; it has sufficient mechanical strength.

MMICs are typically powered from a 4 or 5 V supply through the FET drains and or more variable voltages to set bias condition of the FET (gates). Typically, this voltage is negative (-5 V). Ensure that the negative bias voltage is applied *before* the positive drain voltage. Otherwise, permanent MMIC damage may result. Refer to the component datasheet for power-supply details.

Power supplies must be carefully

filtered. The filters are usually made of a small inductance (the bond wire forms a RF choke) and an RF-shunt capacitor mounted (epoxy-glued) directly near the power-supply pads of the MMIC. Select appropriate capacitors carefully. MIS (metal-insulator-semiconductor) capacitors are very good capacitors for shunting mm-wave frequencies. It is usually good practice to follow the indications given in the MMIC datasheet, since the MMIC designers account for a recommended power supply and bias circuit when optimizing design performance.

The MMICs We Used

Last year (2002), we were investigating what the MMIC market could offer to hams. The MMIC market is substantially held by a few companies, such as Filtronic, UMS, Agilent, TRW-Velocium, Mimix, Raytheon and TriQuint. Some of these have internal GaAs MMIC foundries, while others are mainly MMIC design houses.

Our research resulted in the choice of two MMIC amplifiers (all datasheets are available through the Internet).

CHA-2094B from UMS: 20-dB gain, three-stage low-noise amplifier (LNA) with a maximum output power of 8 dBm and a NF of 0.75 dB.

HMMC-5040 from Agilent: a four-stage medium power amplifier (MPA) to work in the 20-40 GHz band with a typical gain of 22 dB, a 1-dB compression point of 18 dBm and 21 dBm saturated output power. No further information was available at 47 GHz (S-parameters and so on), but a close look at the gain curve made us feel its performance could be acceptable in our frequency band.

Our Prototypes

Fig 5 shows the circuit we used for our prototypes. The positive (drain) power supply is designed around a 7805, and the gate negative voltage is designed around an ICL7660. The devices require three different bias voltages (input stages need V_{gs1} and $e V_{gs2}$, V_{gs3} is for the output stage).

The nominal bias current is approximately 20 mA for the output stage and 15 mA for each input stage; for a total power consumption of 50 mA. The best NF performance is accomplished with 45-mA total power consumption.

We have measured performance of the two MMICs in both single and cascade arrangements.

The CHA2094b, alone, yields poorer results (both in NF and in Gain) than we expected based on the datasheet. Even in-band (36-40 GHz) measure-

ments exhibited 5 dB more noise than on the datasheet. This is not justified by the losses of the waveguide-to-microstrip transitions and losses in the input and output microstrip lines.

Anyway, the results in Table 3 were still very interesting. The measured values must be considered average values since they depend on temperature, which we didn't measure.

Table 4 shows the performance for the two modules connected in cascade and to the transverter.

The same preamplifiers have been used in both transmission and reception by means of a WR22 waveguide transfer relay, and the power measurements have given these results:

Input -6.32 dBm
Output 12.19 dBm,
approximately 16.4 mW
(near saturation)

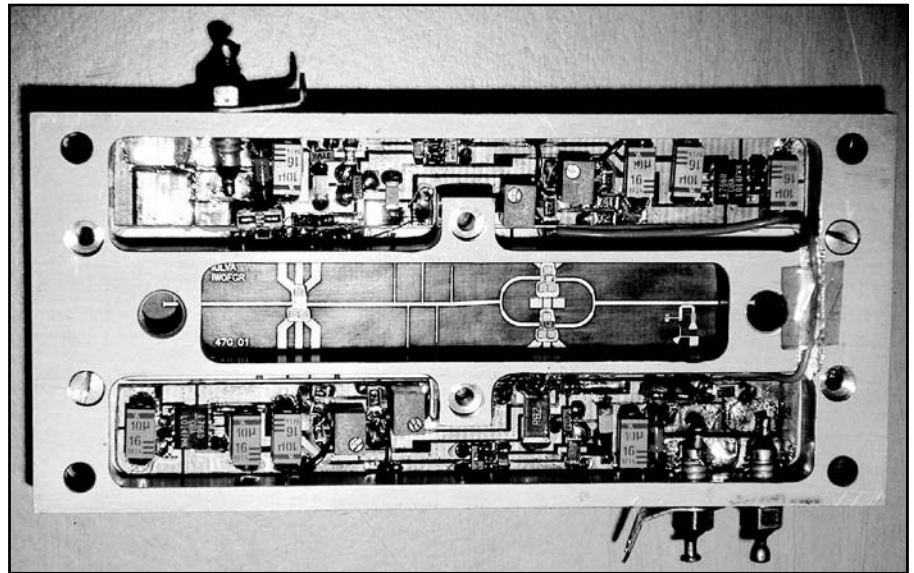
The output shall be used to feed a power amplifier we are designing and we will describe that in our next article.

The output power at the 1-dB compression point, even though it varies with temperature, once stabilized, has been around 10.5 dBm, which is indeed a good result.

We performed measurements on the cascade of two HMMC-5040 MMICs and the results were a gain $\gg 25$ dB; NF ≈ 8 dB; Pout ≈ 15 dBm

Table 4

Parameter	Prototype	Notes
Gain	26.8 dB	36.1 dB together with the transverter of Fig 6
NF	5.10 dB	
I	90 mA	



(A)

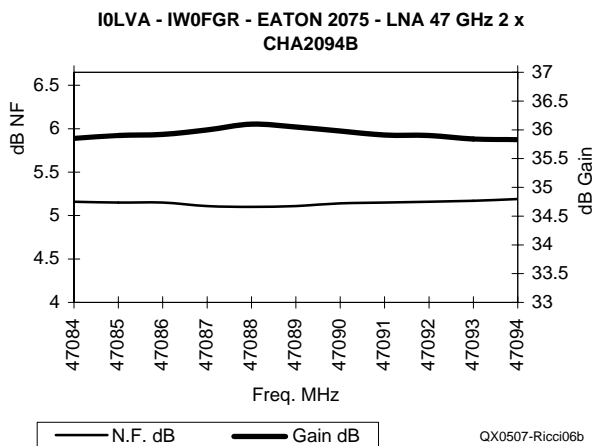


Fig 6—At A, a photo of the test setup with single and cascade MMICs and a transverter. At B, characteristic curves for the LNA with CHA2094B and cascaded transceiver.

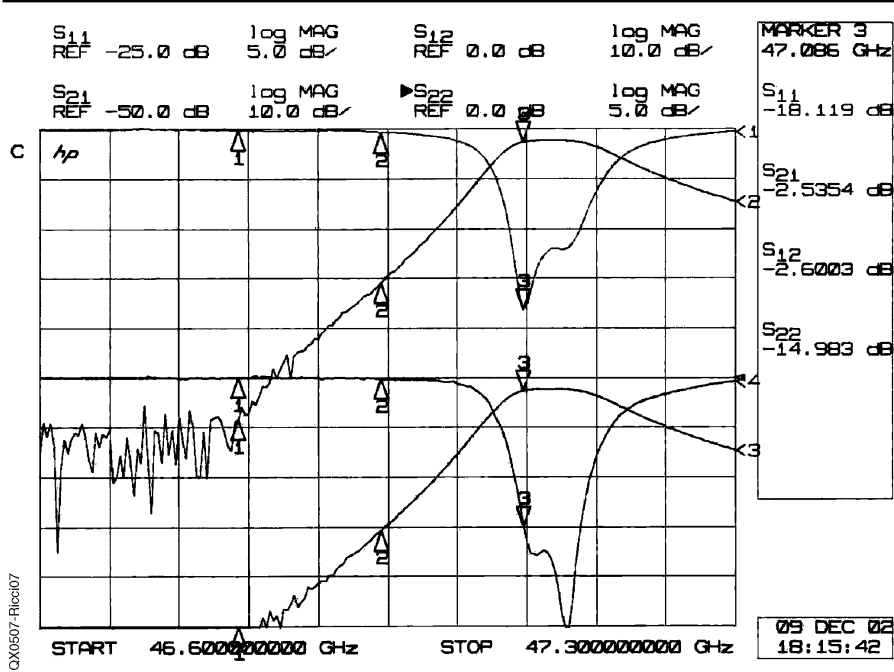


Fig 7—Response curves for the image-rejection filter.

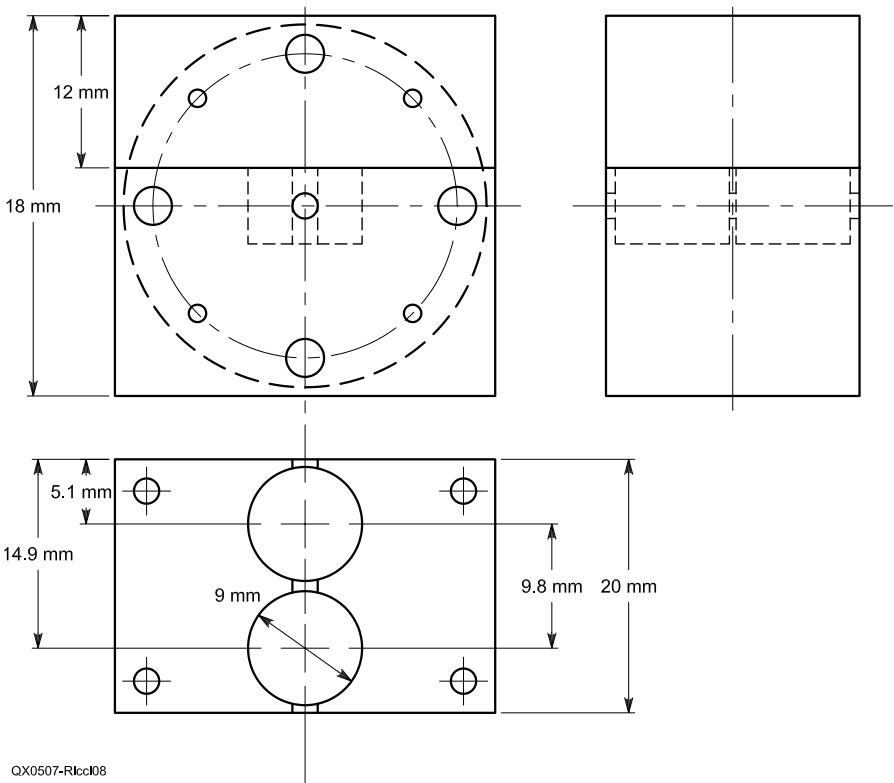


Fig 8—Mechanical details of the image-rejection filter.

and 17 dBm in saturation. The dc power requirement is about 550 mA.

The Image-Rejection Filter

Receiver input noise forced us to use an image-rejection filter in our re-

ceiving chain. Here's a brief introduction and description of our approach with this type of filter in the 6-mm band. The filter we used is a doubly coupled resonant-cavity filter designed in a circular waveguide and

The Test Bench

The following measuring instruments were used:

- Noise Figure Meter Eaton 2075B
- Noise Figure Meter HP 8970A
- Noise Source HP 346A
- Noise Source HP Q347B
- Power Meter HP 346A
- Power Meter HP 435B
- Power Sensor HP8487A

built by our friend Armando, I3OPW, in brass (with no silver plating or other surface treatment). Once the filter was tuned, our first measurements with a network analyzer showed excessive in-band insertion loss of 5 dB, LO attenuation (46,944 MHz) of 50 dB and >60 dB (beyond the sensitivity of our instrument) for f_{IM} (46,800MHz). By increasing the diameter of the coupling hole, we managed to reduce in-band insertion loss to 2.6 dB (maximum) without too much degradation of the out-of-band attenuation levels (>30 dB for LO and >50 dB for f_{IM}), which is acceptable. These measurements are shown in Fig 7. We believe that better results could be obtained with surface plating of the filter capable of enhancing surface conductivity. Fig 8 is a drawing of the filter.

Special Thanks to...

We send a special thanks to our friends who have given us material and moral support.

We are now operational and looking to correspond with other hams to do trials or contests. Our local DX field trials at 47 GHz have produced very good results, but there are still many improvements to be done. A special thanks to M.E.D.S. sas for the assembly of our first prototypes and technical/technological skills and advice.

Daniele Moretti, IW0FGR, has a degree in Electronics Engineering from the University of Rome. He is working as an RF Engineer. He has been a licensed amateur since 1994 with a special interest in the microwave bands.

Silvano Ricci started his radio interest at the age of 14, as an SWL. He was licensed in 1969 as I0LVA. He holds a certificate in electronics and telecommunications. In 1970, he was at the top of the class in the electronics at the transmission school in Naples. He has a special interest in VHF-UHF and the microwave bands from 5.7 GHz to 145 GHz. He has published articles in Radio Revista and DUBUS. He on the roll of honor of the Associazione Radioamatori Italiani. □□

A Do-It-Yourself Noise Figure Meter

*If you want to evaluate receiver noise figure,
this article describes how to fabricate a
semi-automatic system from gear on hand.*

By Fred Brown, W6HPH

My professional experience with an automatic noise figure (ANF) meter has taught me how simple and easy the ANF meter makes optimum noise figure adjustments, compared to the usual tedious and time-consuming on-and-off procedure with a noise generator.¹ With an ANF meter you simply tune everything for minimum meter reading. Because of their high cost, ANF meters are out of reach for most of us.

Presented here is a simple technique that will permit the same ANF optimization without using an ANF meter. It gives a relative noise-figure reading. For measurement of the final absolute noise figure, I would recommend the Calibrated Noise Source by WØIYH.²

This scheme is shown in Fig 1. The AGC of the AM receiver will maintain a constant signal level at the receiver's detector regardless of gain variations in the converter. Any adjustment that will minimize the noise output will also optimize the signal-to-noise ratio and thus the noise figure of the converter. Modern receivers and transceivers have highly effective AGC systems. My Icom IC-706, used as an AM receiver at 28 MHz, can handle an input range of more than 50 dB and hold the audio output constant to less than

¹Notes appear on page 53.

0.1 dB! This may be exceptional, but even if the output varied by a few dB over such a wide range it would be good enough for this task.

Fig 2 shows a typical AGC response curve. For this scheme you will want to set the signal level near the middle of the flat part of the curve. This is usually somewhere above S9 on a typical S-meter.

Ideally the signal generator should be crystal-controlled. If an ordinary tunable generator is used, allow at least an hour for warm-up to avoid frequency drift. Of course the signal generator impedance should equal your antenna impedance. Remember you are optimizing noise figure for whatever impedance your converter or preamp "sees." If you want to optimize for your exact antenna

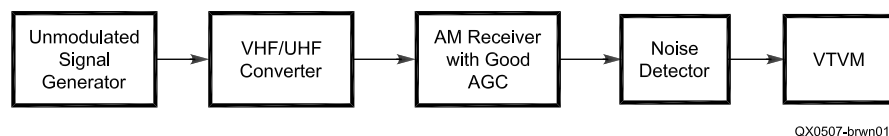


Fig 1—Block diagram of the noise-figure optimization setup.

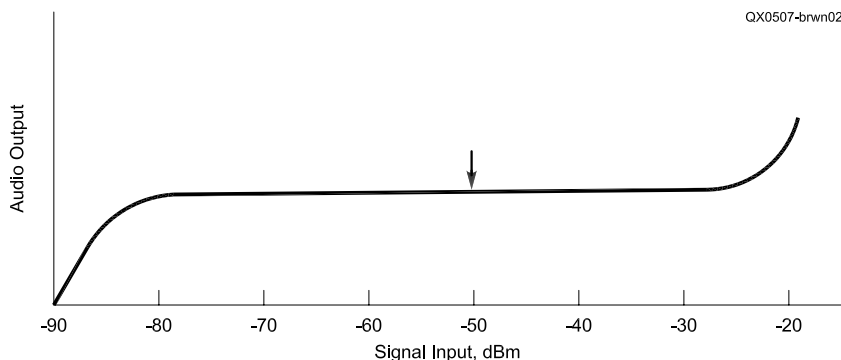


Fig 2—A typical AM communications receiver AGC response curve. The signal level should be set near the middle of the flat part of the curve as indicated by the arrow.

840 Phoenix Way
San Marcos, CA 92078
w6hph@yahoo.es

impedance you can use an unmodulated signal from a friend across town. But antenna noise may mask converter noise, especially on 6 and 2 meters.

For a noise detector I suggest the circuit of Fig 3. Many audio voltmeters respond to peak levels and as a result will give very erratic readings when measuring noise. What is needed is a meter that responds to RMS or average values. The circuit of Fig 3 responds to average values and gives a steady meter reading. Audio output of the receiver is stepped up by the audio transformer and is rectified by the full-wave rectifier. The diodes can be practically any type, but Germanium or Schottky diodes will work better than silicon types. The dc voltage across the 10 kΩ resistor is proportional to the average value of the noise. This is filtered by the 1 MΩ resistor and 1 μF capacitor to give a steady dc value. The 1 second time constant (1 MΩ and 1 μF) is a good compromise between meter fluctuations and speed of response. I use an old-fashioned 11 MΩ vacuum tube voltmeter (VTVM) for an indicator. I do not recommend a digital meter.

Adjustment procedure is as follows:

1. First run an input-output curve such as shown in Fig 2. Determine the S-meter reading corresponding

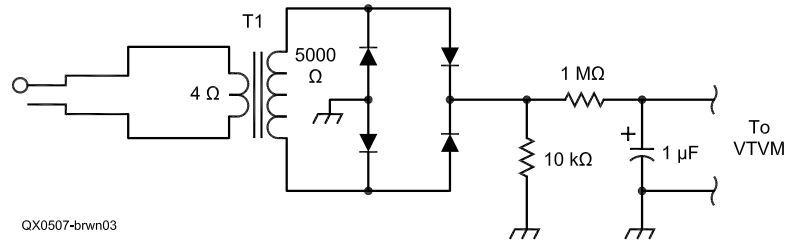


Fig 3—The noise detector. Transformer T1 can be a 5000 Ω to voice coil output transformer, as commonly found on old vacuum tube radios.

to the middle of the flat part of the curve and use this signal level while optimizing.

2. Set the audio gain control to give a mid-scale meter reading on the VTVM.
3. Make all adjustments slowly. Remember that 1 second time constant is added to the AGC time constant.
4. After making an adjustment, check the S meter reading to make sure you are still near the middle of the flat part of the AGC curve.
5. You should be able to observe a pronounced dip in noise output as the converter input tuned circuit is tuned through resonance. This is a good indication that everything is working as it should.

Fred Brown has held the call W6HPH since 1949 and has been Extra class since 1966. He earned a BS in Electronics from Cal Poly and an MSEE from the University of Illinois. He has worked in the electronics industry most of his life and is the author of more than 50 articles published in amateur and professional journals. Currently he operates a completely homemade SSB station on 432 MHz.

Notes

- ¹Noise generators have another disadvantage in that their "on" impedance is usually different from their "off" impedance.
- ²The 2003 ARRL Handbook for Radio Communications (Newington, 2002), p 26.32. See also W. Sabin, W0IYH, "A Calibrated Noise Source for Amateur Radio," QST, May 1994, p 37. □□

We Design And Manufacture To Meet Your Requirements

*Prototype or Production Quantities

800-522-2253

This Number May Not Save Your Life...

But it could make it a lot easier! Especially when it comes to ordering non-standard connectors.

RF/MICROWAVE CONNECTORS, CABLES AND ASSEMBLIES

- Specials our specialty. Virtually any SMA, N, TNC, HN, LC, RP, BNC, SMB, or SMC delivered in 2-4 weeks.
- Cross reference library to all major manufacturers.
- Experts in supplying "hard to get" RF connectors.
- Our adapters can satisfy virtually any combination of requirements between series.
- Extensive inventory of passive RF/Microwave components including attenuators, terminations and dividers.
- No minimum order.

NEMAL

Cable & Connectors
for the Electronics Industry

NEMAL ELECTRONICS INTERNATIONAL, INC.
12240 N.E. 14TH AVENUE
NORTH MIAMI, FL 33161
TEL: 305-899-0900 • FAX: 305-895-8178
E-MAIL: INFO@NEMAL.COM
BRASIL: (011) 5535-2368

URL: WWW.NEMAL.COM

ATOMIC TIME

1010 Jorie Blvd. #332
Oak Brook, IL 60523
1-800-985-8463
www.atomictime.com



ADWA101

12" Arabic Black Wall
WAWG102 \$29.95
This wall clock is great for an office, school, or home. It has a professional look, along with professional reliability. Features an easy time zone switch, just set the zone and go! Runs on 1 AA battery and has a safe plastic lens.

Atomic Digital Chrono Watch
< ADWA101 \$49.95
Our feature packed Chrono-Alarm watch is now available for under \$50! It has date and time alarms, stopwatch backlight, UTC time, and much more!
Use coupon code: ADWA49



5542Z-2

Arcron Atomic Watch
<5542Z-2 \$199.99
This elegant watch features a shock-resistant stainless steel case with hardened mineral lens. Black/grey dial with luminescent numbers/hands, and high quality replaceable leather band. Watch can change to any world time zone. Case diameter 40mm.

1-800-985-8463
www.atomictime.com



WAWG102



WS-8007U-C

^LaCrosse Digital Wall Clock \$34.95
This digital wall / desk clock comes with a beautiful cherry wood frame. It shows time, date, day of week, temperature and moon phase. 12/24 format.

Tell time by the U.S. Atomic Clock - The official U.S. time that governs ship movements, radio stations, space flights, and warplanes. With small radio receivers hidden inside our timepieces, they automatically synchronize to the U.S. Atomic Clock (which measures each second of time as 9,192,631,770 vibrations of a cesium 133 atom in a vacuum) and give time which is accurate to approx. 1 second every million years. Our timepieces even account automatically for daylight saving time, leap years, and leap seconds. \$7.95 Shipping & Handling via UPS. (Rush available at additional cost) Call M-F 9-5 CST for our free catalog.

A Space-Saving Antenna for 40 Meters

*A vertical antenna with short radials
and an electrically long radiator*

By Ron Skelton, W6WO

Constraints and Concepts

This article describes the design, construction and measurement of an unusual vertical antenna that has met my goal to work CW DX at near zero cost. Vertical antennas have well-known strengths and weaknesses, but their unique advantage is that they can be efficient DX antennas in a *very* small space. My constraints include a small back garden in a planned community. Fortunately, the owners association is reasonable about antennas; however, these must be as inconspicuous as possible. There is no space for elaborate horizontal or sloping wire antennas—a vertical is my *only* option.

There are many commercial multi-band verticals that use shortened radiators with a set of very short radials. These are expensive,

hard to duplicate and are not as efficient as an antenna optimized for a single band. I needed something that I could make that would be efficient and aesthetically acceptable.

Neither ground mounted radiators with extensive ground systems nor the common elevated “ground plane” design with quarter wave radials are possible, and short radiators with base and other forms of loading are inefficient. I considered a design using radials in a square form as described by Les Moxon, G6XN,¹ but all that wire would not meet with XYL approval.

A full-length quarter-wave self-supporting vertical radiator of 34 ft made from progressively smaller diameter aluminum tubing is quite feasible mechanically and when painted in a camouflage design is almost invisible.

Model First, Build Later

Using *EZNEC*² 3.0 models, I be-

¹Notes appear on page 56.

gan to experiment with sets of radials of various lengths, diameters and angles. All the models included an even number of radials that are symmetrical. In this arrangement, the currents in the radials themselves produce little or no radiation. This is important because it preserves a vertical radiation pattern with a single lobe at a low angle. I modeled a practical quarter-wave radiator using a set of tubing sections 1.5 inches in diameter at the base and progressively decreasing in diameter to 0.375 inches at the top.

To begin, a conventional elevated ground plane with four quarter-wave-length radials at a base height of 8 ft was modeled and found to have a 50 Ω SWR of about 1.9:1. Reducing radial lengths below quarter wave-length rapidly deteriorated the SWR.

I decided for practical reasons that four wire radials, 10 ft in length, would be my limit. Modeling this design resulted in an exceedingly high SWR with an input impedance of 20 $-j200$ at my design frequency of

4-221 Gull Cove Way
Capitola, CA 95010
w6wo@arrl.net

7.015 MHz. The real part of Z remained at a useful level of 20Ω but with the considerable negative reactance. Adding the positive reactance of an inductance at the base feedpoint was an obvious way to correct the SWR. 200Ω of positive reactance at 7.015 MHz requires a $4.5 \mu\text{H}$ coil, which is an easy component to make. However, the best SWR I could achieve with this model was 2.26:1—not quite good enough. Increasing the base height by a few feet did not change the SWR much, and while reducing height did improve the SWR, this was not an acceptable solution.

Four 10-ft radials were still more wires than I wanted, so I began to investigate even shorter elements. With numerous models, I investigated various combinations of wire and tubing. I hate to think how long it would have taken without *EZNEC*, so my thanks to W7EL. Incidentally, I use the label “Ground-plane” only for *resonant* radials and “counterpoise” where elements are not resonant. In the latter case, I think of the antenna as a vertical form of an off-center-fed dipole.

My next idea was to add inductive loading higher in the radiator. This would allow a reduction of base loading where the current losses are highest and would concentrate useful current at a higher point. I used a well-made coil of about $5 \mu\text{H}$ recovered from an old trap antenna that fit nicely at a point about half way up, where the diameter was 1.0 inch.

The final design uses four horizontal 0.375 inch OD tubing elements, each 4 ft long and two 10 ft wire radials sloping from base height to 6 feet. The effect of adding 5 mH of inductive load 16 feet above the base is to electrically lengthen the antenna, thereby reducing the frequency for best SWR considerably. The base load was then reduced to raise the frequency up to the design goal and this achieved a good match. Fig 1 shows the final plot.

A Practical Approach

It might have been possible to eliminate the base coil altogether by increasing the upper level inductance further. I decided not to pursue this, as I wanted to have the ability to adjust the coil and elements at a base height of 8 feet. I also considered adding some form of top hat but decided this would become a mechanical issue and was not needed. Playing with tubing and radial lengths and angles along with the base coil allows easy ground-

level tuning adjustments.

A low vertical angle of radiation is often good for DX and the angle of the only lobe of this antenna is lowered as the antenna height is increased. It could be reduced from 23° to about 21° by doubling the base height. I kept the base at 8 ft, making the antenna as inconspicuous as possible

Connecting the coax feeder raised the question of whether the coil should be in series with the radiator or the radials. From an impedance matching standpoint, this should be immaterial, but because this is an off-center fed design, I was concerned about common-mode cur-

rents on the coax feeder. I tried it both ways, and to check on shield currents, I used a voltage-canceling probe based on a design by Les Moxon, G6XN.³ I couldn't detect much difference, so for practical reasons I decided to insert the coil in series with the radiator.

Long ago I measured combinations of ferrite toroids over RG303 and RG58 coax as common-mode chokes. The rule of thumb is to add at least 10 times the coax impedance to the shield. The combination I used with this antenna has 25 mix 73 and 15 mix 43 toroids inserted at the feedpoint. This choke adds about

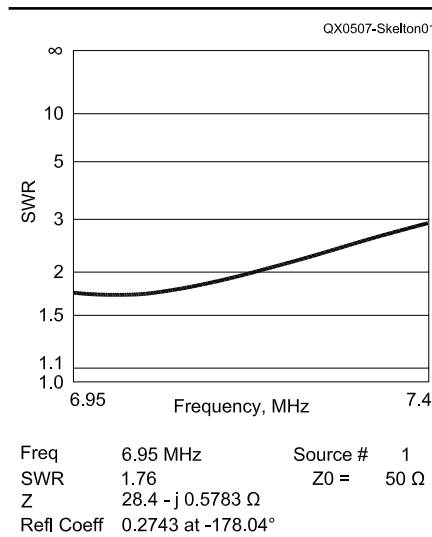


Fig 1—EZNEC plot of final model.



Fig 2—Voltage-canceling probe.

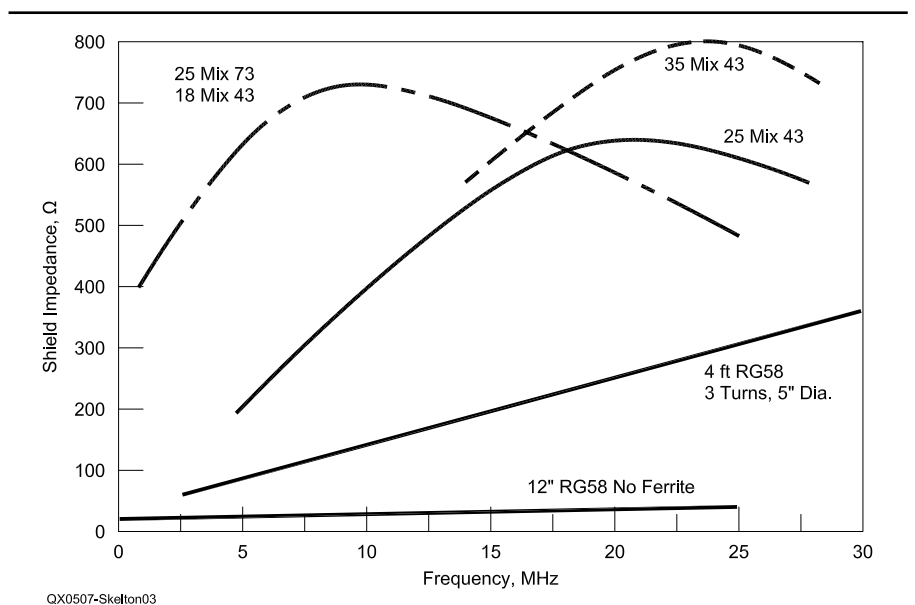


Fig 3—Ferrite common-mode chokes.



Fig 4—Base coil and radial elements.

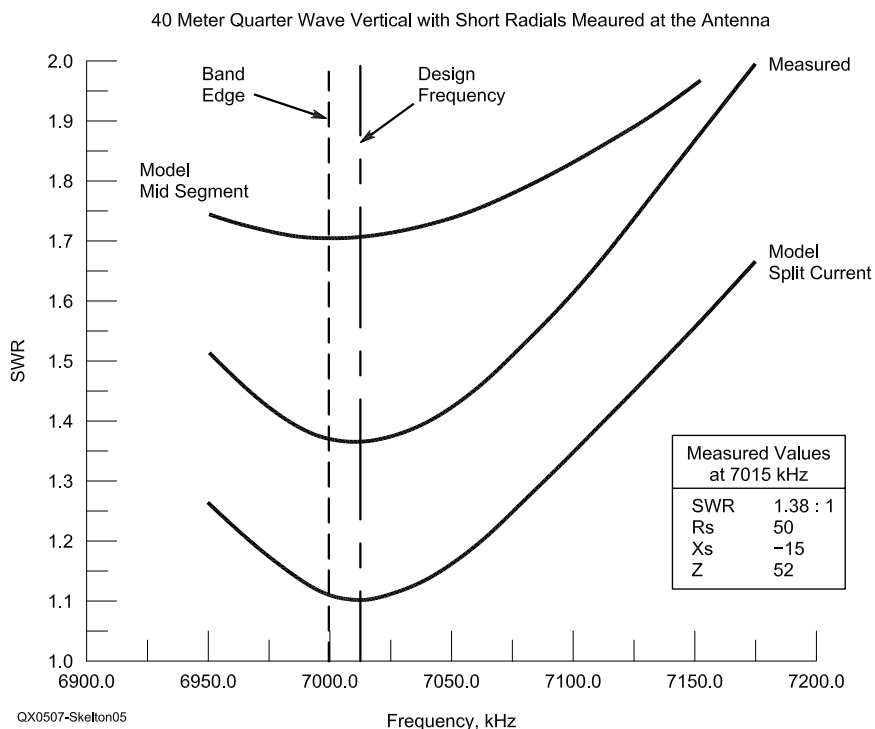


Fig 5—Results: actual versus model.

A picture is worth a thousand words...



With the all-new

ANTENNA MODEL™

wire antenna analysis program for Windows you get true 3D far field patterns that are far more informative than conventional 2D patterns or wire-frame pseudo-3D patterns.

Describe the antenna to the program in an easy-to-use spreadsheet-style format, and then with one mouse-click the program shows you the antenna pattern, front/back ratio, front/rear ratio, input impedance, efficiency, SWR, and more.

An optional **Symbols** window with formula evaluation capability can do your computations for you. A **Match Wizard** designs Gamma, T, or Hairpin matches for Yagi antennas. A **Clamp Wizard** calculates the equivalent diameter of Yagi element clamps. A **Yagi Optimizer** finds Yagi dimensions that satisfy performance objectives you specify. Major antenna properties can be graphed as a function of frequency.

There is **no built-in segment limit**. Your models can be as large and complicated as your system permits.

ANTENNA MODEL is only \$85US. This includes a Web site download **and** a permanent backup copy on CD-ROM. Visit our Web site for more information about **ANTENNA MODEL**.

Teri Software
P.O. Box 277
Lincoln, TX 78948

www.antennamodel.com

e-mail sales@antennamodel.com
phone 979-542-7952

700 Ω and prevents potential feedline problems.

The base uses a high quality coil of 5 μ H from a local flea market, to which I added a number of taps. Fig 4 shows the coil, the four tubing elements, the two wire elements and the ferrite choke.

Results

The final measured result showed close agreement with the model only with regard to the frequency of best SWR. The measured values showed lower SWR and a 125 kHz SWR bandwidth that is narrower than that of the model with the preferred mid-segment placement of the source.

I varied the Q of the coils and ground types in the model, but this did not substantially change the result and could not account for the difference. Most differences are probably related to environmental unknowns, but W7EL also cautions that **EZNEC** is very sensitive to placement and selection of the source used in the model. What I measured fell midway between the split-current source and the mid-segment source methods.

To obtain some idea of the antenna efficiency, I modeled the final design in free space to remove all ground loss and this showed a radiation resistance of 20 Ω . The re-

sistive component actually measured was quite incidentally 50 Ω . The 50 Ω represents the combination of radiation resistance (which is good) and power wasted in the ground and other objects. The ratio of 20/50 in this instance indicates an efficiency of 40%. So far so good, but how well does it perform? I have been very pleased with the results. For example, in competition with the huge pileup to work XV1X, I snagged him on my first call.

Ron was first licensed in 1951 as G3IHP and spent many tears as DX when there were still colonies. Retired in 1998 following a communication-systems career in government, telecommunications, financial services, computer and electric power sectors. Ron pioneered the use of digital microwave, carrier and switching systems, both in the US and in other countries. He is a Fellow of the Institution of Electrical Engineers and likes to build little boxes with knobs on them.

Notes

¹L. Moxon, G6XN, *HF Antennas for All Locations* (RSGB, available through ARRL), p 45, "Compact Two-radial Ground Plane."

²EZNEC Registered trademark, Roy W. Lewallen, W7EL.

³L. Moxon, G6XN, "HF Antennas for All Locations", p 280, "Voltage-cancelling Probe." □□

Octave for Signal Analysis

The GNU Octave analysis tool can be used to move data between the frequency and time domains—find out how below.

By Maynard A. Wright, W6PAP

Introduction

In *Octave—Calculations for Amateurs*,¹ we looked at using GNU *Octave*² to ease the workload of making and checking repetitive calculations. *Octave* offers a lot more than that, though.³ When we're operating, working on our gear, or reading technical literature, we often think about signals in either or both the time and frequency domains. Among other useful mathematical functions, *Octave* includes a powerful means to move signals back and forth between the two domains.

Why would we want to do that? Well, we might want to see what happens to the spectrum of a modulated signal when we crank up the mic gain a bit too high, we might specify a keying waveshape in the time domain and wonder just what its spectrum looks like, or we might have acquired a train

of measurements in the time domain from a digitizing oscilloscope and would like to see whether there are any surprises in the spectrum.⁴

This article is intended to illustrate how to use *Octave* to perform some useful transforms of signals. For a more comprehensive tutorial on transforming signals, and on other aspects of signal processing, see Chapter 18 of the *ARRL Handbook*.⁵

Let's begin with a simple sine wave. Although we could use normalized times and frequencies, it's easier to think about real signals, so we'll start with a sine wave at 16 kHz. We'll use a relatively low carrier frequency here so that we can display both the carrier and the modulating waveform with good resolution in our graphs without having to use really large vectors of samples. We'll set the amplitude of the sine wave to 1.0. We can think of this as representing the peak voltage level of the signal, although it might also represent a peak current.

Since we are using a digital computer here, we must represent our continuous (analog) sine wave as a sequence of discrete (digital) values in

time. The more values, the closer the representation. Such a sequence of values representing the amplitudes of a continuous signal at equally spaced instants of time is called a sampled signal.

We will choose 1024 points to represent the sine wave. The values will be stored in an array, called a vector in *Octave* when one of the dimensions is unity. The number 1024 results from our desire to choose a value that is a power of two because the fast Fourier transform (FFT) works more efficiently when dealing with vectors having such lengths. Although *Octave* can handle vectors of arbitrary lengths, some implementations of the FFT cannot work on vectors of lengths other than powers of two. 1024 points is actually overkill for the signals we will consider here, but the vectors we generate will plot nicely and will take very little time to compute, so we will use this relatively high number of samples. It is possible to completely represent a signal by sampling it at just more than twice the rate of the highest frequency component of the signal (see Chapter 18 of the *ARRL Handbook*), but it is

¹Notes appear on page 61.

often advantageous to sample at a higher rate and we are doing that here.

We'll start the program with the following code:

```
time1 = linspace(1, 1024, 1024);
v_cxr = sin(2 * pi * time1 / 32);
```

This code builds a vector of 1024 real numbers in *v_cxr* that represents a sine wave that includes 32 full cycles. Next, we add some code to plot the sine wave. The plot appears in Fig 1:

```
title "TIME DOMAIN SINUSOID";
xlabel "TIME: 1.95 us PER DIVISION";
ylabel "AMPLITUDE";
grid
axis([0, 60, -abs(max(v_cxr)) - 0.1,...
abs(max(v_cxr)) + 0.1]);
plot(time1, v_cxr);
pause;
```

The "pause" command causes execution of the code to halt with the plot displayed until any key is pressed to cause the code to continue.

We will have occasion to plot other curves as we go along, and we will change the code above as is appropriate for each plot, but without further discussion. An explanation of the plotting capabilities and options of *Octave* is included in Chapter 14 of the *GNU Octave Manual* (see Note 2). The changes we make will involve the title and the second argument to `axis()`, which determines how much of the vector gets displayed.

We could also change the y-axis to a logarithmic plot, which you might want to do in practical analysis as many signals you will simulate or capture are measured in decibels, a logarithmic measure. You can change the y axis to a logarithmic scale by using the function `semilogy()` instead of `plot()`. Or you might convert your data from linear to logarithmic before plotting and then use the linear plot. All the figures in this article use linear plots for simplicity.

Now that we have our sine wave described in the time domain, let's see what it looks like in the frequency domain. Most of us are aware that a sine wave signal in the time domain is represented by a single line in the frequency domain. Can we verify that using *Octave*? *Octave* provides a pair of functions, `fft()` and `ifft()`, that can be used to move the representation of a signal back and forth between the time domain and the frequency domain. Let's try that with our sine wave using the following code:⁶

```
s_cxr = fft(v_cxr) / 512;
s_cxr(1) /= 2;
```

The second line above divides the dc component of the signal by two since it is not affected by the need to compensate for discarding the negative frequencies.

The function `fft()` performs a transformation from the time domain to the frequency domain and stores the result in a vector *s_cxr*. The vector names *v_cxr* and *s_cxr* were chosen to represent the time and frequency domain representations of the signal. You can choose any names you want for such

signals as long as they don't conflict with reserved names in *Octave*.⁷

Once we execute the code, we have a vector, *s_cxr*, in the frequency domain, but what does it mean? The *Octave* function `fft()` produces an output vector that contains three components:

1. amplitude of a dc component
2. amplitudes of components at positive frequencies
3. amplitudes of components at negative frequencies

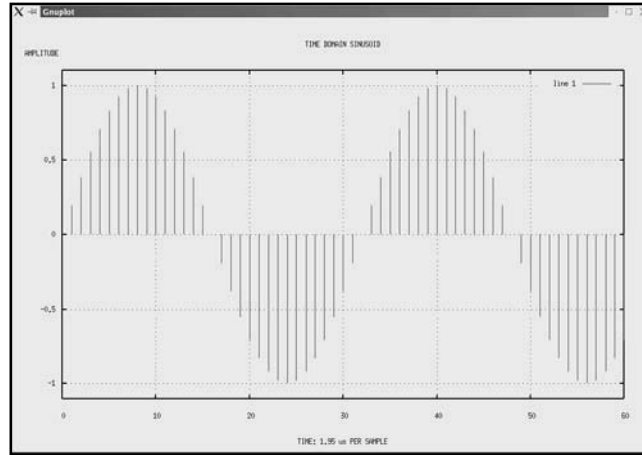


Fig 1—A 16 kHz sine wave that is sampled 32 times per cycle of waveform.

Table 1—The *Octave* code used in this article

```
# Octave program for investigating modulation products
time1 = linspace(1, 1024, 1024);
A_cxr = 1;
#m = input("\n\n ENTER MODULATION FACTOR:");
m = input("\n\n ENTER MODULATION INDEX ");
#v_cxr = A_cxr * cos(2 * pi * time1 / 32) .* (1 + m * ...
# sin(2 * pi * time1 / 512)); # AM modulation
v_cxr = A_cxr * cos((2 * pi * time1 / 32) + m * ...
sin(2 * pi * time1 / 512)); # FM modulation
title "TIME DOMAIN SINUSOID";
xlabel "TIME: 1.95 us PER SAMPLE";
ylabel "AMPLITUDE";
grid
axis([0, 60, -abs(max(v_cxr)) - 0.1, abs(max(v_cxr)) + 0.1]);
plot(time1, v_cxr, "A");
pause;
s_cxr = fft(v_cxr) / 512;
for n = 1:80
    trunq(n) = s_cxr(n);
endfor
w1(1) = 0;
for n = 1:79
    w1(n + 1) = 0.5 * n;
endfor
title "FM SIGNAL FREQUENCY SPECTRUM";
xlabel "FREQUENCY IN kHz";
ylabel "AMPLITUDE";
grid
axis([0, 30, 0, abs(max(trunq)) + 0.1]);
plot(w1, abs(trunq), "A");
pause;
```

Tables 2 and 3 show how this data is stored in *s_cxr*.

There are many good textbooks that discuss the representation of the frequency spectrum using positive and negative frequencies (see, for instance, Chapter 2 of the reference in Note 8). If our input signal consists of a series of real rather than complex variables, though, we can ignore the issue by discarding the negative values, which consist of the upper half of what's in *s_cxr*, and by doubling the values in the lower half to compensate for discarding the negative information. The dc (average) component will be zero in the case of our sine wave.

Now, where is all this stuff stored in the vector? The dc component is stored in the first element of the vector, *s_cxr(1)*. If you type *s_cxr(1)* from within *Octave* after executing the *fft()* function, *Octave* will print the dc value, zero in our example, on the screen. The positive values are stored in ascending order in elements 2 through *N/2*, where *N* is the number of samples, or 1024 in our case. The values above *N/2* are all related to negative frequencies and we will simply ignore them for all the examples in this article.

We now know where the information is stored, but what does it mean in terms of frequencies? Each element stored in *s_cxr* represents the peak amplitude of a sine wave at some frequency that is one of a number of sine waves that can be added together to produce the time domain signal *v_cxr*. The maximum frequency that can be represented is half the sampling frequency, sometimes called the Nyquist frequency, sometimes called the Nyquist frequency. We defined our sine wave so that there will be 32 cycles represented by 1024 samples. This means that each cycle will be represented by 32 samples.⁹ The length of one cycle will be $1 / (16 \text{ kHz}) = 62.5$ microseconds. Since there are 32 samples per cycle, the spacing between samples will be about 1.95 microseconds and the sampling frequency is the inverse of that spacing, or 512 kHz.

Element *N/2*, the highest frequency that can be stored, will be at the Nyquist frequency which is half the sampling frequency, or 256 kHz. There are 512 samples representing that range of frequencies, so there is a spacing of 500 Hz between samples. If we plot the transform of our 16 kHz sine wave, we can then expect the signal to be represented by the 32nd line in the plot.

You may not always be dealing with a simple signal such as a sine wave. Keep in mind that the highest frequency that will be represented by the

output of *fft()* will be the Nyquist frequency, or half the sampling rate, and you can determine the frequencies of all the elements of the vector from there.

It would be nice to have the x-axis of the plot represent the frequency in kHz. We can make that happen by generating a new vector, *w1*, that increments at values of 0.5 along the x-axis. We then plot *s_cxr* as a function of *w1* using the following code:

```
for n = 1:80
    trunq(n) = s_cxr(n);
endfor
w1(1) = 0;
for n = 1:79
    w1(n + 1) = 0.5 * n;
endfor
title "FREQUENCY DOMAIN SINUSOID";
xlabel "FREQUENCY IN kHz";
ylabel "AMPLITUDE";
grid
axis([0, 30, 0, abs(max(trunq)) + 0.1]);
plot(w1, abs(trunq), "A");
pause;
```

The plot of the frequency spectrum of our signal is shown in Fig 2. As we would expect, it consists of a line in the spectrum at 16 kHz. The code we used is shown assembled into an *Octave* program in Table 1.¹⁰ The code as shown will calculate and plot the time and frequency domain representing our 16 kHz sine wave. Included, but commented out using the symbol “#” at the beginning of each line, is code that we will use later in this article. Note that some code

is included for accepting a modulation index from the keyboard during execution of the program.

As an exercise, you might want to use *ifft()* to transform *s_cxr* back into the time domain to see whether you get a signal that is identical to *v_cxr*, the signal with which we began.

So far, we've done quite a bit of arithmetic to calculate and plot something that we knew in advance. Can we do anything useful with this tool?

Let's take a look at amplitude modulation to see what we can learn. We'll consider an amplitude-modulated (AM) signal first and we'll use equation 8 on page 15.5 of the *ARRL Handbook* to define the signal. Our code is to generate the time domain signal is:

```
v_cxr_AM = sin(2 * pi * time1/32) .* (1 + m *
sin(2 * pi * time1/512));
```

The period immediately preceding the multiply sign (“*”) indicates that the multiplication is to be carried out element-by-element over the two vectors. If we omit the period, *Octave* will attempt to carry out a matrix multiplication, something mathematically illegal for these two vectors and which would not give us what we want anyway.

The variable *m* is the modulation factor (see page 15.5 of *The ARRL Handbook*) and is accepted from the keyboard in our code. Note that dividing by 512 in the modulating signal

Table 2—Assignment of elements of the output vector of *fft()* when the number of samples, *N*, is even:

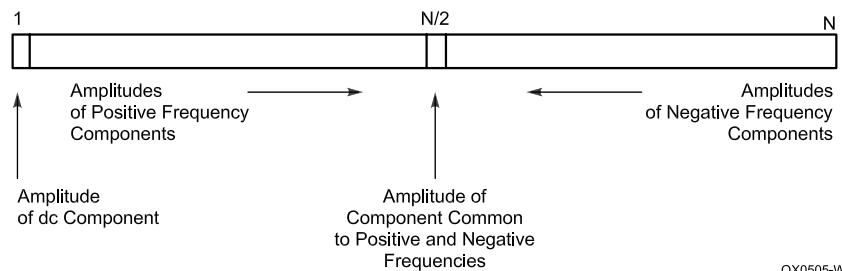
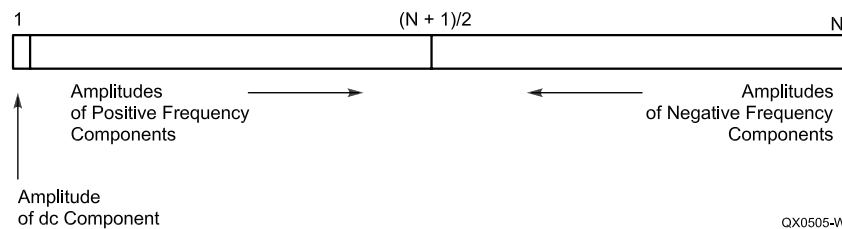


Table 3—Assignment of elements of the output vector of *fft()* when the number of samples, *N*, is odd:



produces two cycles of waveform over the 1024 samples for a modulating frequency of 1000 hertz.

In a practical modulator, though, there are other considerations. If we are

using plate modulation of a vacuum tube amplifier, for example, the modulating signal consists of the dc plate current as modulated by the modulating signal, just the expression in the

second set of parentheses above. If the negative swing of the modulating signal amplitude exceeds the dc plate current value, the current stops as current can't flow backward through a vacuum

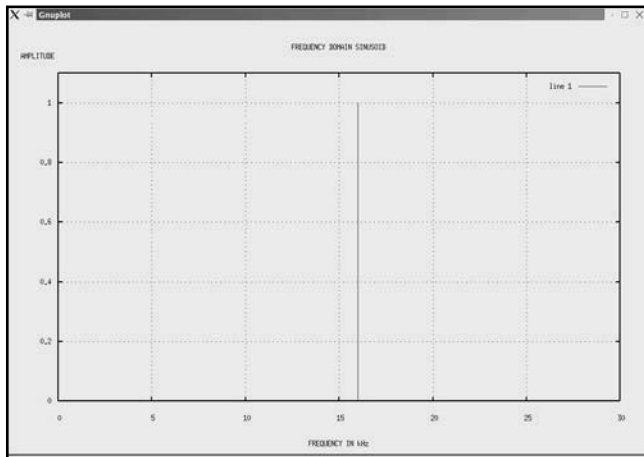


Fig 2—This line in the frequency spectrum represents the same signal that is shown in the time domain in Fig 1. Note that the peak amplitude is 1.0 in both figures.

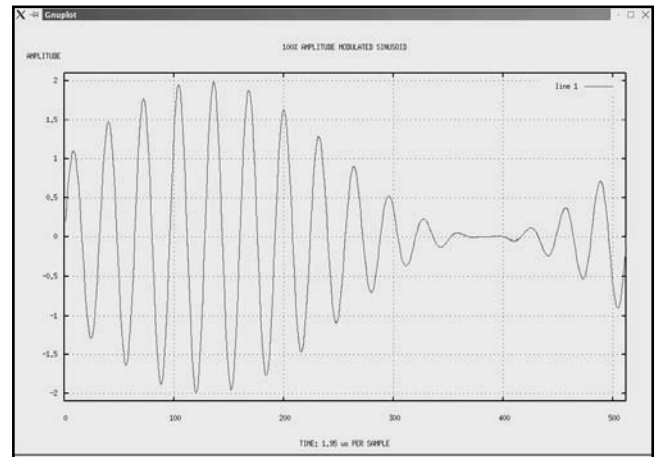


Fig 3—A 16 kHz sine wave 100% amplitude modulated by a 1 kHz sine wave.

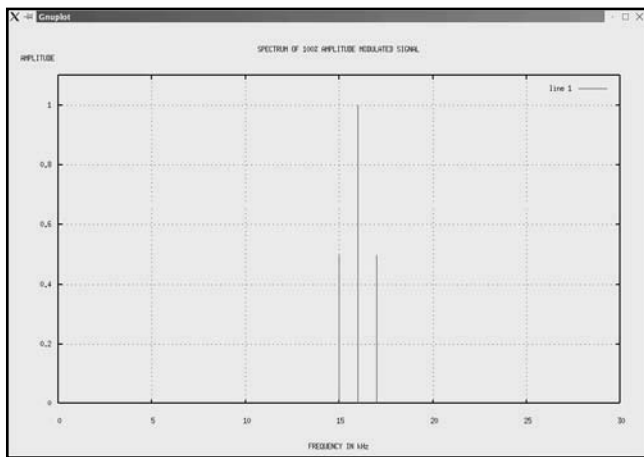


Fig 4—The frequency spectrum of the signal in Fig 3.

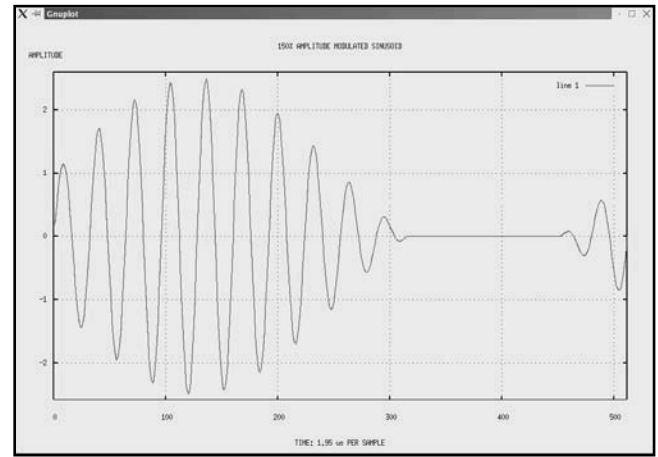


Fig 5—A 16 kHz sine wave 150% amplitude modulated (overmodulated) by a 1 kHz sine wave.

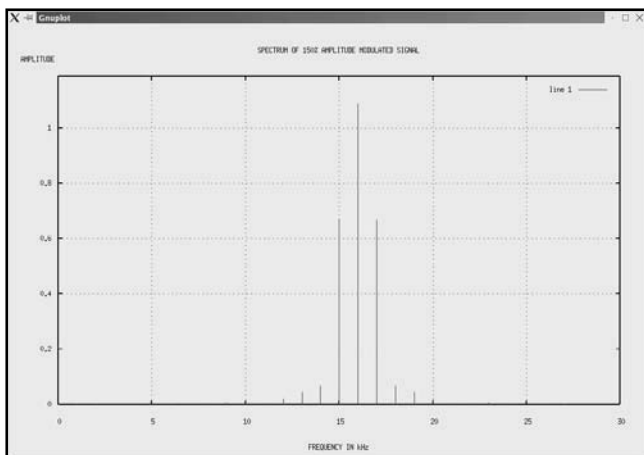


Fig 6—The frequency spectrum of the overmodulated signal in Fig 5.

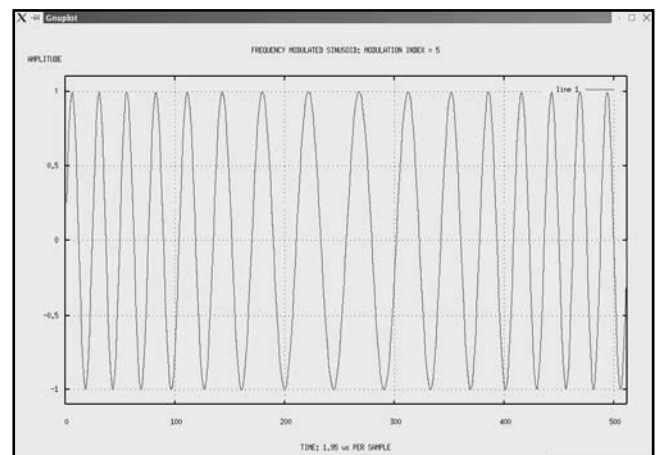


Fig 7—A 16 kHz sine wave frequency modulated by a 1 kHz sine wave with a modulation index of 5.

tube. Let's split up the expression above so that we can take that into account. We keep our original expression for the unmodulated carrier:

```
v_cxr = sin(2 * pi * time1 / 32);
```

We define the modulating waveform separately and then prevent it from going below zero by setting it to zero anytime it is below that value:

```
v_mod = (1 + m * sin(2 * pi * time1 / 512));
for ctr = 1:1024
    if(v_mod(ctr) < 0)
        v_mod(ctr) = 0;
    endif
endfor
```

Now we modulate the carrier by multiplying it by the modulating signal:

```
v_cxr_AM = v_cxr .* v_mod;
```

Fig 3 shows our 16 kHz sine wave 100% modulated (modulation factor = 1) by a 1 kHz sine wave. Fig 4 shows the corresponding frequency domain plot. Note the two sidebands spaced at 1 kHz to each side of the carrier. The carrier amplitude remains at 1.0 and each sideband has an amplitude of 0.5.

Fig 5 shows what happens when we modulate the carrier at 150 percent by setting m equal to 1.5 from the keyboard. Note the long period of time during the cycle when the signal is cut off by the attempt to force plate current backward through the final amplifier tube. Fig 6 shows the frequency domain representation of that same signal. The two desired sidebands are still there, but there is also energy at other multiples of 1 kHz away from the carrier, causing the signal to splatter out beyond the desired bandwidth. The carrier has also been distorted and has a peak value of greater than 1.0 due to addition of spurious energy at its frequency.

We can also use *Octave* to analyze an FM signal. A little rearrangement of our modulating signal gives us equation 10 on page 15.9 of the *ARRL Handbook*:

```
v_cxr_FM = sin(2 * pi * time1 / 32) .*
sin(m * ... sin(2 * pi * time1 / 512));
```

where m is termed the modulation index. We usually refer to a table or chart of Bessel functions to determine the relative amplitudes of the various sidebands comprising an FM signal as in Fig 12.8 of the *ARRL Handbook*, but

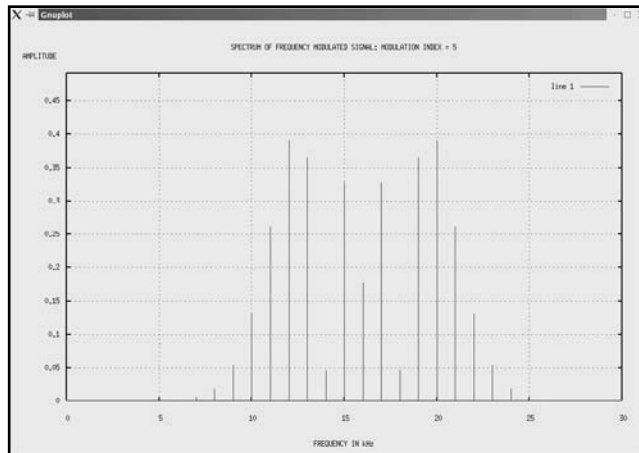


Fig 8—The frequency spectrum of the signal in Fig 7

we can also use *fft()* to analyze an FM signal.

Let's assume a modulation index of 5.0. We can change our prompt to specify MODULATION INDEX instead of MODULATION FACTOR, but whether or not we do that won't affect the results. The resulting time domain waveform is shown in Fig 7 and the corresponding frequency spectrum in Fig 8.

As another exercise, you might want to convert the values in Fig 8 to decibels with respect to one volt and compare them with the values in Fig 12.8 of the *ARRL Handbook*.

As you acquire experience in using *Octave*, you will find more applications for this versatile software tool. When you are reading the *ARRL Handbook* or any other technical text material, use *Octave* to try out some of the results that are shown in tabular form or are graphed. You will be able to change some of the input data, as well as the equations, and see what effects you observe in the output data. Doing this can fix the principles of interest in your mind, enhance your understanding of those principles, and make the process of learning something new more enjoyable.

Notes:

- ¹M. Wright, W6PAP, *Octave - Calculations for Amateurs, QEX*, May/June 2005, pp 48-50.
- ²J. Eaton, *GNU Octave Manual*, Network Theory Limited, 1997.
- ³This assumes that you are willing to comply with the GNU Public License, which you can read at www.gnu.org or www.octave.org. See www.octave.org to obtain a copy of *Octave* for your system. The code featured in this article was tested using two versions of *Octave* running under *RedHat Linux 8* and *Microsoft Windows 98SE*.
- ⁴Many test instruments and systems can output acquired data to a file which can be transferred via diskette or data channel to the computer that hosts *Octave*. *Octave*

makes provision for reading such a datafile into a matrix or a vector.

- ⁵The *ARRL Handbook for Radio Communications, 2004*, The American Radio Relay League, Inc., 2003. All references to the *Handbook* in this article are from this edition.
- ⁶The Fourier transform pair that moves signals back and forth between the time and frequency domains includes coefficients that vary among different implementations. *Octave* uses no coefficients in implementing the direct transform (*fft()*), but uses a coefficient 1/N in implementing the inverse transform (*ifft()*). The divisor (512) that we have supplied represents a combination of a divisor of 1024 (the number or points, or N) and a multiplication by 2 to compensate for ignoring the negative frequency information. We chose this coefficient because it causes a time domain signal measured in volts to be transformed into a frequency domain signal in which each component is measured in volts.
- ⁷J. Eaton, *GNU Octave Manual*, Network Theory Limited, 1997, chapter 30.
- ⁸B. Lathi, *Modern Digital and Analog Communication Systems*, Third Edition, Oxford University Press, 1998.
- ⁹This is because 1024 is 32². For other numbers of samples, the number of cycles per vector and the number of samples per cycle will not necessarily be equal.
- ¹⁰Good coding practice calls for carefully and extensively commenting source code. In this case, the code in Table 1 is presented with few comments for simplicity with the intent that the text of the article will adequately comment the code.

Maynard Wright, W6PAP, was first licensed in 1957 as WN6PAP. He holds an FCC General Radiotelephone Operator's license with Ship Radar endorsement, is a registered professional engineer in California and a Senior Member of IEEE. He has been involved in the telecommunications industry for 41 years. Maynard is a member of the North Hills Radio Club in Sacramento, California. You can reach him at 6930 Enright Dr, Citrus Heights, CA 95621-2837; 916-726-1673; w6pap@arrl.net. □□

Letters to the Editor

ATX Adventures (Nov/Dec 2004)

Doug,

This is a little late, but I want to say how much I enjoyed the article by Phil Eide, KF6ZZ, on his repair and conversion of an ATX power supply for ham use. My experience has been that most discussions of switchers leave the impression that they are far too complex for hams to tamper with. The few articles on switchers I've seen use a strict cookbook approach. Mr. Eide's article takes a lot of the mystery out of the design process and almost leads me to believe that a mere mortal could take on such a project. I thought the informal and lighthearted writing style, mixed in with practical pointers and just enough theory, made it hard to avoid learning at least a little.

Topics involving magnetics are often pretty foreboding for both engineers and amateurs, excepting a small group of specialists. I'd like to see more articles like this one, to throw some more light on the subject.—73, Nicholas R. Kennedy, WA5BDU (E), 300 S Vancouver Ave, Russellville, AR 72801-5632; wa5bdu@arrl.net

Coaxial Traps for Multiband Antennas (Nov/Dec 2004)

Dear Doug and Tony (VE6YP):

In consideration of the marvelous article appearing in the Nov/Dec issue of *QEX* regarding coax traps and the underlying theory, I was wondering if you plan to update your [VE6YP's] coax trap "calculation" program?

As an aside, I have recently constructed several coax traps; one is a "single" winding trap using RG-213, and the another a "double" winding

trap using Belden 8263. My experience has been that your program under-estimates the number of turns that are necessary.

My first attempt (using RG-213) was to construct a trap resonant at about 3900 kHz. Using your calculations (number of turns equals ~ 7 for a 4 $\frac{1}{2}$ -inch OD form). It resonated at about 5.600 kHz, not 3900, as desired.

For the second trap (using Belden 8263), with a double winding in parallel, I decided to add turns (that could be removed, later, if necessary). Your program calculated that each coil should use ~ 7.7 turns. I wound the trap using 9 turns (on a 3 $\frac{1}{2}$ -inch OD form). Upon completion, I found the (unloaded) resonance to be at 3772 kHz. (Had I used 7.7 turns per coil, I would have wasted another batch of coax.)

Considering how (mechanically) difficult it is to construct these traps, I decided to install the trap "as is." Much to my delight, my 160 m inverted L antenna is now a dual-bander, with resonance on 80 meters at ~ 3750 kHz. That's close enough (to 3900) for "government work." My resonance on 160 dropped from 1890 kHz to 1865. I have no trouble matching it (anywhere) on either band.

Most importantly, the trap seems to be unconditionally stable. Prior traps (conventionally constructed) that I tried would drift as they warmed—even with only 100 W applied. This one does not drift (applying 1 kW CW for 30 seconds), neither is it affected by weather. (I sealed it rather well with liquid tape.) Figs 1 and 2 show the trap.

Incidentally, it's wound on a 3 $\frac{1}{2}$ inch OD ABS form, 6 inches long, the trap weighs-in at about 17.7 ounces, a bit heavy, but manageable. Needless to say, I am delighted with the ultimate success. Please let me know what, if any, changes (per the analy-

sis and measurements by Mr. Muller) that you have made (or plan to make) to your coax trap design software, particularly to correct the calculation of *L*, *C* and *Z*.

Thanks and regards—Jim Gorman, W6SQZ; JGormanRed@aol.com

An Inexpensive Terminal Node Controller for Packet Radio (Mar/Apr 2005)

Doug and TNC Builders,

I have received more feedback on the TNC article, so I want to pass it on to everyone to expedite your building efforts.

1. The text on page 24 of the article describes the monitor command. In the software implementation, it is actually "mon" (that is, mon off/all/me). Thanks to Philip R. Gaudet Jr, K1IRK, 81 Pascal Ave Rockport, ME 04856-5916; k1irk@arrl.net

2. If you plan to reassemble the software and use MPLAB 7.01 or later you will see 3 undefined symbols due to MicroChip's unexpected change in name. As pointed out by Leo Coleman, this can easily be fixed by making the following changes in the provided tnc.asm file:

```
Change TOIE to TMR0IE
Change TOIF to TMR0IF
Change _WRT_ENABLE_OFF to
_WRT_PROTECT_OFF
```

3. Phil, K1IRK and Rod, Kreuter WA3ENK, have experienced some high frequency oscillation in the receive circuitry causing the receive LED to oscillate. Phil and Rod recommend a more robust design that would include a slight amount of negative feedback to insure this doesn't happen. They suggest the following:



Fig 1—A side view photo of W6SQZ's trap.



Fig 2—An end view photo of W6SQZ's trap.

A. Lift ground from Pin 1 of the 16F88 (leave ground on pin 18). Insert a 470 Ω resistor from pin 1 to ground.

B. Insert a 100 kΩ resistor from pin 1 to pin 2 on the 16F88. This will provide a small of hysteresis and stabilize against oscillations.

C. They also recommend putting a 0.001 μF capacitor from pin 17 to ground to remove any potential 20 MHz clock signal from the comparator.

I haven't experienced this oscillation on any of the five units I have built. That might have been dumb luck! I think that Phil and Rod have a good idea and plan on modifying one of my units to try it. Thank you Phil and Rod!

5. Phil also has the following suggestion on the transmit circuitry:

I have looked at the output on a scope using the calibration function, and it looks okay. I thought it might be a good idea to put a capacitor across the potentiometer to smooth the steps on the sine-wave approximation, rather than letting the radio do that.

6. Rod Kreuter, WA3ENK sent some e-mail about a terminal setup problem he experienced with the TNC. The TNC expects a Line Feed character at the end of a command sequence from the terminal. If it sees only a carriage return for the line end, it echoes the individual characters but then times out after about 7 seconds, since it thinks the operator went to get a drink in the middle of the command! I use *Hyperterminal* under *XP*, which has the option set to send line feeds (file->properties->settings->ASCII setup->"send line end with LF"). Rod experienced the problem with *Procomm* under *DOS*. If you experience this problem and can't set your particular terminal program to work, please let me know.

Thanks to Rod for digging into the source code and figuring this one out. Nice piece of detective work!—*Bob Ball, WB8WGA, 23 Ingerson Rd, Jefferson, NH 03583-6230; wb8wga@arrl.net*

Receiver Audio Processing Using a Phase-Locked Loop (May/June 2005)

Hi Doug,

I have received my complimentary copies of May/June *QEX*. Thanks. I'm glad to see my article in print. Now, there is one problem.

I received an e-mail message from K8CU a couple of days ago. He had built my audio processing device (already!) but found that it didn't work. He wondered whether there might be

an error in the schematic as published in *QEX*. So, I checked the schematic against my original and, sure enough, there are errors in one section.

In Fig 4, in the section of the schematic involving U1 and the adjacent ½ U2, the following corrections should be made:

1. The 1000 pF capacitor should be shown connected between pins 7 and 8 of U1.

2. The 47 kΩ resistor above ½ U2 should be connected between pins 6 and 7 of the ½ U2.

3. Pin 8 of U1 is *not* connected to pin 6 of the ½ U2.

Thanks and 73—*Bob Kavanagh, VE3OSZ; ve3osz@rac.ca* □□

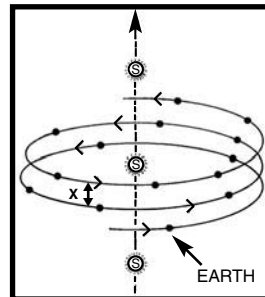
In the next issue of QEX/Communications Quarterly

In the next *QEX*, Rod Brink, KQ6F, describes his new direct-conversion phasing rig for 75 m and 40 m. The unit uses a Stamp II module for control and an AD9835 DDS for tuning. Rod combines modern subsystems to achieve an up-to-date version of an old idea. □□

Scientist - Author - Publisher of "Physics - Astronomy - Sciences - New Theories with Interpretations".

WALTER H. VOLKMANN

Will an Object Launched Into Space Ever Stop?
Answer in Book.



Hardcover, 6" x 9", 15.2 x 22.8 cm
137 pages, 46 photos and illustrations

\$30.00 Postpaid USA - Surface US
\$34.00 Postpaid Foreign - Surface Dollars
\$40.00 Postpaid Foreign - Air

Order by Mail	- or -	Order by Fax
Walter H. Volkmann		Walter H. Volkmann
QEX - Ad		QEX - Ad
P.O. Box 271797		972-874-0687
Flower Mound, Texas, USA		
75027-1797		

Credit Card:
MasterCard, or Visa, Money Order.
No Billing, all orders prepaid.



ARRL
225 Main Street
Newington, CT 06111-1494 USA

For one year (6 bi-monthly issues) of QEX:

In the US

- ARRL Member \$24.00
- Non-Member \$36.00

In the US by First Class mail

- ARRL Member \$37.00
- Non-Member \$49.00

Elsewhere by Surface Mail
(4-8 week delivery)

- ARRL Member \$31.00
- Non-Member \$43.00

Canada by Airmail

- ARRL Member \$40.00
- Non-Member \$52.00

Elsewhere by Airmail

- ARRL Member \$59.00
- Non-Member \$71.00

Remittance must be in US funds and checks must be drawn on a bank in the US.
Prices subject to change without notice.

QEX Subscription Order Card

QEX, the Forum for Communications Experimenters is available at the rates shown at left. Maximum term is 6 issues, and because of the uncertainty of postal rates, prices are subject to change without notice.

Subscribe toll-free with your credit card 1-888-277-5289

Renewal New Subscription

Name _____ Call _____

Address _____

City _____ State or Province _____ Postal Code _____

Payment Enclosed to ARRL

Charge:



Account # _____ Good thru _____

Signature _____ Date _____

06/01

Down East Microwave Inc.

We are your #1 source for 50MHz to 10GHz components, kits and assemblies for all your amateur radio and Satellite projects.

Transverters & Down Converters, Linear power amplifiers, Low Noise preamps, coaxial components, hybrid power modules, relays, GaAsFET, PHEMT's, & FET's, MMIC's, mixers, chip components, and other hard to find items for small signal and low noise applications.

We can interface our transverters with most radios.

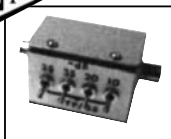
Please call, write or see our web site www.downeastmicrowave.com for our Catalog, detailed Product descriptions and interfacing details.

Down East Microwave Inc.
954 Rt. 519
Frenchtown, NJ 08825 USA
Tel. (908) 996-3584
Fax. (908) 996-3702

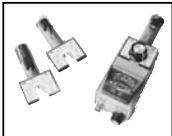
NATIONAL RF, INC.



VECTOR-FINDER
Handheld VHF direction finder. Uses any FM xcvr. Audible & LED display.
VF-142Q, 130-300 MHz \$239.95
VF-142QM, 130-500 MHz \$289.95



ATTENUATOR
Switchable, T-Pad Attenuator, 100 dB max - 10 dB min BNC connectors
AT-100, \$89.95



DIP METER
Find the resonant frequency of tuned circuits or resonant networks—ie antennas.
NRM-2, with 1 coil set, \$219.95
NRM-2D, with 3 coil sets (1.5-40 MHz), and Pelican case, \$299.95
Additional coils (ranges between 400 kHz and 70 MHz avail.), \$39.95 each



DIAL SCALES
The perfect finishing touch for your homebrew projects. 1/4-inch shaft couplings.
NPD-1, 3 1/4 x 2 3/4 inches 7:1 drive, \$34.95
NPD-2, 5 1/8 x 3 3/8 inches 8:1 drive, \$44.95
NPD-3, 5 1/8 x 3 3/8 inches 6:1 drive, \$49.95

S/H Extra, CA add tax

NATIONAL RF, INC
7969 ENGINEER ROAD, #102
SAN DIEGO, CA 92111

858.565.1319 FAX 858.571.5909
www.NationalRF.com

ENHANCE DX RECEPTION !

ASAP-2 Antenna Switch & Preamp

- > Use With HF Transceivers
- > 1.8-30 MHz Freq. Coverage
- > Select 1 of 4 Receive Ant. or Xmit Antenna
- > Select -20, 0, +20 dB Gain
- > 5 dB NF, +30 dBm 3rd OIP
- > Uses Rig Key Line for T/R
- > Great for N,S,E,W Beverages, Shielded Loops, Whips
- > ASAP-1 Receive Only/SWL model



ASAP-2 @ \$149.50
ASAP-1 @ \$119.50
PS-1 12V AC Adapter @ \$13.95

Check, M.O. Buy-On-Line (Pay-Pal)
Post Paid- Priority Mail (U.S.)

STOP IN-RUSH !

SS-811 Soft-Start Module

- > For Ameritron 811 Amplifiers
- > Extends Tube and Power Supply Component Life
- > Limits Turn-On In-Rush
- > 2-Sec. Full HV Time Delay
- > Easy to Install, Only 3 Wires
- > Step-by-Step Instructions
- > Can be used with other 115VAC, 15 Amp Draw Linear Amplifiers (Please Call for Details)



SS-811 @ \$49.50

(850) 936-7100

www.j-tecradio.com

J-TEC

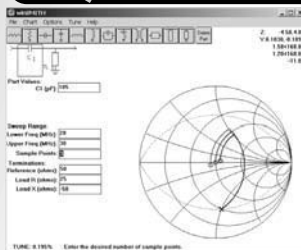
Big Savings for Amateur Radio Operators!

"Noble Publishing is offering these titles to amateurs at half price!
We don't pay royalties for these titles and you can save."

Randy Rhea, N4HI

\$74.50

~~\$149~~ winSMITH 2.0



Automate the design of transmission line & lumped element networks, & learn how the Smith chart works.

TUTORIAL CDs

\$49.50

\$99

Introduction to the Smith Chart

A great way to learn about the Smith chart & to begin solving antenna, matching & other problems.

\$49.50

\$99

Q from A to Z

Fully understanding Q will give you tremendous insight to circuit behavior.

\$148.50

\$297

Practical Issues in HF Frequency Design

This series of 3 CDs explains why HF circuits often don't behave as expected. You'll learn how to fix them.

\$49.50

\$99

AMW Magazine Archive

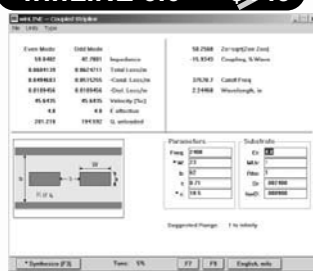
A searchable archive of over 500 great technical articles from Applied Microwave & Wireless magazine published from 1989 to 2002.

SOFTWARE

written by the engineers at Eagleware

\$74.50

~~\$149~~ winLINE 6.0



Relate physical & electrical parameters of transmission lines such as microstrip, stripline, coupled lines, inverted, coplanar, suspended & others.

BOOKS

HF Filter Design

& Computer Simulation

Complete coverage of L-C and printed filter design. Best seller!

\$34.50

\$69

Microwave Transmission Line Impedance Data

Formula & graphs of impedance data for many types of line. This book complements winLINE.

\$27

\$54

Oscillator Design & Computer Simulation

The popular & authoritative book on oscillator design. Covers VCO, xtal & transmission line oscillators.

\$34.50

\$69

ORDER DIRECT at WWW.NOBLEPUB.COM

To take advantage of this sale, order direct at our website and use the discount coupon code QEX05A

NEW ADDRESS

1334 Meridian Rd
Thomasville, GA 31792

TEL 229.377.0587
FAX 229.377.0589

NOBLE PUBLISHING

NEW! Fourth Edition

ON4UN's

Low-Band DXing

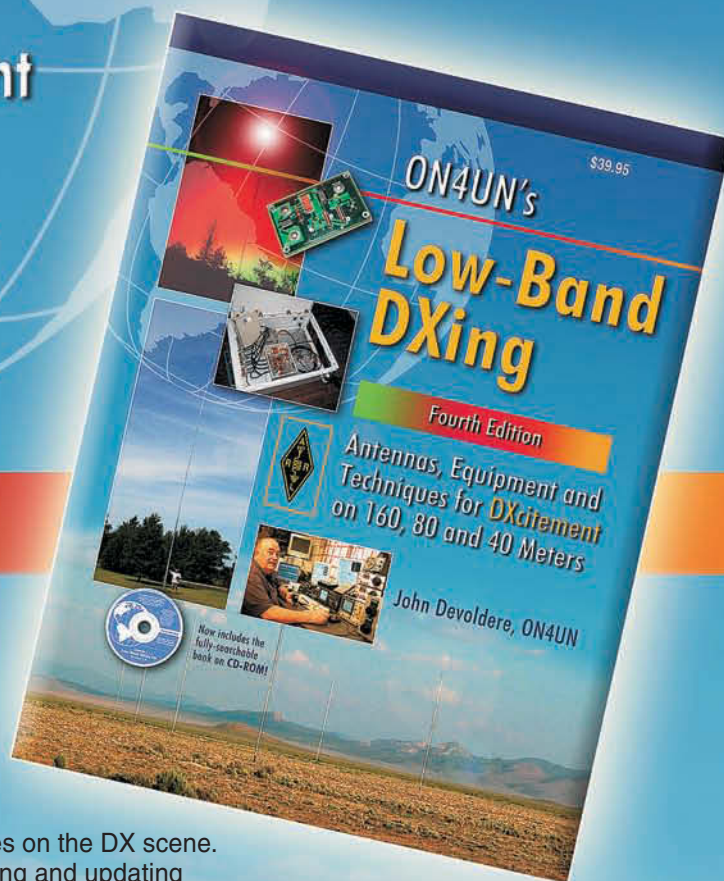
Antennas, Equipment
and Techniques for
DXcitement on 160,
80 and 40 Meters

by John Devoldere, ON4UN

Thoroughly updated with entirely new material on low-band antennas and high-gain transmitting arrays. Includes new insights and new design techniques for receiving antennas and vertical arrays.

"John is one of the most recognizable figures on the DX scene. He has spent more than 1,500 hours rewriting and updating **ON4UN's Low-Band DXing**, known far and wide as the 'low-bander's bible.'"—R. Dean Straw, N6BV, Editor

CD-ROM included! This edition is bundled with the fully searchable and complete book on **CD-ROM** for *Windows*[®] and *Macintosh*[®] systems. (Also contains additional **ON4UN software** and over 2000 quality pictures.)



ARRL Order No. 9140—**\$39.95***
*shipping: \$9 US (ground) / \$14 International

Shipping and Handling charges apply.
Sales Tax is required for orders shipped to CA, CT, VA, and Canada.

Prices and product availability are subject to change without notice.

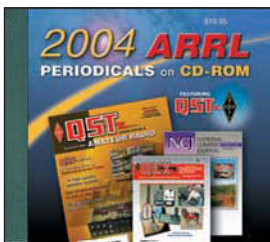
ARRL The national association for
AMATEUR RADIO



SHOP DIRECT or call for a dealer near you.
ORDER TOLL-FREE 888/277-5289 (US)
ONLINE WWW.ARRL.ORG/SHOP

QEX 7/2005

CD-ROM Collections



ARRL Periodicals on CD-ROM are fully-searchable collections of popular ARRL journals. Every word and photo published throughout the year is included!

SEARCH the full text of every article by entering titles, call signs, names—almost any word. SEE every word, photo (including color images), drawing and table in technical and general-interest features, columns and product reviews, plus all advertisements. PRINT what you see, or copy it into other applications.

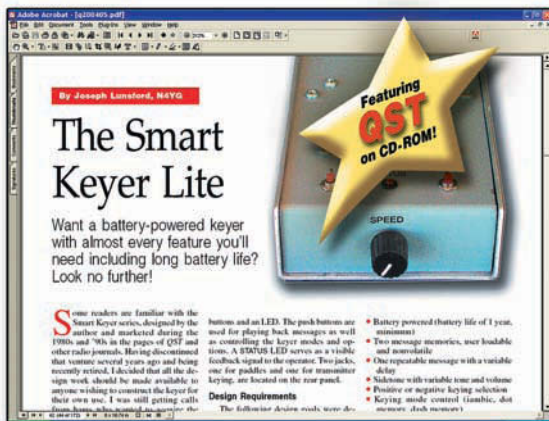


System Requirements:

Microsoft Windows™. 1999, 2000, 2001, 2002, 2003, and 2004 editions support Windows and Macintosh systems, using the industry standard Adobe Acrobat Reader® (included).

Communications Quarterly CD-ROM

This CD-ROM collection covers volumes of *Communications Quarterly* published from 1990-1999. Gain access to advanced technical topics in articles which cover transmitter, receiver and transceiver projects, theory, antennas, troubleshooting and much more. High quality black-and-white page scans can be read on your computer screen or printed. Quickly **search** for articles by title and author, **select** specific year and issue, and **browse** individual articles and columns. Requires Microsoft Windows™.



QST View

Every page of QST—all the ads, articles, columns and covers—has been scanned as a black-and-white image that can be viewed or printed.

BONUS! Latest, enhanced viewer—**AView**—included with any QST View purchase. **AView** is compatible with all sets of QST View.



ARRL CD-ROM Collections

ARRL Periodicals CD-ROM (includes QST, QEX, NCJ)

#9396 Year 2004	\$19.95
#9124 Year 2003	\$19.95
#8802 Year 2002	\$19.95
#8632 Year 2001	\$19.95
#8209 Year 2000	\$19.95
#7881 Year 1999	\$19.95
#7377 Year 1998	\$19.95
#6729 Year 1997	\$19.95
#6109 Year 1996	\$19.95
#5579 Year 1995	\$19.95

QST View CD-ROM

#7008 Years 1915-29	\$39.95
#6710 Years 1930-39	\$39.95
#6648 Years 1940-49	\$39.95
#6435 Years 1950-59	\$39.95
#6443 Years 1960-64	\$39.95
#6451 Years 1965-69	\$39.95
#5781 Years 1970-74	\$39.95
#5773 Years 1975-79	\$39.95
#5765 Years 1980-84	\$39.95
#5757 Years 1985-89	\$39.95
#5749 Years 1990-94	\$39.95
#8497 Years 1995-99	\$39.95
#9418 Years 2000-2004 ... NEW!	\$39.95
#QSTV (all 13 sets) . Only \$399 (Save \$120)	

Communications Quarterly CD-ROM

#8780 (1990-1999)	\$39.95
Ham Radio Magazine CD-ROM*	
#8381 Years 1968-76	\$59.95
#8403 Years 1977-83	\$59.95
#8411 Years 1984-90	\$59.95
#HRCD (all three sets)	\$149.85
QEX Collection CD-ROM	
#7660 (1981-1998)	\$39.95
NCJ Collection CD-ROM	
#7733 (1973-1998)	\$39.95

*Ham Radio CD-ROM, © 2001, American Radio Relay League, Inc. Ham Radio Magazine © 1968-1990, CQ Communications, Inc.

Shipping & Handling charges apply: US orders add \$6 for one CD, plus \$2 for each additional CD (\$12 max.). International orders add \$5.00 to US rate (\$17.00 max.). Or, contact ARRL to locate a dealer. Sales Tax is required for orders shipped to CA, CT, VA, and Canada.



www.arrl.org/shop
1-888-277-5289 (US)